Hierarchical Structured Materials for Controlled Oral Drug Delivery

Dissertation

zur Erlangung des Grades

„Doktor der Naturwissenschaften”

im Promotionsfach Chemie

am Fachbereich Chemie, Pharmazie und Geowissenschaften

der Johannes Gutenberg‐Universität in Mainz

vorgelegt von

Wei He

geboren in Shanghai, China

Mainz 2018

1. Table of contents

2. Introduction

Orally delivered drugs, especially chemically sensitive peptide drugs peptide drugs are prone to enzymatic degradation and acidic hydrolysis in the gastrointestinal environment [1], and therefore should be protected from deactivation before reaching their targeted site [1-3]. An ideal oral drug carrier that maximizes the bioavailability of the payload should be nano-sized [4, 5], pH-responsive [6, 7], muco-adhesive [8], targeting to a certain site of the intestine [7, 9], and favorable for cellular uptake [1-3]. At first glance, these requirements can seem overwhelming or even conflicting, but these properties are not required simultaneously in the human body. Thus, relevant functions could be triggered in a temporally sequential manner by designing a spatially hierarchical structure.

Hierarchically structured drug delivery systems, including nano-in-nano [10-16], nano-in-micro [17-20], micro-in-micro[21], micro-in-macro [22, 23], or nano-in-macro [24-26] systems are a current topic of research for maximizing the protection and efficient delivery of drugs in the human body [27, 28]. The multi-barrier nature of the hierarchical structures usually delays the release of the payload [11, 13, 16, 29, 30]. Meanwhile, different drugs can be loaded into each level of the hierarchy to achieve a sequential release [19, 25, 31, 32]. Furthermore, various stimuli-responsive coatings have been utilized to regulate the release of peptide upon environmental triggers [10, 11, 24, 25]. However, current stimuli-responsive drug nanocarriers lack the ability to retain peptide before they reach the targeted tissue. Thus, they cannot take full advantage of a hierarchical structure. Besides, the overall encapsulation efficiency of peptides is limited because the peptides are either loaded after the formation of the carriers [11] or are partially not encapsulated during the formation of carriers [24]. To overcome these limitations, we have designed a hierarchical peptide delivery system that consists of a new type of pH-responsive nanocarriers [33] and pH-responsive nanofibers in

which nanocarriers are loaded. In section 4.4, such nanoparticle-in-nanofiber (NP-in-NF) system is discussed in detail.

The nanocarriers are based on chitosan (CS), which is a popular oral drug excipient [34-36] because of its mucous adhesiveness, biodegradability, and biocompatibility [37, 38]. Pioneering works of CS-based drug carriers were mainly based on interfacial crosslinking in water-in-oil emulsions which lead to immobilization of the payload due to non-specific crosslinking reactions [39]. Physical crosslinking such as polyelectrolyte complexation [40-44] avoids chemical immobilization of the payloads and enables a pH-responsive swelling and triggered release [41]. However, the CS NPs prepared with polyelectrolyte complexation (PEC) method requires the use of low concentrations of polymers, thereby implying that only a low concentration of NPs can be produced. Besides, part of CS is not converted into NPs and is present as residual polymer dissolved in the continuous phase [45]. Furthermore, polyelectrolyte complexes, also called "polyplexes", lack mechanical stability: dissolution and chain rearrangement can take place in the presence of salt or after dilution [39]. These properties of CS-based polyplexes limit their application as nanocarriers for oral peptide delivery. In this work, we fabricated nanocarriers based on glycol chitosan (GC) with the polyelectrolyte complexation method. The drawbacks of this method could be prevented by confining the PEC reaction in miniemulsion droplets and subsequently crosslinking the surface of the NPs. The peptide can be encapsulated under mild conditions with high drug encapsulation efficiency, and the pH-responsive nanocarriers allow for the release of peptide over five days. In section 4.2, the crosslinked nanocarriers based on polyplexes is described in detail.

Despite that nanocarrier prepared in inverse miniemulsion possess advantages like better size-control and improved efficiency of encapsulation in comparison to other preparation methods [33, 46], the recovery of the resulting nanocarriers and their transfers to water is a non-trivial

task. Required by the biological application, nano-drug carriers prepared in inverse emulsions must be transferred to and stabilized in aqueous media, which is traditionally facilitated by coating the nanocarriers with a hydrophilic layer via physisorption, chemisorption, or covalent grafting [47]. Especially, polymeric nanocarriers are typically transferred to water by the solvent evaporation method with the help of hydrophilic surfactants [48-50]. Recently, such method further evolved to a universal two-step method: hydrophobization followed by amphiphilic coating [51], which has shown successful recovery of both inorganic [52-56] and polymer NPs [57, 58]. Furthermore, an ultraviolet (UV)-responsive copolymer has been developed as a switchable emulsifier for non-aqueous emulsions [59]. The NPs stabilized by this emulsifier could be redispersed in water upon UV radiation followed by solvent evaporation. Nevertheless, for hydrophilic excipients, the additional stabilizing amphiphiles are unnecessary, or even harmful due to their cytotoxicity [60] or undesirable interference with proteins [54]. Thus, methods involving the phase inversion of microemulsion are irrelevant in this context, because a large excessive amount of surfactants is left in the final dispersion of the NPs [61, 62]. Nevertheless, attempts to remove the hydrophobic surfactants by centrifugation and resuspension often affront a compromise between the undesirable aggregation and limited recovery rate [63-65]. To overcome such problems, we propose a new strategy to recover polymeric hydrophilic nanocarriers from inverse emulsion under mild conditions. The resulting self-stabilizing nanocarriers have minimal aggregation and quasi-qualitative rate of recovery while no additional coating layer is needed. Inspired by the cryoprotectants in the freeze-drying process [66], our approach involves the insertion of a temporary water-soluble molecular “cushion” into the nanodroplets of inverse emulsions before the removal of the surfactants. Therefore, the irreversible aggregation of nanocarriers during the washing process is minimized thanks to the molecular “cushion”. Meanwhile, these small molecules can be easily dissolved upon the redispersion of nanocarriers in water. We monitored the location of nanocarriers during the washing process, characterized the colloidal

properties of the final dispersion, studied the residue of surfactant, and tested the concept with various other molecules. In section 4.5, the recovery of NPs from inverse miniemulsion is discussed in detail.

3. Theoretical background

3.1. Oral drug delivery systems

3.1.1. Hierarchical systems for oral drug delivery

Orally delivered drugs experience harsh gastrointestinal environments until they reach the targeted site, especially for drugs based on nucleotides, proteins or peptides, enzymatic degradation and acidic hydrolysis [1, 67]. Therefore, an oral drug carrier should protect and transport its payloads before releasing them at their targeted site. The drug carriers should protect the peptide from the degradative gastrointestinal environment, release the peptide to a certain region of the intestine, transport the peptide through the epidermal cells, and release the peptide in the blood. To fulfill these tasks, such carriers should possess simultaneously four main properties. Firstly, the material embedding the drug, *i.e.* the drug carrier, should be pH-responsive so that it protects the drug at low pH value and release the drug at higher pH value near the regions of the duodenum or ileum [6, 7]. Secondly, mucoadhesive properties for the drug carrier are suitable so that they can be preferentially adsorbed at the intestinal epidermal mucus layer. Thirdly, the drug needs to be selectively delivered to the targeted organ or in the blood [7, 9]. Finally, the endocytosis of the drug carrier is enhanced if the carriers are in the submicron range [4, 5]. Many different properties of an efficient drug carrier can, therefore, appear at first glance conflicting. However, such a drug carrier could be achieved by designing hierarchical structures with properties that are programmed to be triggered in a sequential manner.

Hierarchically structured drug delivery systems, including nano-in-nano [10-16], nano-in-micro [17-20], micro-in-micro [21], micro-in-macro [22, 23], or nano-in-macro [24-26] systems are a current topic of research for maximizing the protection and efficient delivery of drugs in the human body [27, 28]. The multi-barrier nature of the hierarchical structures

usually delays the release of the payload [11, 13, 16, 29, 30]. Meanwhile, different drugs can be loaded into each level of the hierarchy to achieve sequential release [19, 25, 31, 32]. Furthermore, various stimuli responsive coatings have been utilized to regulate the release of peptide upon environmental triggers. For example, gold NPs grafted with protein drugs have been encapsulated into crosslinked gelatin capsules, which released the NPs upon ultrasound trigger [25]. Porous silica NPs were coated with an acid-degradable coating, the degradation rate of which regulates the release of anticancer drugs [10]. Similarly, porous silica NPs loaded with an anti-diabetic peptide drug have been coated with a pH-responsive polymer containing enzyme inhibitor. The peptide drug and the enzyme inhibitor were released in a sequential manner upon an increase in environmental pH value [11]. Multi-responsive systems were also fabricated by loading pH-responsive NPs into gelatin capsules with a pH-responsive coating. Encapsulated insulin could be released at a pH value of 7.4 and be transported to the blood. An *in vivo* study on diabetic rats shows an increased insulin level and decreased glucose level after oral administration of the optimized formulation [24].

However, current drug nanocarriers lack the ability to retain peptides before they reach the targeted tissue. Therefore, they cannot take full advantage of a hierarchical structure. Besides, the overall encapsulation efficiency of peptides is limited because the peptides are either loaded after the formation of the particles [11] or are partially not encapsulated during the formation of particles [24]. These limitations can be overcome by the nanocarriers recently reported by our approach [33]. The peptide can be encapsulated under mild conditions with high drug encapsulation efficiency, and the pH-responsive nanocarriers sustain the release of peptide over five days. In this work, we present a hierarchical peptide delivery system for which two components in the hierarchy of structure are pH-responsive.

3.1.2. Recent advances in responsive drug delivery systems

Nano-drug carriers based on liposomes, micelles, dendrimers, polymeric NPs, or inorganic NPs have been made with different architectures or surface properties for their enhanced cellular permeability and extended systematic retention. To further improve the drug efficacy, the therapeutic agents should be delivered in a special-, temporal-, or dosage-controlled manner upon stimuli in their microenvironments. Therefore, the diffusion of the payload from the nanocarriers should be switchable via the protonation, hydrolytic cleavage, or conformational change of the polymer. Such changes can be induced by endogenous stimuli, such as the concentrations of a proton (pH-responsive), glutathione (redox-responsive), and degradative enzyme (inflammation-responsive); or by exogenous stimuli, such as heat, light, ultrasound, or electromagnetic field [6]. In this section, recent advances in the stimuli-responsive system that are relevant to oral drug delivery are reviewed, among which the pH-responsive system is the focus of this work.

3.1.2.1. pH-responsive systems

In the human body, the pH value varies among different organs, especially those along the gastrointestinal tract. At the cellular level, intracellular compartments also exhibit different pH values. Indeed, the pH value of endosomes shift from 7.4 to 5 ~ 6 during their acidification and is further reduced to 4~5 after their fusion with lysosomes [6, 68]. Moreover, under pathological changes such as sites of solid tumor and inflammation, the pH value near diseased site deviates from 7.4 for a healthy tissue to 6.5 ~ 7.2 due to elevated acidic metabolites in the extracellular environment [6, 69, 70]. Hence, the pH change can serve as an endogenous stimulus for various responsive drug delivery systems.

In general, strategies that render pH-responsiveness to polymers can be categorized into chemical or physical approaches. In the physical approach, polymers containing ionizable

functional groups can change their solubility or conformation at different pH values, which causes the swelling/dissolution of the matrix, the dissociation of micelles, or the change of configuration polymer chain at the surface. Typically, a polymer with side groups that can be protonated such as dimethylaminoethyl groups [71] is used, so that the resulting NPs can swell at the pH value that is below or above the acid dissociation constant (pK_a) of the side group. In the chemical approach, polymers containing acid labile bonds in the backbones [72-74], side groups [75], or crosslinkers [76], can undergo acidic hydrolysis, which leads to the change of the nature of the surface, the swelling of the matrix, or the release of the conjugated drug. For example, polymeric NPs can swell upon acidic cleavage of hydrophobic protecting groups, and thus reveal hydrophilic side groups, yielding a rapid release of the payloads [75].

The release of drugs can be triggered by (1) the change of permeability of drug upon the swelling/disassembly of the polyelectrolyte based carrier [77-79]; (2) the cleavage of anchored drug molecules from the matrix [68]; or (3) the change of the electrostatic interaction between drugs and their matrix [80]. The strategy (1) is milder compared to the strategy (2) because no chemical modification of the drug is required. The strategy (1) is more universal compared to the strategy (3), as it is non-selective to the charge of the drug. Hence, the change of permeability has been widely adopted, especially for macromolecular drugs. For example, bovine serum albumin has been loaded and released from CS decorated porous silica NPs, where the swelling of the CS coating at lower pH was considered responsible for the accelerated release of bovine serum albumin under pH 4.0 compared to that under pH 7.4 [77]. On the other hand, a polymeric micelle-based on a copolymer of polyethylene glycol (PEG), PEG-*block*-poly(β-amino ester) can disassemble at pH 6.4 ~ 6.8 and released entrapped camptothecin, a small molecular anticancer drug [78]. Similarly, human serum albumin has been delivered into brain ischemic areas in mice via pH-triggered disassembly of micelles based on piperidine- and imidazole-modified PEG-*block*-poly(β-amino ester) [79].

The surface properties of drug carriers can be altered by modifying their charge or exposing the protected ligands for targeting. The ionization of the polyelectrolytes on the surface of nanocarriers can lead to a switch of charge, which promotes the cellular uptake of nanocarriers. For instance, a systematically administered bacteria targeting NP based on poly(lactic-co-glycolic acid)-*block*-polyhistidine-*block*-PEG copolymer has been designed to switch its charge at the site of infection, where the anaerobic fermentation and inflammation reduce the local pH value. The negatively charged NPs remain non-targeting during their circulation in blood while switching to positive charge and target at the negatively charged bacterial wall upon charge switching under acidic environment. The internalization of NPs was enhanced at pH 6.0 compared to that at pH 7.4, and the antibiotic-loaded NPs have shown effective inhibition in both Gram-positive and Gram-negative bacteria [69]. The pH-triggered charge switching concept has also been realized by chemical cleavage. A cysteamine modified polyphosphoester-*block*-PEG copolymer has been partially conjugated with a 2,3-dimethylmaleic anhydride to obtain a charge conversion block copolymer which can switch the charge from negative to positive upon acidic cleavage of dimethylmaleic anhydride at pH 6.8. Such copolymer can be conjugated with doxorubicin, and the resulting micelle can be more efficiently internalized by cancer cells at pH 6.8 than they are at pH 7.4. Afterward, the doxorubicin can be further cleaved and thus released at pH 5.0 inside the endosome [68].

To improve the cellular targeting and internalization of drug carriers, cell penetration peptides or targeting ligands on the surface of nanocarriers can be activated via the conformational change of polyelectrolytes after their ionization at certain pH range. For instance, a poly(L-lactic acid)-*block*-polyhistidine based micelle has been developed for the targeted delivery of doxorubicin to cancer cells. The micelle is decorated with PEG-*block*-polyhistidine ligands, the polyhistidine side of the ligand is further grafted with transactivator of transcription (TAT), which is a transactivating regulatory protein. The exposure of TAT was realized by the

protonation of the polyhistidine segments at the acidic extracellular pH value around the tumor. [81]. Alternatively, the functional ligand can also be exposed by the cleavage of the masking ligands. For example, a liposome decorated with TAT was grafted with acid cleavable long PEG ligands, which masked the TAT during circulation. Doxorubicin encapsulated liposomes showed increased cytotoxicity after acid incubation compared with those without acid incubation. Such increased cytotoxicity was believed to be the result of the exposure of the TAT sequence upon the cleavage of PEG ligands [82]. Moreover, the activation of cellular targeting ligand can also be realized by the acidic cleavage of masking PEG. The targeting property of the micelles was switched off until the removal of the PEG ligands in the acidic tumor sites [83].

During the internalization of the drug carriers, the pH value in the lumen of endosomes evolves during their maturation. The pH value reduces from 6.0 to ~ 6.2 in early endosomes to ~ 5 in late endosomes after the acidification process, and finally to 4 - 5 after the fusion of late endosome with lysosomes [72, 84]. Various payloads have been released at endosomal pH value upon the swelling of polyelectrolyte-based NPs [75], the disassociation of micelles [68, 85, 86], the hydrolysis of protein nanocapsules [87], the acidic etching of mesoporous magnetic NPs [88], and the cleavage of drug from silica NPs [89-91].

To avoid the acidic hydrolysis and enzymatic degradation of therapeutic molecules in lysosomes, efforts have been made to eject drug carriers from the late endosomes via the eruption of endosomal compartment due to the reduced endosomal pH value. Such a process is often referred to as “endosomal escape”. The pH-induced eruption of endosomes can be facilitated by weak polycations, such as poly(L-lysine) [84], poly(β-amino esters) [85, 86], or polyhistidine [87, 88]. The polyelectrolyte in the drug carriers was protonated at endosomal pH value, thus increasing the osmotic pressure inside endosomes, and consequently led to the eruption of the endosome. However, a potential concern of endosomal escape, in general, is

that the eruption of the lysosomal membranes and the leakage of lysosomal enzymes can lead to autophagy and cell death [6]. Besides, in the case of transcytosis drug delivery, drug carriers are expected to leave the cell with the help of the late endosome via exocytosis. Hence, endosomal escape caused by polyelectrolytes should be avoided. In this respect, nanocarriers based on CS and its derivatives have shown a low buffering effect compared to other polycations. Moreover, the endosomal escape of CS-based nanocarriers requires additional membrane-destabilizing polyelectrolytes [89]. Therefore, CS and its derivatives, are safe candidates as a pH-responsive excipient for transcytosis drug delivery.

pH-responsive systems are popular for oral drug delivery thanks to a significant variation of pH value along the gastrointestinal tract. The two major tasks of oral drug delivery are to protect the drug from the degradative environment and to improve their cellular uptake. Various pH-responsive NPs have been designed for the oral delivery of peptide/protein drugs or hydrophobic drugs, which has been thoroughly reviewed [93]. In general, the drugs can be released in the intestine (pH ~ 6) upon the ionization of anionic polyelectrolytes, which causes the swelling of the matrix [94], dissolution of the coating [95], disassembly of micelles [96], or reduction of electrostatic retention to anionic drugs [80]. Among these oral drug carriers, CS is an especially attractive component because of its mucoadhesiveness, biocompatibility, and biodegradability [94]. In section 3.2, CS-based nanocarriers are discussed in detail.

3.1.2.2. Thermo-responsive systems

Drug carriers based on thermo-responsive polymers, typically poly(*N*-isopropyl acrylamide) [90], enable a sharp response in a conformational change of polymer chain at their lower critical solution temperature so that the encapsulated payload can be released under conditions such as hyperthermia [91]. Among thermo-responsive drug carriers, thermosensitive

liposomes are the most popular ones [90-94], and several of them have been used in clinical trials [6]. Furthermore, the lower critical solution temperature can be further tuned by modifying the chemical structure of the thermo-responsive polymer, so that the responsive temperature is even close to that of human body temperature [90, 92]. Recently, leucine zipper peptide, a thermo-responsive peptide, has been introduced to liposomes. At an elevated temperature, the peptide unzips, and therefore a channel can be opened on the shell of the liposomes for the release of doxorubicin [93]. Alternatively, gas generated during a thermo-induced chemical reaction can also disrupt the liposome and release the encapsulated doxorubicin in a temperature-sensitive manner [94]. Besides, the cellular permeability can also be tuned by thermo-trigger to improve the overall efficacy of the encapsulated drug. NPs coated with cell penetrating peptides, can be activated by external thermo-trigger, and the resulting NPs exhibit 8-fold enhanced HeLa-cell uptake [95]. In the scenario of oral drug delivery, the temperature profile along the digestive system is not profound enough for a thermo-responsive system, hence simple thermo-responsive systems are not often found in such application. However, the thermo-responsive property could be coupled with other stimuli-responsive functions, especially those lead to local hyperthermia (refer to section 3.1.2.4).

3.1.2.3. Redox-responsive system

Redox-responsive drug carriers are designed to be sensitive to the change of redox potentials that can trigger the site-specific release of payloads. The redox potential in various physiologic environments is frequently determined by the concentration of glutathione, which is found to be different between extracellular (2 to 10 μM) and intracellular (2 to 10 mM) compartments, and between tumor and healthy tissues [6]. The glutathione-sensitive typically contain disulfide bonds, which can serve as a cleavable part of polymer backbone [96], a crosslinker [97-99], the connecting node of di-block copolymers [100], the linker that

immobilizes functional building blocks [101, 102], or the anchor that immobilizes the payload [103]. The disulfide bonds are prone to rapid cleavage via reductive degradation, which triggers the release of the payloads via various mechanisms including but not limited to: destabilizing self-assembled micelles [96-98, 100], liposomes [102], or polyelectrolyte complex [104]; cleaving crosslinks of crosslinked nanogels [99]; cleaving anchoring bonds of polymer-drug conjugates [103]; or opening blocked pores of drug loaded mesoporous materials [101].

Beside reduction-responsive systems, oxidation-responsive systems have also been developed so that the release of the drug is triggered by reactive oxygen species, which is typically found in inflammatory tissues. For example, an oral drug delivery system that targets the inflammatory site of intestine was described [105]. The siRNA loaded NPs based on poly-(1,4-phenyleneacetone dimethylene thioketal) have shown the capability of gene silencing after oral administration. The nanocarrier degraded at the site of colitis and protect the mice model from colitis by releasing the payload siRNA.

Despite the rich variety of the redox-responsive systems available, it is still challenging to control the release of drug by a specific redox mechanism in a complex biological environment, as was illustrated by the withdrawal of Mylotarg, a commercialized redox-responsive drug, which failed to confirm benefits to patients [6]. Caution should be made in the design of redox-responsive drug delivery systems for the realistic physiological environment, as redox agents other than the glutathione/glutathione disulfide couple could also affect the drug carrier. Besides, the side effects of the redox-responsive carrier itself on the drug molecule could also compromise the effectiveness of the drug delivery system.

3.1.2.4. Magnetoresponsive systems

Ferromagnetic NPs can be incorporated into nano-drug carriers, and thus enable them to respond to the external magnetic field. Various magnetic drug carriers have been developed, such as core-shell NPs [106, 107], liposomes [108, 109], micelles [110, 111], polymeric nanoreservoirs [112], porous magnetic nanocapsules [113], or bacterial magnetic particles [114]. These carriers have shown the capability to deliver both small molecules, such as cancer drugs [115], and macromolecules such as RNA [116-118], DNA [119], and enzymes [120]. Being ferromagnetic, these carriers can facilitate the magnetic resonance imaging and can be guided under a focused external magnetic field for improved accumulation [6]. Furthermore, magnetic drug carriers can serve as magnetism-heat transducers under an alternating external magnetic field via hysteresis lose or Neel relaxation. Such ability can be directly applied to heat the solid tumors selectively and kill them via hyperthermia induced cytotoxicity [121]. Moreover, these magnetism-heat transducers can be combined with thermo-responsive polymers to yield magnetism-thermo-responsive systems. For example, the permeability of a porous membrane that is embedded with a mixture of poly(*N*-isopropyl acrylamide) nanogels and magnetic NPs can be altered by magnetic radiation [122]. The magnetic NPs can have been embedded into nanostructures, such as drug-loaded micelles [110], hydrogels [123], or the shell of liposomes [108] so that the release of drug can be regulated by external magnetic radiation in a non-destructive manner. Moreover, magnetic-thermo-responsive NPs can serve as gate-keepers that block the mesoporous matrix. For example, the pores on the surface of mesoporous silica NPs have been blocked by magnetic-thermo-responsive nanovalves, which are closed at physiological temperature, while opened upon heating. Consequently, the release of loaded doxorubicin can be triggered by an external magnetic radiation [124]. More complex systems can be engineered to execute complicated tasks. For instance, a heat sensitive TRPV1 channel in the cell membrane can be modified

with magnetic NPs. The magnetic modified TRVP1 channel can pump in calcium ions upon electromagnetic radiation to stimulate the production and release of bioengineered insulin *in vivo* [125]. Alternatively, oligonucleotides can serve as temperature sensors, as the double strands melt at elevated temperatures and couple at lower temperatures. Thus, complementary single strands of nucleotides can be separately conjugated to a host-guest pair, whose self-assembly behavior can be precisely controlled via fine-tuning the nucleotides [126]. For example, the pores of mesoporous silica NPs can be blocked with magnetic NPs via DNA linkage. The resulting drug carrier can be switched on and off by magnetic radiation [127].

3.1.3. Drug delivery systems for fragile molecules

Hydrophilic macromolecular drugs such as proteins, peptides, and nucleic acids, attract increasing interest in the treatment of a wide range of diseases, while their application is still limited due to low bioavailability [128]. Macromolecular drugs are liable to enzymatic and hydrolytic degradation, and thus they have a short biological half-life in the circulatory system. Besides, proteins and peptides easily denature upon environmental changes and lose their bioactivity [129]. Therefore, hydrophilic macromolecular drugs are considered more fragile than traditional small molecular drugs, and the delivery of hydrophilic macromolecular drugs, especially proteins and peptides, remains a challenge. To address this problem, a spectrum of technologies has been developed for the delivery of fragile molecules [128, 130]. In general, the loading of hydrophilic molecules can be achieved by either entrapment in a polymeric matrix, adsorption onto a functionalized surface, or encapsulation in the liquid core of a capsule. The methodologies for the loading of drugs have been thoroughly reviewed by Vrignaud et al. [128]. In this section, drug-loading strategies are reviewed from the perspective of the preservation of fragile molecules.

In general, a mild procedure is favored for the loading of fragile molecules. A very popular strategy for the preservation of drug is to load the drug to a preformed carrier. At low

temperatures, adsorption or absorption are thermodynamically favored, and the possibility of undesired side reactions with drug due to the synthesis of the carrier is eliminated. Such a "post-loading" method is especially popular among carriers for protein/peptide drugs. Various peptides [12, 131, 132] and proteins [77, 133, 134] have been loaded into various carriers, such as mesoporous silica (MPS) NPs [132], silica nanocapsules [77], polymeric nanocapsules [131, 135], or MPS microparticles [12] by simply mixing a cooled aqueous solution of drugs with a dispersion of preformed carriers. For example, tumor necrosis factor alpha was successfully loaded into silica nanocapsules after mixing for 48 h under magnetic stirring in an ice-water bath, while bovine serum albumin was loaded in the same manner at room temperature [77].

The "post-loading" method enjoys the merit that the target drug is not affected by the synthesis of the carrier. However, such merit is only applicable to simple drug carriers that do not require further functionalization. Besides, such kind of carriers is insufficient for the protection of payloads against harsh environments, such as that the one experienced in oral drug delivery. Finally, the drug release rate for those carriers is usually high [128]. To address these drawbacks, additional coatings were applied to those type of nanocarriers resulting in nano-in-micro [19, 135] or nano-in-nano [11] multifunctional systems. Using a droplet-based microfluid device, functional MPS NPs loaded with a hydrophilic model drug were further encapsulated into a hydroxypropylmethylcellulose acetate succinate-based polymer, which endowed the particle with pH responsibility and muco-adhesion properties. Furthermore, a hydrophobic model drug was also loaded into this pH-responsive polymer matrix, so that two drugs of different hydrophobicity were co-encapsulated into the nano-in-micro system [19]. Similarly, glucagon-like peptide-1, an anti-diabetic peptide, was loaded into functional MPS NPs by immersion. Afterward, the peptide-loaded NPs were further coated with a pH-responsive enteric polymer that contained a second peptide dipeptidyl peptidase-4, which is

an enzyme inhibitor using an aerosol flow reactor. The resulting functional coating regulated the release of a peptide, preserved the peptide via simultaneously physical isolation and biological inhibition of the enzyme that could degrade the glucagon-like peptide-1[11].

Another popular technique for fragile molecules is the polyelectrolyte complexation method, or the PEC method, in which two types of polymers, a polycation, and a polyanion, are mixed in an aqueous media and form a polyelectrolyte complex, a so-called "polyplex" by electrostatic interactions [136]. The PEC method is mild and aqueous based, and the resulting polyplex particles have a high charge density. Therefore, the PEC method is very popular among the carriers for nucleic acids, because the polyanionic nucleic acids are complexed with polycations, and the resulting polyplex is positively charged, which is favored for their cellular internalization. Such kind of systems has been applied in gene transfection [62] or gene silencing [104, 137-139]. For example, to improve the gene silencing effect, RNA was complexed with a redox-sensitive polycation such as poly(disulfide amine) [137], disulfide-containing poly(amido-amine) [138], or histidine-containing polycations [104]. The resulting polyplexes can quickly disassemble under reductive intracellular conditions via the degradation of the polyelectrolyte matrixes [128, 138]. On the other hand, the disulfide linkages can be inserted between the siRNA and the polyelectrolyte matrix [140] or between the RNA themselves [139], so that the release of RNA can also be triggered by the cleavage of RNA from the matrix [140], or by the depolymerization of multimerized RNA [89, 139].

Contrary to polyplex NPs based on strong polyelectrolytes for the formation of compact and stable particles, polyplex-based on weak polyelectrolytes can swell or even disassemble upon the change in pH values. At intermediate pH values, when the net charge of the polycation and polyanion approach zero, the polyplex NPs are stable and compact. At both lower and higher pH, when the net charge of the polyplex increases, the polyplex swells and triggers the release of the payloads. For example, insulin was trapped in a polyplex-based on CS and poly-

γ-glutamic acid (PGA). The polyplex NPs at pH 6.0 have an average diameter of about 220 nm when they are in their most compact form. At pH 2.0, the particles can swell due to the protonation the polycationic CS and have an average diameter of 315 nm. At pH 7.0, the particle can swell due to the deprotonation of PGA and have an average diameter of about 270 nm. At pH 7.4 the polyplex NPs disassemble completely. The release of insulin corresponds to their swelling behavior: the release of insulin is suppressed at pH 6.0 and promoted at higher and lower pH values. Therefore, such CS-based polyplex was proposed to be a pH-responsive oral drug carrier for insulin. [43, 141] Similarly, heparin [142] and nucleic acids [143, 144] were also trapped in the CS-based polyplexes [142, 143] or ionotropic gels, in which a multi-valent counterion was used in the place of one of the polyelectrolytes for complexation [38, 133].

Nanocarriers for complicated tasks such as endosomal escape usually requires multiple steps of synthesis. Fragile drugs protected in polyplexes can survive the reaction thanks to the compact structure of polyplexes. For example, a siRNA was first complexed with a polyaspartamide derivative that can disrupt endosomal membrane at pH 5.5. Then a silica shell was precipitated onto the surface of the polyplex for transient stabilization. Afterward, the silica layer was further functionalized with a disulfide-containing PEG that was detached upon reduction, so that the endosomal escaping ligands were exposed when the nanocarriers were in the late endosome. The resulting mRNA loaded nanocarrier displayed prominent sequence-specific gene silencing ability in tumor-bearing mice [104].

Fragile molecules can also be encapsulated into various polymeric nanocapsules with an aqueous core. In these cases, the target drugs need to be protected from the side reactions during the formation of the shells of nanocapsules. A common method is to avoid high temperature. For example, during interfacial radical photopolymerization, a low-temperature process (4 °C) was selected to ensure that the level of proteolysis was minimized during the

shell formation of peptide-based nanocapsules [135]. To avoid an oxidation reaction, sodium metabisulfite was added to the aqueous phase to preserve the DNA during the radical polymerization [71]. It was also suggested in some work that a shell material containing antioxidants, such as disulfide groups in the thiol-conjugated hyaluronic acid [129], can preserve fragile drugs like RNA against oxidation [65]. Finally, the encapsulation of an aqueous core into a nanocapsule does not necessarily require a chemical reaction. Indeed, a shell can also form by the adsorption and precipitation of the pre-formed polymer so that the payload is not affected by any side reaction. For example, salmon calcitonin was encapsulated into CS-based nanocapsules. The hydrophobic peptide was dissolved in the oil phase of miglyol and acetone, and an oil-in-water nanoemulsion was formed by the solvent-displacement technique, in which no high-energy shearing was involved. The partially PEGylated CS was then added to the continuous phase. The formation of a hydrophilic shell resulted from the adsorption of PEGylated CS onto the water-oil interface [131].

Drug delivery systems designed for oral drugs must meet extra requirements because of the harsh and complicated environment along the gastrointestinal tract. Oral drug carriers should protect their payloads from enzymatic degradation and acidic hydrolysis while transporting their payloads to the desired location [145]. Furthermore, sometimes drugs should ideally be protected and released in the circulatory system, which means that the carriers should also penetrate the intestine and enter the blood via either a paracellular or transcellular route [3, 130, 146].

Chitosan is an extensively studied promising candidate as a drug excipient because of its mucous adhesiveness, biodegradability, and low cytotoxicity [38]. Therefore, various carriers based on CS for the oral delivery of protein drugs were developed to improve the oral bioavailability of therapeutic proteins, such as insulin, calcitonin, and cyclosporine A [34-36, 147, 148]. Pioneering works were mainly based on interfacial crosslinking in water-in-oil

emulsions under mild conditions. This strategy suffers from the non-specific crosslinking reactions, which lead to the immobilization of the payload [39]. Therefore, research shifted toward physical crosslinking strategies, such as ionic gelation and polyelectrolyte complexation [40-44]. These approaches avoid chemical immobilization of the payloads and polyplexes, which enable a pH-responsive swelling and triggered release [41]. For example, the polyplex of CS and heparin is stable at lower pH (1.2, 2.5), swells at intermediate pH (6.6 and 7.0), and disintegrates in the blood (pH 7.4). Such property allows the heparin to survive the acidic environment of the stomach and be released in the intestine. In-vivo tests in a mouse via oral administration showed that the CS-heparin nanocarriers displayed improved bioavailability of heparin as an anticoagulant. Besides, CS was chosen to improve the absorption of heparin through the paracellular pathway by transiently opening the tight junction between epithelium cells [142]. However, a comparative study of CS-based polyplexes and CS free polymers shows that the paracellular opening ability of CS should be interpreted with care. Although free-soluble CS derivatives can reversibly open the tight junctions and increase the permeation of insulin via the paracellular pathway, polyplex made from the same polymers show the low effect on the opening and take intracellular pathway instead, which is much less efficient in the transportation of payloads [134].

It is noteworthy that the CS NPs prepared with the PEC method requires the use of low concentrations of polymers, thereby meaning that only a low concentration of NPs is produced. Besides, part of CS is not converted into NPs and is present as the residual polymer in the continuous phase [45]. Furthermore, polyplexes lack mechanical stability: dissolution and chain rearrangement can take place in the presence of salt or after dilution [39]. Moreover, the CS ligands on the surface of nanocarriers can also be cleaved in the degradative environment in the stomach, which render the loss of their mucoadhesive property and

undesirable leakage of payloads [11]. These properties of CS-based polyplexes limit their application as nanocarriers for oral peptide delivery.

3.2. Chitosan-based nanocarriers

3.2.1. Chitosan and its derivatives

3.2.1.1. Chitin, chitosan, and their chemical structures

The use of renewable biopolymer in the pharmaceutical field has become a trend as it offers advantages such as biocompatibility and biodegradability [149, 150]. A very important class of biopolymer are polysaccharides, such as cellulose, starch, pectin, and chitin. Chitin is the most abundant natural biopolymer second to cellulose: it is available to the extent of over 10^{10} ton globally [150]. Chitin in nature forms ordered microfibrillar crystallines and serves as a structural component such as in exoskeleton shells of arthropods and cell walls of fungi and yeast [149]. Although chitin can be extracted commercially from fungi and bacteria, the main commercial source of chitin is crustacean shells. Industrial production of chitin involves acid treatment to remove CaCO3, base treatment to remove protein, and decolorization to remove residual pigments [149].

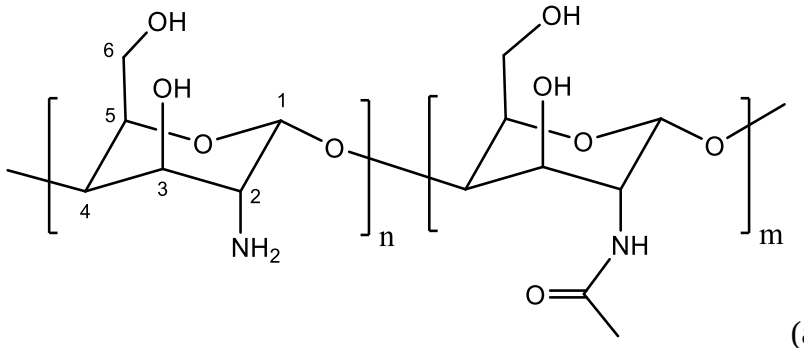

(a)

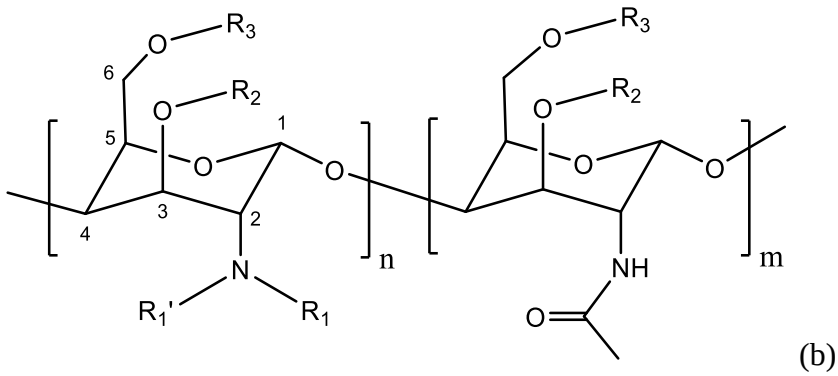

(b)

Figure 1. Chemical structure of chitin, chitosan, and their derivatives. (a) chitin (n = 0) chitosan (n ≠ 0); (b) derivatives of chitosan: R_1, $R_{1'}$ R_2, and R_3 refer to mono-N-substituted, di-N-substituted, O-3-substituted, and O-6-substituted functional groups respectively.

Chemically, chitin was first identified in 1884 as poly (b-(1-4)-N-acetyl-D-glucosamine) [149] (**Figure 1**a), despite that chitin in nature can be deacetylated to a low extent, depending on the source [151]. The 1,4-beta glycosidic bond endows chitin with a linear, rigid chain, compared to its branched counterpart, 1,6-beta glycoside, in glycogen or its helix counterpart, 1,4-alpha glycoside, in amylose [150]. Such 1,4-beta glycosidic bond is also featured in cellulose (as shown in **Table 1**). Therefore, chitin can be viewed as a modified cellulose, with the hydroxyl group on C-2 replaced by an acetylamino group. With the rigid and linear chain of chitin, intra- and interchain hydrogen bonds easily forms between the primary hydroxyl group on C-6, the secondary hydroxyl group on C-3, and acetylamino group on C-2 of glucopyranose ring (**Figure 1**a). Consequently, chitin has a good crystallinity in solid form, but poor solubility in a usual solvent, which is a major obstacle to the application of chitin [149].

Table 1. Glycosidic bond configuration and examples

glycosidic bond	**configuration of the polymer chain**	**Example**
1,4-alpha	linear, helix	Amylose
1,6-alpha	branched	glycogen (1 branch per 10 unit), amylopectin (1 branch per 30 unit)
1,4-beta	linear, rigid	cellulose, chitin, chitosan

Chitosan (CS), as a partially deacetylated derivative of chitin, is a copolymer of D-glucosamine (GlcN) and N-acetyl-D-glucosamine (GlcNAc) linked with 1,4-beta glycosidic bond [149] (**Figure 1**b). The degree of deacetylation (DD%) or the degree of acetylation (DA%, DA% = 100% - DD%) is, therefore, an important parameter of chitin and CS. Although there is no clear boundary between CS and chitin, it is widely adopted that when the average DA% of chitin reaches below 50%, the resulting polyelectrolyte is called “chitosan”

[149], which is soluble in acidic aqueous media thanks to the protonation of the amine group. The structure and properties of pure CS, including molecular weight, DA%, distribution of deacetylated unit, solubility, and persistence length, has been thoroughly characterized and reviewed [149].

The aqueous solubility of CS depends on both the properties of the polymer and that of the dissolution media [149]. Generally, the charge density determines the aqueous solubility of CS. Average DA% limits the total amount of amine group available for ionization: usually, a DA% below 50% or 60% is required for dissolution in neutral media and acidic media respectively [152]. The distribution of GlcN dictate the distribution of charge along the polymer chain, therefore a random distribution is favored over a block-wise distribution of GlcN for dissolution [152]. Besides, the high molecular weight of CS was also reported to be unfavorable for dissolution [153]. In terms of dissolution media, the ionic strength, the pH value, and the pK_a value of the acid collectively influence the degree of ionization of amine group, and therefore the dissolution of CS [149].

3.2.1.2. Derivatization of chitosan

CS as the most important derivative of chitin can be further derived for various purposes via de-polymerization, adjustment of the distribution of GlcN, and modification on the side-chain [149, 150, 154, 155].

The molecular weight of CS can reach as high as 10^6 Dalton [150], but the high-molecular CS is unsuitable for application due to its low solubility and high viscosity. CS has thus been depolymerized either chemically, physically, or enzymatically [150, 156, 157] to yield low-molecular CS or CS oligomers. Chemical or physical depolymerization of CS aims at the cleavage of the glycosidic bond by strong acids (e.g. hydrochloric acid, phosphoric acid, nitrous acid), strong oxidants (e.g. H_2O_2, $FeCl_3$), high temperature, or high dosage of radiation [150]. Despite the ease in preparation, these methods suffer from inevitable side reactions

[158] and low efficiency, as the product contains a large amount of undesirable monomer, while oligomers, especially hexamers [159], are required for the optimal physiological activity.

Enzymatic depolymerization/degradation of CS yields CS oligomers without monomers and has fewer side reactions compared to chemical methods. Besides, depolymerization can be more controlled in terms of a sequence of GlcNAc and GlcN units [156]. Cellulase can cleave 1,4-beta glycosidic bond regardless of the sequence of GlcNAc or GlcN units [157]. Furthermore, chitinolytic enzymes, such as chitinase, chitosanase, and lysozyme can degrade CS in a more specific manner, and the specificity of chitinolytic enzymes has been studied in detail via NMR technique [156]. Lysozyme and chitinase preferentially attack GlcNAc-GlcNAc linkage, and the resulting oligomer has dominantly GlcNAc units as the end group [160]. Chitosanase specifically attacks GlcN-GlcN linkage [161], with some exceptions that show the ability to cleave GlcNAc-GlcN linkage [160].

The distribution of GlcNAc and GlcN depends on the condition of deacetylation reaction [149]. Heterogeneous deacetylation of chitin leads to a blockwise distribution of GlcN, which is typical for commercial CS [149, 162]. The same reaction carried under homogeneous condition lead to random distribution [150, 160]. Besides, re-acetylation of highly deacetylated CS with acetic anhydride leads to a random distribution of GlcN [152, 162].

Various modifications can be done on the side chain of CS [149, 150, 154, 155]. The reactivity of these nucleophilic functional groups sort as follows: primary NH_2 group on C-2 (N-substitution) >> primary hydroxyl group on C-6 (O-6-substitution) > secondary hydroxyl group on C-3 (O-3-substitution). Therefore, the amine group and the hydroxyl groups can be randomly or regioselectivity functionalized according to specific needs.

CS or slightly deacetylated chitin, as a weak cationic polyelectrolyte, has an only limited solubility in acidic aqueous media. Therefore, a major motivation for the modification of CS is to improve its aqueous solubility in basic media. For example, carboxymethyl chitosan has been prepared with sodium monochloroacetate, and the substitution reaction takes place at O-6, O-3, and amine groups [149]. The selective N-carboxymethylation by glyoxylic acid has been achieved via reductive amination in a mono- or di-substituted manner [163] Selective N-substitution of CS can also be achieved by amidation with an anhydride [164]. Selective O-substitution can be achieved via protection and deprotection of amine group [165]. Similarly, CS or chitin has been O-6-sulfated [165, 166], O-3-sulfated [165], N-sulfated [167], O-6-phosphated [168], or N-phosphonomethylated [169]. These anionic groups transform CS into an amphoteric polymer, therefore enable their dissolution in both acidic and basic media. The above mentioned amphoteric CS derivatives can be potentially applied as an anticoagulant [167], an antiretroviral agent [165], a metal absorbing agent [169, 170], or pH-responsive coating [164]. Beside amphoteric modification, CS can also be quaternized and form a strong polyelectrolyte. The resulting N-trimethylated CS is soluble in water at all practical pH values [171]. N-quaternized CSs have been applied as flocculating [172] or anti-static agent [173]. Finally, GC, or O-6-ethoxylated CS, show excellent aqueous solubility at all pH values. Compared to quaternized CS, GC has a lower charge density and therefore non-toxic to mammalian cells regardless of its molecular weight [174]. Besides, GC has shown good biocompatibility *in vivo* [175], which makes it a good candidate for biological applications.

Beside aqueous soluble CS, amphiphilic CS is another important CS derivative. Started from an aqueous soluble polymer, CS can be tuned to be amphiphilic [176], or even soluble in organic solvents [177]. Various vinyl monomers, including methyl acrylate, methyl methacrylate, acrylonitrile, and styrene can be grafted to CS via radical polymerization [150]. The resulting graft copolymer usually has a low grafting density and therefore is

biodegradable via cleavage of CS. A higher grafting density can be achieved by grafting hydrophobic ligands to the CS via acylation [177, 178]. The highly substituted CS can be soluble in chloroform [177]. More commonly, hydrophobic ligands can be introduced to amine groups via reductive amination [179-183]. With an increased degree of substitution and an increased length of aliphatic ligand, amphiphilic CS shows decreased solubility and biodegradability [178], but increased viscosity in acidic media [184]. The thermogelation behavior of the alkylated CS has been studied in detail, which shows that the pH value and salt concentrations affect the balance between the repulsive charged groups and attractive aliphatic ligands [182, 183, 185]. The hydrophobic ligands also confer interfacial activity to CS, so that amphiphilic CS can serve as a polymeric surfactant [176]. Besides, the amphiphilic CS can further complex with ionic surfactants of opposite charge [183], and the resulting surfactant-polymer complex can form a stable interfacial membrane and hence efficiently reduce the interfacial tension [176, 183, 186]. Thanks to the diversity in functional groups and tunability, amphiphilic CS can be used as a potential polymeric surfactant in cosmetic or pharmaceutical formulations [179, 187].

CS and its derivatives have been widely applied in bio-applications, such as antibiotics [188], tissue engineering [189], and nucleotides/protein delivery [67, 190] thanks to their bioactivity, biodegradability, and biocompatibility [37]. Various functionalities have been introduced to CS by chemical modification. Poly(ethylene glycol) (PEG) has been grafted to CS via reductive amination or amidation [191]. The PEGylated CS obtains the water-soluble and anti-fouling property of PEG, and therefore PEGylated CS shows reduced cytotoxicity and increased colloidal stability [146]. Short peptides, with a degree of polymerization around 6, have been conjugated to amine group via ring-opening polymerization of an N-carboxy anhydride of amino acids to improve the hydrophilicity of CS [192]. Sulfhydryl bearing agents, such as thioglycolic acid, cysteine, N-acetylated cysteine, and glutathione can be

grafted to CS via EDC catalyzed amidation [193, 194], the thiolated CS significantly increased mucoadhesive strength and hence is attractive polymer for oral or nasal drug delivery [146]. Various carbohydrates have been grafted to CS to enable lectin recognition, and thus drug targeting [155, 195, 196]. Aldehydo- or keto-sugar like glucose, cellobiose, lactose, galactose can be grafted to CS via reductive alkylation [196], while carboxylic acid or lactone containing sugars can be grafted via EDC/NHS amidation [196, 197]. Cyclodextrin can be grafted to CS via reductive amination [183, 198], grafted β-cyclodextrin as the same association constant as free β-cyclodextrin, can for dynamic physical gel adamantine-cyclodextrin dynamic linkage [183].

3.2.2. Nanoparticles based on chitosan and its derivatives

NPs, compared to other drug delivery carriers, such as tablets, capsules, beads, liposome, microparticles, and microemulsions, improve the bioavailability of the encapsulated drugs via enhanced transmucosal transport, cellular targeting, or improved cellular uptake [38]. In the last decades, various therapeutic agents including vaccines, genes, proteins, and peptides have been encapsulated into polymeric NPs, especially in CS-based nanoparticles (CS-NPs) [38, 146], and among the protein drugs loaded in CS-NPs, insulin is the most widely studied [199]. CS-NPs can be prepared via self-assembly, precipitation, polyelectrolyte complexation or emulsion-based methods.

CS and its derivatives can be physically crosslinked by anionic small molecules in aqueous media. Such process is usually called “ionotropic gelation” or simply “ionic gelation”, which is believed to be a result of electrostatic attraction between the cationic CS and the polyanionic molecules. Nonetheless, a gain in entropy via the liberation of metallic mono-valent counterions also contributes to the complexation [45]. Ionotropic gelation allows facile entrapment of hydrophilic drugs under mild conditions. Moreover, the resulting NPs can swell at low environmental pH thanks to the polycationic nature of the CS. For example, CS

crosslinked by tripolyphosphate can form NPs with a diameter of 300-400 nm. The resulting NPs swell at lower pH while deswell at pH 6.4, and the diffusion-controlled release rate of the encapsulated insulin can thus be adjusted by the pH value. The dispersion was used for nasal delivery of insulin, and a ~ 50% maximal reduction of glucose level was observed *in vivo* in the blood of the tested rabbits [200]. Similarly, thiolated CS was used to prepare CS-NPs via ionotropic gelation for nasal delivery of insulin [193] or leuprolide [194]. Take insulin, for example, the NP based on thiolated CS (150-200 nm in diameter) was believed to enhance the mucoadhesiveness of NP. A larger decrease of blood glucose level (40%) was observed in thiolated CS-NPs compared to that of unmodified CS-NPs (25%), suggesting that insulin loaded in thiolated CS-NPs are better absorbed compared to that in pristine CS-NPs [193]. Ionotropic gelation allows for reasonable loading efficiency and loading capacity of a hydrophilic drug in aqueous media under mild condition. However, CS-NPs formed by ionotropic gelation suffer from a lack of mechanical stability especially under high or low pH or high ionic strength. Efforts were made to stabilize the CS-NPs via introducing additional multi-valent ions and oppositely charged polymer [43].

3.3. Re-dispersion of nanoparticles in other media

Drug nanocarriers, compared to their macroscopic counterparts, improve the drug bioavailability thanks to their enhanced transmucosal transport, cellular targeting, and cellular uptake [38]. In the last decades, various hydrophilic therapeutic agents including nucleotides, proteins, and peptides have been encapsulated into nanocarriers [33, 38, 46, 67, 146, 190, 199]. Required by their biological application, drug nanocarriers prepared in inverse emulsions must be transferred to and stabilized in aqueous media, which is a non-trivial task because nanoparticles tend to aggregate during the transfer process. Polymeric nanocarriers are typically transferred to water by a solvent evaporation method with the help of hydrophilic surfactants [48-50]. Recently, such method was further evolved into a universal two-step method: Hydrophobization followed by an amphiphilic coating [51], which has shown successful recovery of both inorganic NPs [52-56] and polymeric counterparts [57, 58].

Nevertheless, for hydrophilic excipients, the additional stabilizing amphiphiles are unnecessary, or even harmful due to their cytotoxicity [60] or undesirable interference with proteins [54]. Besides, the hydrophobic surfactant on the surface of nanocarriers alters the permeability of the shell, and the actual surface of the nanocarriers is formed from the coated surfactant instead of shell materials, which further complicate the study of particle-cell interaction. Attempts to remove the hydrophobic surfactants by precipitation and redispersion often affront a compromise between the undesirable aggregation and limited recovery rate [63-65], as the strong centrifugal force required for the precipitation of small NPs also leads to their irreversible aggregation, whereas an insufficient precipitation causes the loss of small NPs during the repeated washing processes. To overcome these problems, a new strategy for the redispersion of polymeric hydrophilic nanocarriers from inverse emulsion into aqueous media is needed. The recovery process should be fast, mild, and cost-efficient. The resulting

self-stabilizing nanocarriers should ideally preserve their pristine surface and the final dispersion should have minimal aggregation and qualitative rate of recovery.

Early studies concerning the transfer of NPs prepared in micellar nanotemplates in non-polar media were focused on inorganic NPs, as reviewed by Krumpfer et al. [47]. The review discusses mainly the redispersion of NPs into hydrophobic media, but it still provides insightful strategies for the general process of NP recovery. The authors summarized four strategies for the redispersion of NPs: surface modification by graft-from reactions, graft-to reactions, chemisorption of crosslinkable surface functionalities, and physisorption of amphiphiles. The common idea behind these methods is to insert an intermediate layer between the nanomaterial and the embedding matrix or the dispersing media.

The general concept to stabilize NPs in a media is illustrated in **Figure 2**. For a pair of materials of distinct hydrophobicity, a surfactant is routinely used to compatibilize the mismatched polarity. For example, a hydrophobic NP can be stabilized with a hydrophilic surfactant. Due to the weak interaction of physisorbed surfactant, a chemisorbed ligand or covalently grafted layer is favored, especially under a high-shear condition in a polymer matrix. As illustrated in **Figure 2**, via route B, the stabilizing layer fills the gap between the material pair, even when the difference in polarity between the material pair is insignificant. For example, to stabilize CdS NPs in water, a chemisorbed ligand is used.

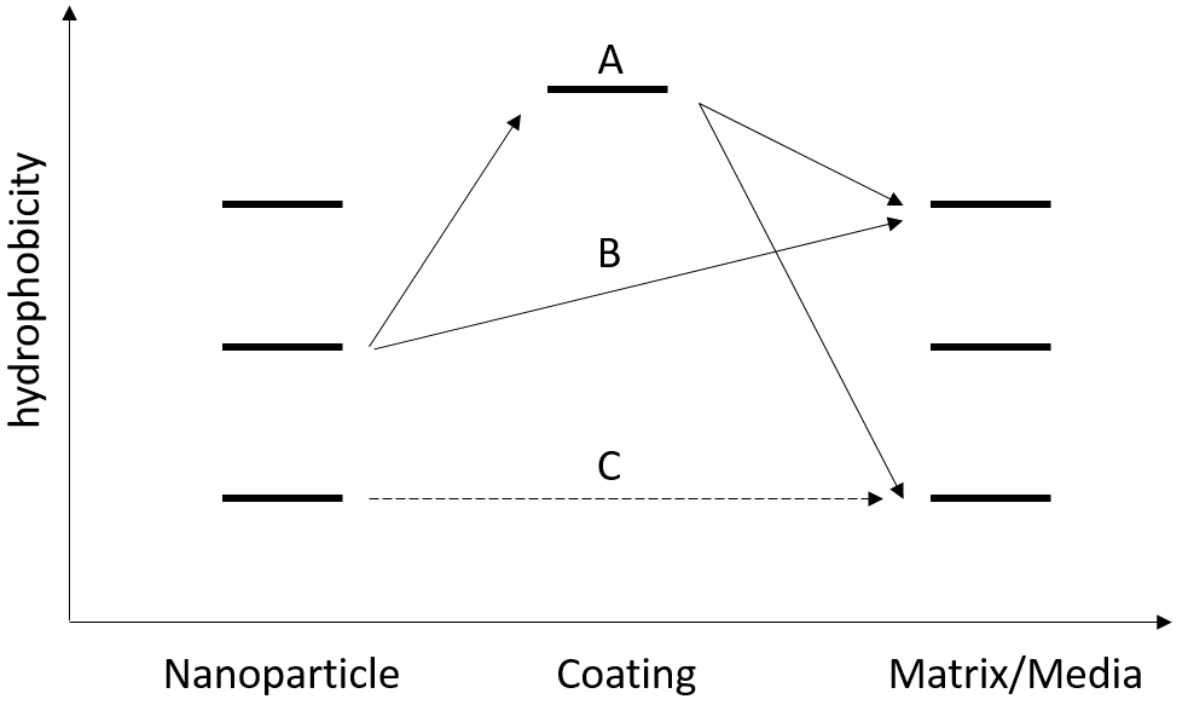

Figure 2. Modification of NPs to compatibilize the materials with mismatched polarity.

Alternatively, with route A, initially hydrophobized inorganic NPs can be coated with an additional layer that is compatible with the final media or matrix. As a result, regardless of the nature of the material pair, the polarity mismatch between the pristine surface of NPs and the final matrix is compatibilized by the engineered intermediate layer. Such a layer is frequently an amphiphilic copolymer, which has shown the ability to promote a homogeneous dispersion of the inorganic NP into a matrix or a solvent. This method is called one-phasic solvent mixture method [47]. Experimentally, a large amount of solvent of intermediate polarity (*e.g.* ethanol, acetone) is added to a two-phase system, in which the NPs are originally in the aqueous phase, and a single phase is formed. When additional water is added, a biphasic system form again and then the NPs partition into the oil phase. In application, such method has been used purposely to hydrophobize the hydrophilic NPs so that they can be homogeneously embedded into the non-polar polymeric matrix.

Inorganic NPs hydrophobized by the one-phasic solvent mixture method can be directly mixed with a hydrophobic polymer [201] or can be stabilized with an amphiphilic copolymer in water [52, 53]. The same strategy is also frequently used for a material pair that has the same polarity, especially in the redispersion of hydrophilic gold NPs synthesized in inverse emulsion into the water for biological applications [54-56]. Besides, these copolymers have been applied to polymeric NPs like poly(lactic acid)-based NPs prepared in either inverse emulsion [57] or nonaqueous emulsion (an acetonitrile-in-cyclohexane emulsion) [58] and was purified by repeated precipitation-redispersion circles and redispersed with the help of a hydrophilic surfactant.

One would expect that NPs based on water-soluble polymers should be automatically dispersed in water, which follows Route C in **Figure 2**. Counterintuitively, an additional surfactant is often required to redisperse such NPs when they are prepared via inverse emulsions. For example, toluene diisocyanate (TDI) crosslinked gelatin NPs [63] prepared in water in the p-xylene emulsion were finally stabilized in water by a poly[(butylene-*co*-ethylene)-*block*-(ethylene oxide)] surfactant. The removal of the surfactant is achieved by washing with a large amount of acetone followed by drying. In another example, a dimethylformamide-in-isooctane emulsion was stabilized by a poly[(butylene-*co*-ethylene)-*block*-(ethylene oxide)]surfactant, the recovery of NPs was achieved by solvent evaporation, and the NPs were stabilized in a sodium dodecyl sulfate (SDS) solution [48]. Similarly, NPs based on the polylactide-*block*-polypeptide-*block*-polylactide copolymer requires a hydrophilic surfactant for redispersion [49]. TDI crosslinked protein nanocapsules prepared in inverse emulsion require SDS for stabilization, after evaporation of the organic solvent [50]. The solvent evaporation method is widely used. Briefly, a hydrophobic organic phase containing the prepared NPs is directly emulsified in a solution of hydrophilic surfactants. After evaporation of the organic solvent, the NPs can be dispersed in aqueous media. The

residual hydrophobic surfactant can be trapped together with the hydrophilic NPs, and consequently, hydrophobize the NPs. Therefore, NPs recovered by solvent evaporation method actually follows the route A in **Figure 2**, *i.e.* the NPs are hydrophobized by the hydrophobic surfactant in the droplet of organic solvent and then stabilized by the hydrophilic surfactant.

The solvent evaporation method requires a lengthy procedure under heating and an inevitable aggregation of NPs. The number of aggregated NPs is determined by the sizes of droplets after the re-emulsification process and the stability of the resulting emulsion during solvent evaporation. To address these problems, efforts have been made to improve the re-emulsification or the evaporation process. For example, after the reaction mixture was centrifuged to remove the majority of the hydrophobic surfactant, the centrifuge cake containing the NPs was redispersed in cyclohexane by ultrasonication. The cyclohexane phase was further emulsified in Lutensol solution, and the resulting emulsion was subjected to lyophilization. The dried NPs can be redispersed in water [202]. The modified solvent evaporation method avoids the heating, which is favorable for fragile molecules but is still time-consuming and energy inefficient.

Another approach is to use a responsible surfactant that changes hydrophilicity upon request. For example, a UV-responsive copolymer has been developed as a switchable emulsifier for non-aqueous emulsions [59]. The emulsifier coated NPs can be redispersed in water upon the UV induced cleavage of hydrophobic group 1-pyrene which is followed by solvent evaporation. However, this method still suffers from the lengthy process of dialysis, and the large dosage of UV radiation (4 W, 3 h), thus making it unfavorable for fragile molecules like protein drugs.

Ideally, hydrophilic NPs prepared in the aqueous phase of inverse emulsions are directly dispersed in water, *i.e.* via route C in **Figure 2**. In the field of microemulsions, phase

inversion methods can serve this purpose by raising the temperature. For example, calcium alginate NPs prepared in inverse microemulsion were redispersed in water without additional surfactant [61, 62]. However, the final dispersion still contained a large amount of the initial surfactant and the recovery rate of NPs is limited.

Inspired by the cryoprotectants in the freeze-drying process [66], our approach involves the insertion of a temporary water-soluble molecular “cushion” into the nanodroplets of inverse emulsions before the removal of the surfactants. Therefore, the irreversible aggregation of nanocarriers during the washing process is minimized thanks to the molecular “cushion”. Meanwhile, these small molecules can be easily dissolved upon the redispersion of nanocarriers in water. We monitored the location of nanocarriers during the washing process, characterize the colloidal properties of the final dispersion, study the residue of surfactant, and tested the concept with various other molecules.

4. Results and discussion

4.1. Polyelectrolyte complexation in miniemulsion droplets

4.1.1. Introduction

Colloidal polyplex NPs are known to form upon mixing of two oppositely charged polymers in dilute solution, which is driven by the gain in entropy via the liberation of counterions [45]. PGA and GC were selected as two biodegradable polymers from renewable feedstocks to form the polyplex NPs [144]. We first investigated the formation of the complex from solutions of GC, polypeptide YY (PYY), and PGA. In a first step, the PYY solution was added to a PGA solution. The positively charged PYY (isoelectric point pI = 7.6) acts as polycation at pH 6.0 and is therefore complexed by the excess amount of negatively charged PGA (pK_a = 4.5). In the second step, the PGA-PYY mixture is complexed with an excess amount of GC (pK_b = 6.5). The complexation between the PYY-PGA pair and the PGA-GC pair is obvious at high concentrations (PYY: 1 mg/mL, PGA, and GC: 10 mg/mL, pH = 6.0). Instant precipitation was observed upon mixing of these polymers. Due to concentration restrictions reported in the literature [43], the polymer concentrations were lowered 10 times to allow for the formation of NPs. Section 4.1 to 4.3 are based on our publication (He, W., Parowatkin, M., Mailander, V., Flechtner-Mors, M., Graf, R., Best, A., Koynov, K., Mohr, K., Ziener, U., Landfester, K. and Crespy, D., Nanocarrier for Oral Peptide Delivery Produced by Polyelectrolyte Complexation in Nanoconfinement, Biomacromolecules, 2015 [33]).

4.1.2. Polyelectrolyte complexation in aqueous media

To study the interaction between the peptide and the two polymers at low concentration, the diffusion coefficient of a fluorescein isothiocyanate (FITC) labeled rat-PYY (rPYY-FITC) was measured by fluorescence correlation spectroscopy (FCS) before and after mixing with GC or PGA (**Figure 3**). When a short fluorescent peptide (M_w ~ 4 kDa) binds to the

oppositely charged polymer (M_w = 100 to 200 kDa) via Columbic attraction, the diffusion coefficient of the peptide should decrease, and its apparent hydrodynamic radius should correspond to that of the peptide-polymer complex. Unexpectedly, we found that the apparent hydrodynamic radius of rPYY-FITC remained constant at 1.1 nm when mixed with PGA but increased significantly to 8.3 nm when mixed with GC (**Figure 3**). These results suggest that rPYY-FITC interact strongly with GC at pH 6.0 instead of PGA. We attribute such behavior to the pI shift of the peptide due to fluorescence labeling. When a FITC molecule reacts with rPYY, it consumes an amine group while introducing a carboxylic acid group (pK_a of FITC = 4.3) [203]. As a result, the pI of rPYY shifts from 7.6 (non-labeled rPYY) to 5.5 (single labeled rPYY-FITC1) or 4.9 (double labeled rPYY-FITC2) (**Figure 4**). Therefore, at pH 6.0, the rPYY-FITC is negatively charged, and thus interacts with the cationic GC, rather than the anionic PGA. We can speculate that non-labeled rPYY is still positively charged at pH 6.0 and interacts with PGA rather than GC. Therefore, the nanocarriers prepared with the PEC method lack effective encapsulation and the entrapment of peptide also depends on pI. Furthermore, only experimental conditions with very low polymer concentration (< 1 mg/mL) and the high excess ratio of the two polyelectrolytes are allowed to ensure NP formation and the resulting particles are not stable against dilution, especially in the presence of salts [204].

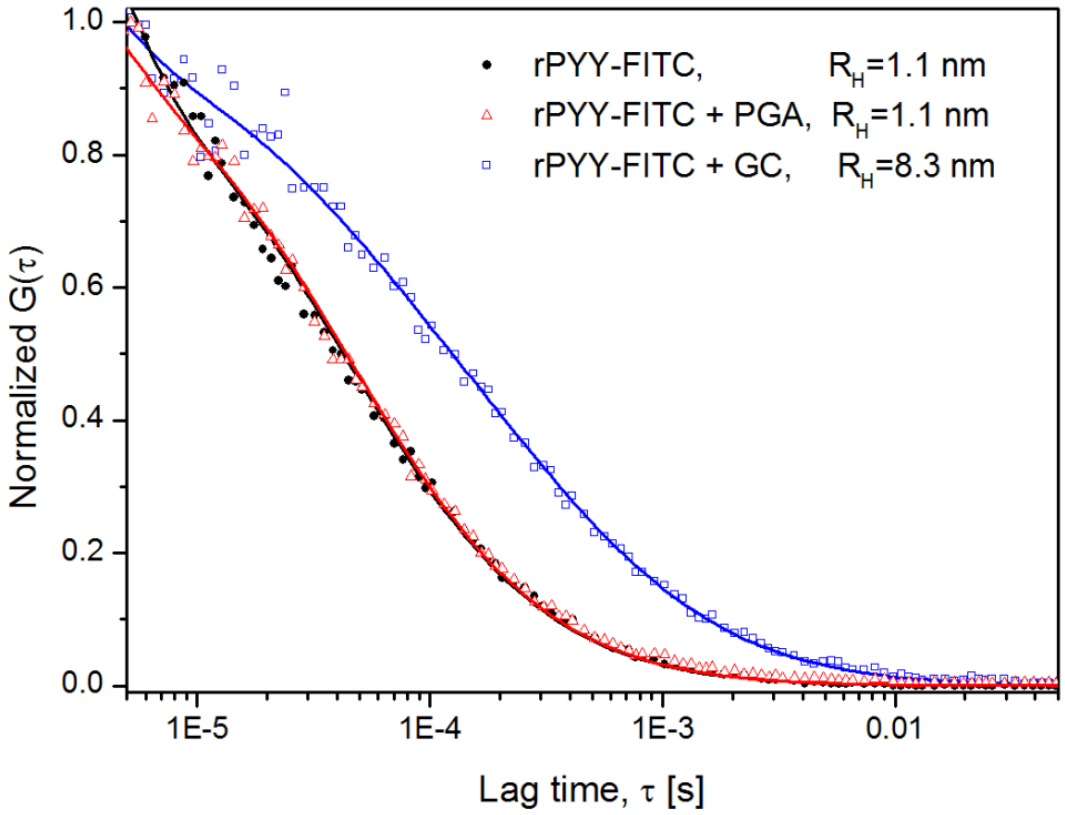

Figure 3. Normalized FCS autocorrelation curves for rPYY-FITC. Measured before (circles) and after mixing rPYY-FITC with PGA (triangles) or GC (squares). The solid lines represent the corresponding fits with a simple diffusion model.

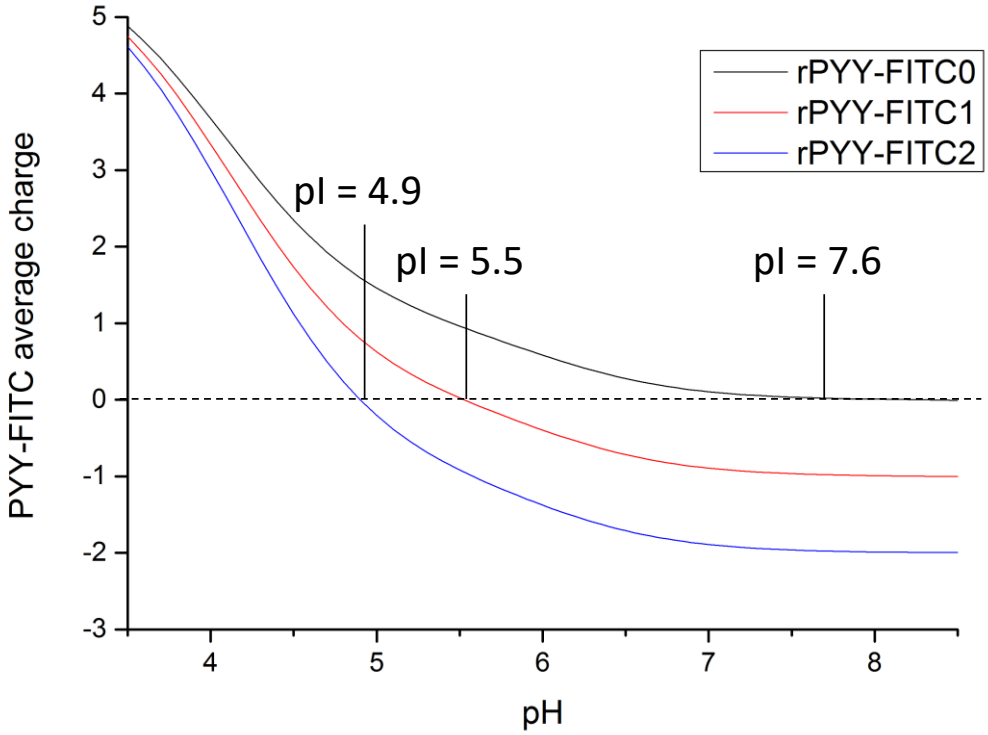

Figure 4. Calculated average charge ~ pH curve of rPYY-FITC. The average charge is based on a calculation of ionization degree of all side groups. rPYY-FITCn, *n* is the number of FITC conjugated to rPYY. The corresponding pI of the rPYY-FITCn is 7.6, 5.5, and 4.9 for *n* = 0, 1, and 2, respectively.

Therefore, we designed new nanocarriers with high encapsulation efficiency that can be prepared at higher concentrations and that are robust against dilution. The concept is shown in **Figure 5**. In the first step, the polyelectrolyte is not anymore present in bulk solution but confined in miniemulsion droplets. The PYY solution was first mixed with PGA solution, and the aqueous solutions of GC and PGA were separately emulsified to form two inverse miniemulsions and complexation occurred upon coalescence of the droplets induced by ultrasound. The coalescence between droplets was forced by the application of ultrasound because miniemulsions are stable against coalescence [205].

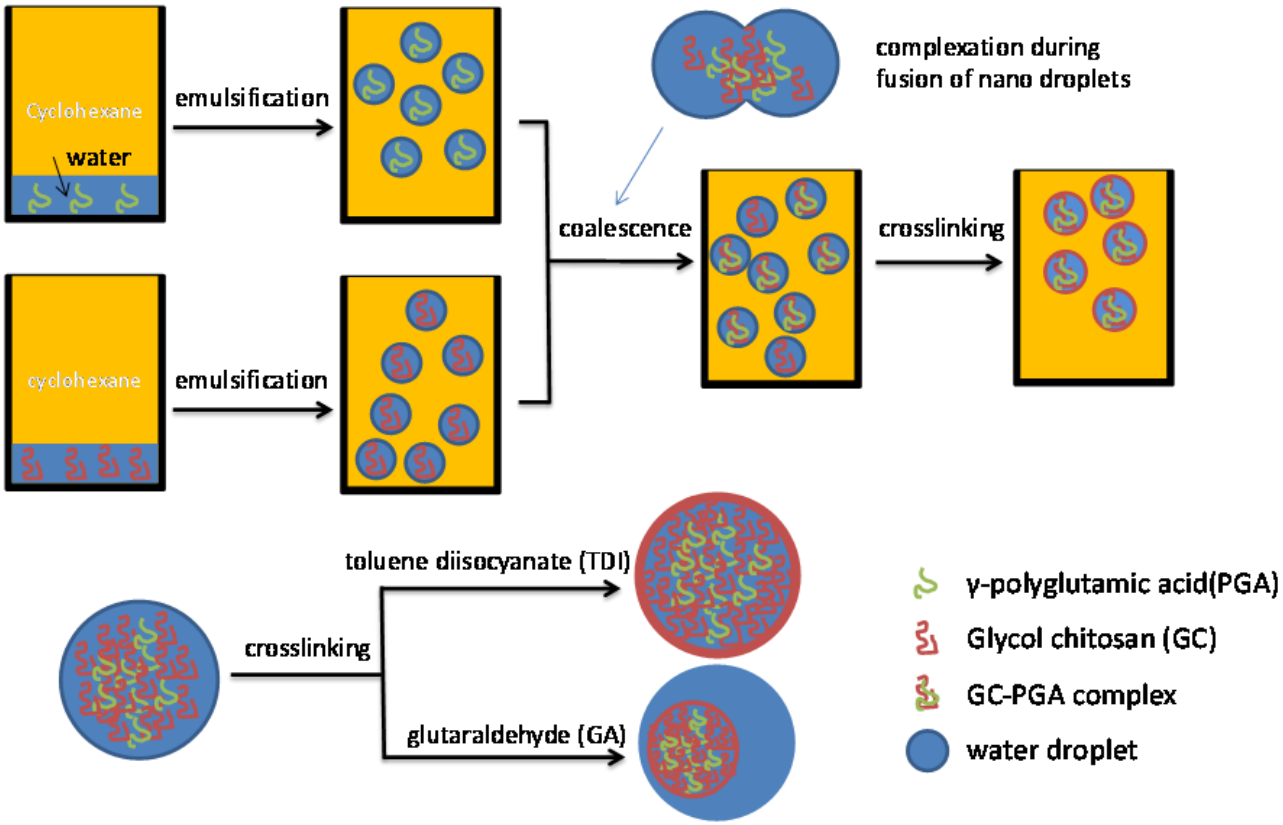

Figure 5. Procedure for the formation of the nanoparticles by polyelectrolyte complexation confined in miniemulsion droplets followed by interfacial crosslinking.

In this section, we introduced an improved strategy for the synthesis of pH-responsive nanocarriers based on polyelectrolyte complexes of GC and PGA. The main drawbacks of the widely used complexation method were successfully overcome by confining the complexation in nanodroplets. To mechanically reinforce the formed GC-PGA polyplex, they were crosslinked at the interface of nanodroplets, which is described in the next section.

4.2. Surface-crosslinked polyelectrolyte complexes

In the second step, a defined amount of TDI or glutaraldehyde (GA) was introduced to crosslink the NPs. The NPs crosslinked with TDI yielded core-shell structures (**Figure 6**a-c) with an average hydrodynamic diameter of 209 ± 110 nm whereas monolithic NPs with an average hydrodynamic diameter of 113 ± 46 nm were obtained with GA as crosslinker (**Figure 6**d). The difference in morphology suggests that the crosslinking with TDI takes place at the interface of the droplet. This can be attributed to the higher hydrophobicity of TDI compared to GA, preventing it to diffuse inside the aqueous droplets. GA is hydrophilic and therefore will immediately partition into the aqueous phase. The crosslinking reaction with TDI is therefore limited to the interface of the droplets and the covalent immobilization of the peptide in the NPs can be avoided. Furthermore, it is difficult to assess the amount of crosslinking with GA because of side reactions such as self-polymerization and acetal formation with hydroxyl groups that can occur [206].

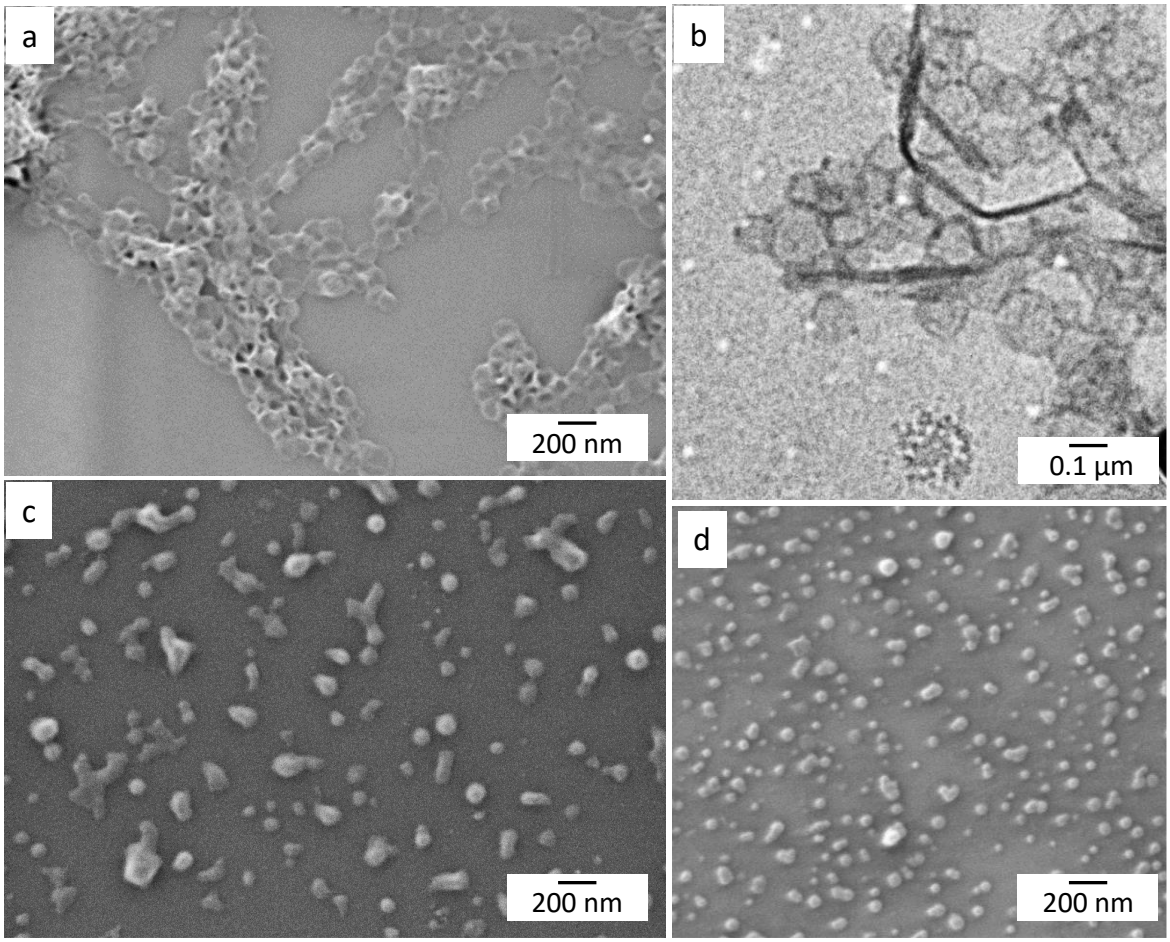

Figure 6. Morphology of GC based nanocarriers. Scanning electron microscopy (SEM) (a) and transmission electron microscopy (TEM) (b) micrographs of the GC NPs crosslinked by TDI (initial isocyanate group to amine group ratio = 100%). (c) SEM micrograph of the TDI crosslinked GC-PGA NPs prepared in miniemulsion (initial isocyanate group to amine group ratio = 2%). (d) SEM micrograph of glutaraldehyde crosslinked CS NPs (aldehyde group to amine group ratio = 100%).

GA crosslinked CS NPs (aldehyde group to amine group ratio = 26%) were analyzed with solid-state ^{13}C-NMR spectroscopy. After the aldehyde-amine reaction, a potential peak of the resulting Schiff-base (-C=N-CH-) is expected to be at 173 ppm, which overlapped with the C=O signal from acetyl units in CS. The C=C double bond formed during GA self-polymerization could also be used to estimate the degree of crosslinking. Unfortunately, the resulting signal did not yield a sufficient signal-to-noise ratio for quantification (**Figure 7**). For these reasons and because TDI is suitable for interfacial polyaddition in inverse miniemulsions [207], we selected TDI as a crosslinker for further investigations. The PYY-

PGA-GC polyplex was prepared in a non-stoichiometric ratio so that an excess of CS is present in the NPs delivering amine groups for the crosslinking reaction. The crosslinked nanocarriers were dispersed in buffer solutions of different pH values (4.5, 6.0, and 7.4) and their zeta potential values were monitored (**Table 2**). The nanocarriers showed a positive potential at pH 4.5 and a weakly negative potential at pH 7.4, indicating that the surface of nanocarriers contains mainly cationic species and partly anionic species. Although hydrolyzed TDI could also contribute to the positive potential, we can still conclude that the surface of crosslinked polyplexes is mainly formed of GC. The nanocarriers are therefore composed of a PYY enriched core and a GC shell crosslinked with TDI.

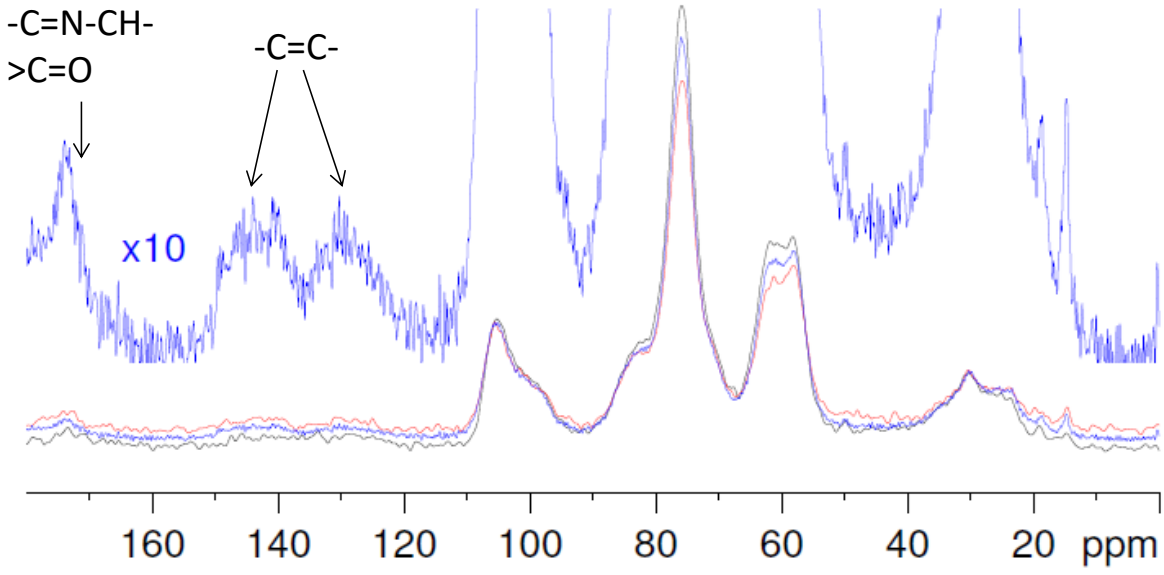

Figure 7. Solid-state ^{13}C-NMR spectrum of glutaraldehyde cross-linked CS NPs (initial aldehyde group to amine group ratio = 26%). Overlay of 3 replicate spectra and blue curve: 10-time magnification of one spectrum. 124 ppm and 133 ppm are assigned as C=C double bond, 173 ppm is assigned as ketone bonds or Schiff-base.

Table 2. Zeta potential and average hydrodynamic diameters of the nanoparticles during the release experiments

Release medium	measured pH	%PYY release	zeta potential (mV)	D_h (nm)
pH 4.5 buffer	4.5	2.4%	+21.0 (5)	333 ± 166
pH 6.0 buffer	6.4	1.8%	0 (flocculate)	> 1000
pH 7.4 buffer	7.5	8.7%	-8.4 (4)	531 ± 302
distilled water	7.3	-	-8.3 (4)	435 ± 217

The NPs were dispersed in various buffer (0.1 M) or water. The %PYY release was calculated as the released rPYY-FITC after 2 h.

4.2.1. Estimation of the degree of crosslinking

Because the degree of crosslinking of the nanocarrier can affect the surface properties and the subsequent release of the payload, the kinetics of TDI crosslinking reaction was investigated. The amount of TDI at different times of reaction was estimated by ^{1}H-NMR spectroscopy. The free TDI was first quenched with an excess amount of dibutylamine at a predetermined time and the resulting product was separated from the NPs and quantified by ^{1}H-NMR spectroscopy. The consumption of TDI during 6 h of reaction with different initial TDI (100% or 25% compared to amine groups in GC) amounts is shown in **Figure 8**. Both curves display a ~ 40% initial reduction of TDI during the first minute of the reaction, which indicate that the interfacial crosslinking reaction took place instantly after the injection of TDI and that a polyurea membrane formed at the interface of the droplets. The crosslinker then penetrated the primary membrane with a reduced rate as the membrane permeability decreased due to the reaction. As expected, TDI consumption was faster at a higher initial concentration of TDI. According to this TDI consumption curve, 70% of TDI was consumed in 20 min when polyplex was crosslinked with 25% TDI. If we assume that all the TDI was consumed by GC, then the corresponding crosslinking density is 17.5%. Therefore, we selected 25% TDI to crosslink the polyplex and stopped the reaction by dilution with toluene after 20 min of reaction without quenching.

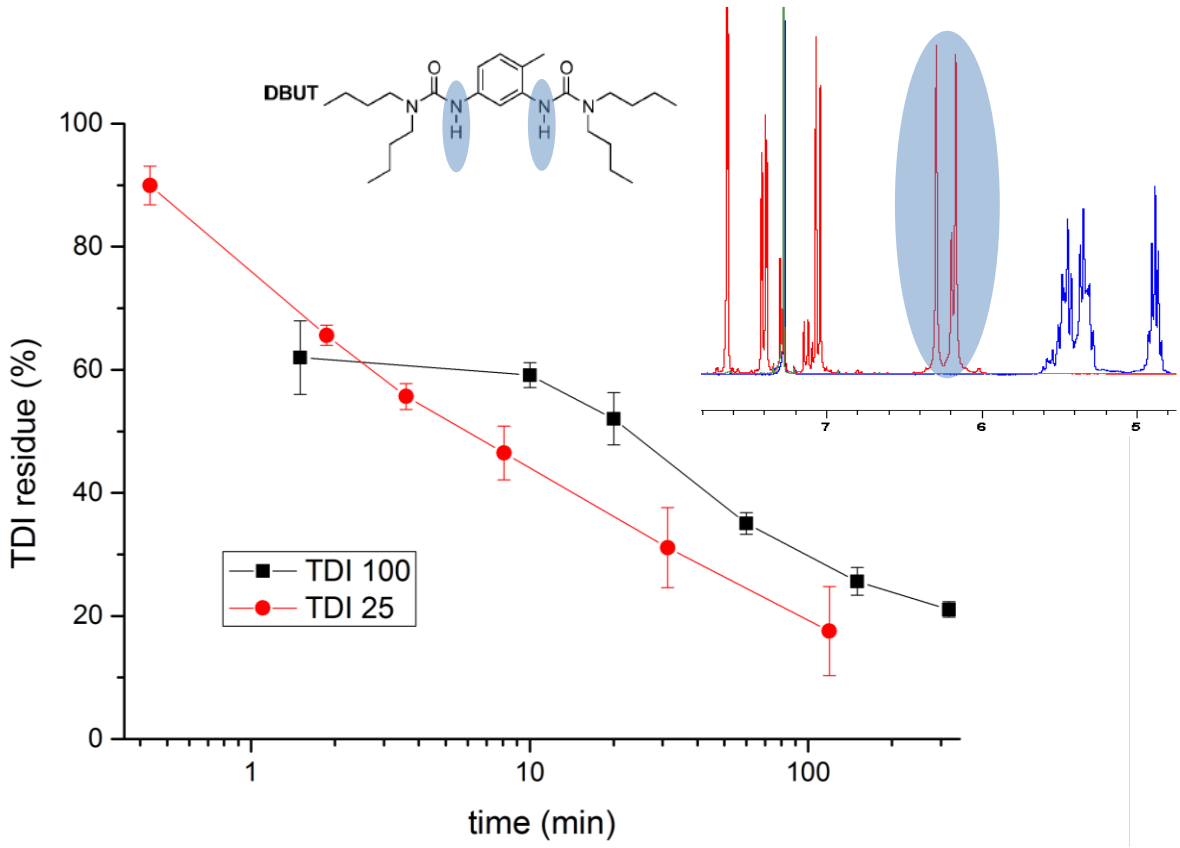

Figure 8. Temporal evolution of the TDI consumption during the interfacial crosslinking reaction. The TDI residue is expressed as the ratio of detected TDI to the initial TDI used for crosslinking. The molar ratios of initial isocyanate groups in TDI to amine groups in GC equals 100% (square) and 25% (dot).

For the preparation of peptide encapsulated particles, rPYY-FITC was encapsulated and the release of peptide and the properties of the NPs (**Table 2**) were monitored at different pH values (4.5, 6.0, and 7.4) over 12 days. The relative release of the peptide was expressed as the ratio of the detected peptide in solution to the total amount of encapsulated peptide. Two main factors can influence the pH-responsive release of peptides: The responsive swelling of the polyplex matrix, and the ionic retention effect of the polyplex matrix on the peptide. The release profile during the first 3 days is shown in **Figure 9**. In general, more peptides were released at pH values of 4 and 7, which agrees with the typical behavior of PEC. Indeed, the polyplex matrix swells at higher and lower pH values and shrinks when the overall charge of polyplex approaches zero (**Figure 10**).

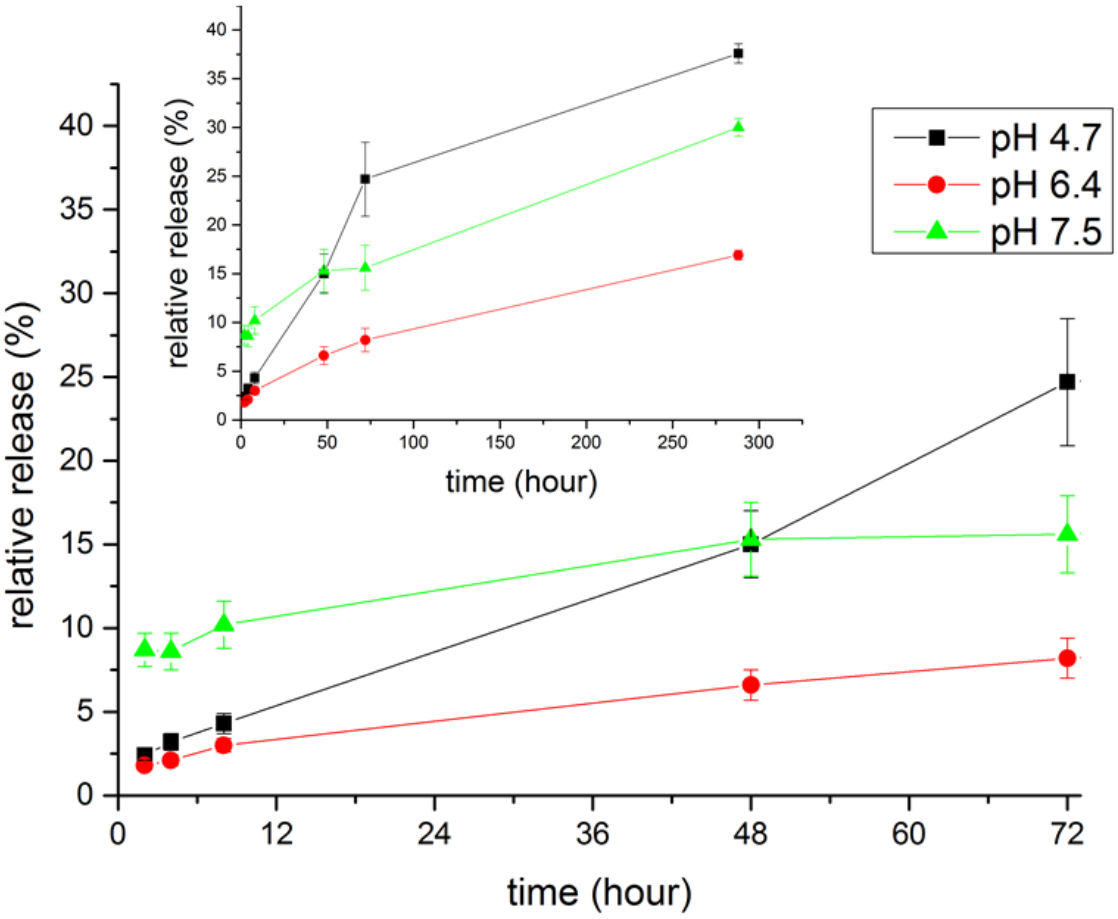

Figure 9. The release profile of the peptides from the NPs GC-PGA-TDI_25% at various pH values. Inlet: the release of rPYY-FITC over 12 days. Relative release: Percentage of released PYY compared to total PYY.

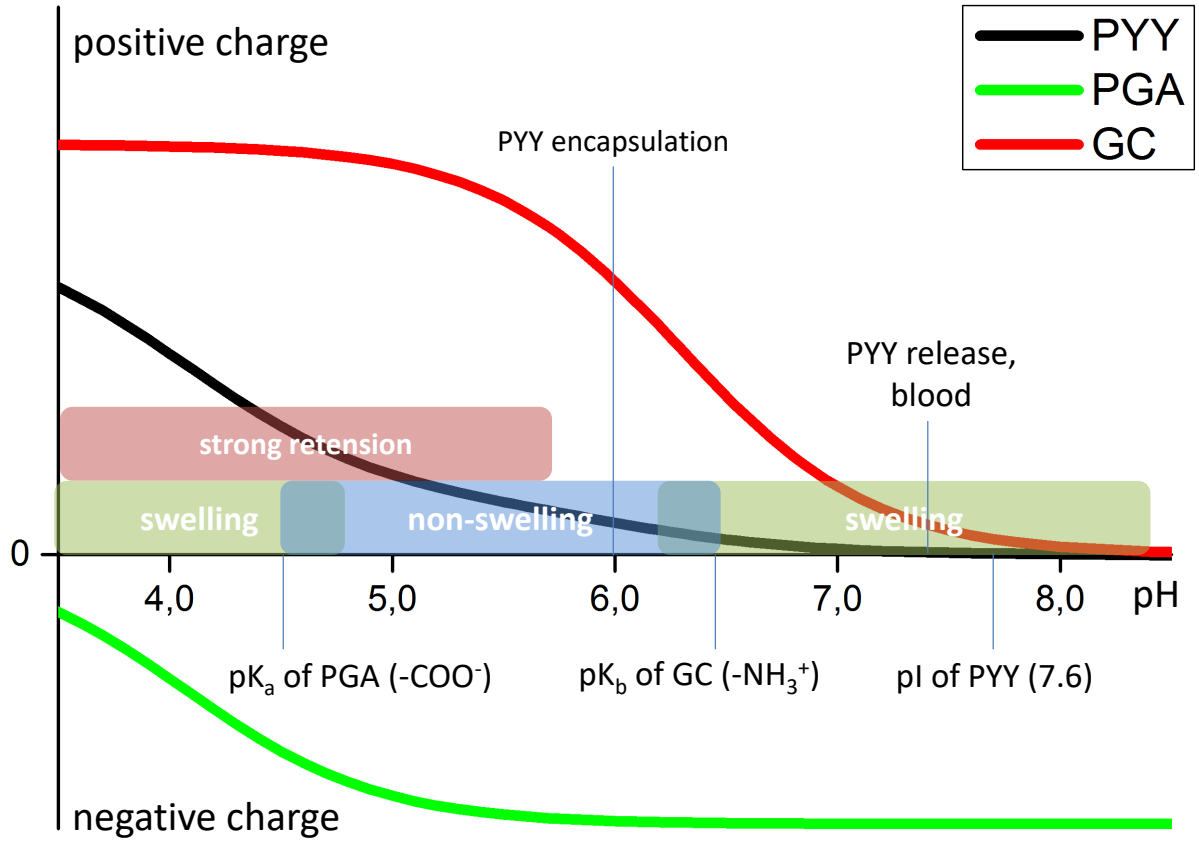

Figure 10. Swelling behavior of GC-PGA PEC. Calculated average charge ~ pH curves are based on the degree of ionization. The red curve shows a positive charge of the protonated amine group in GC, the green curve indicates the negative charge of deprotonated carboxylic acid group in PGA, the black curve indicates the overall charge of PYY. The polyplex matrix swells at both low and high pH and the PYY-PGA interaction is stronger at lower pH value.

In our GC-PGA matrix, the theoretical net charge of polyplex is zero at pH 6.0, which confirms the measured release profile. The peptide release rate at pH values of 6 and 7 was similar, while the release was faster at a pH value of 4. Besides, burst release took place at pH 7, which did not happen at pH 4 or pH 6. We attribute these two features to the ionic retention effect of polyplex matrix and aggregation of NPs. At pH 4.7, the polyplex matrix was supposed to be swollen by the cationic GC network (**Table 2**) when part of PGA was deionized. However, only small amounts of the peptides were released, which can be explained by the strong retention effect between the anionic PGA and the cationic PYY. The cationic surface of the NPs (zeta potential ~ +20 mV) stabilized the NPs and thus the release

kinetics was not affected by aggregation. At pH 6.4, the polyplex matrix was shrunk, and the surface charge approached zero. Thus, the NPs flocculated, and the release rate was low over 3 days, like that at pH 7.5. At pH 7.5, most of the amine groups were deprotonated and the polyplex is expected to be swollen by the anionic PGA network. Meanwhile, the peptide approaches its isoelectric point and therefore the overall ionic interaction was the weakest. As a result, the diffusion of the peptide was maximized, and 8.7% of the peptide was released during the first 2 h. However, the surface charge of NPs at pH 7.5 (zeta potential -8 mV) was too weak to prevent gradual aggregation of the colloids. As a result, the release rate decreased over time and finally approached the release rate at pH 6.4. The maximum release (38%) took place on the last day, pH 4.7 (**Figure 9** inset). The corresponding encapsulation efficiency was estimated to be 68% as the ratio of the total detected amount of PYY-FITC in the dispersion to the theoretical amount of rPYY-FITC in NP dispersion. This is an underestimation due to the self-quenching effect of rPYY-FITC [208]. The GA crosslinked CS nanocarrier also showed the pH-responsive release of rPYY-FITC (**Table 3**). In general, less peptide was released at room temperature over 5 h and the release at lower pH was suppressed when more crosslinker (100% GA) was used. These observations can be attributed to the consumption of amine groups by GA during the crosslinking reaction. It also suggests that the crosslinking reaction with GA led to more crosslinking of the NPs and/or immobilization of the peptide in the NPs in accordance to the morphology of the particles found in transmission electron microscopy (TEM) (**Figure 6**d).

Table 3. The relative release of the labeled peptide from the CS nanoparticles crosslinked with glutaraldehyde (GA)

Medium	**25% GA**	**100% GA**
pH 4.5 buffer	(2.8 ± 0.1)%	(0.8 ± 0.1)%
pH 6.0 buffer	(4.3 ± 0.1)%	(6.6 ± 0.1)%
pH 7.4 buffer	(8.2 ± 0.4)%	(8.1 ± 0.1)%

Initial aldehyde group to amine group ratio = 25% or 100%.

4.2.2. In-vitro release of a peptide drug

Finally, we verified that the released fluorescent species are intact peptides. Fluorescently labeled rPYY-FITC and hPYY were simultaneously encapsulated in NPs and the release of both was investigated by fluorescence measurements and with the human PYY (hPYY) enzyme-linked immunosorbent assay (ELISA), respectively. Because hPYY was not fluorescently labeled and the rPYY was not active for human PYY ELISA, there were no interferences and the measurements were independent. As shown in **Figure 11**, the amount of detected hPYY by an ELISA was close to the amount of rPYY-FITC quantified by fluorescence intensity. The hPYY detected was ~ 20% lower than that of rPYY-FITC. This reduction can be attributed to hydrolysis or denaturation of the peptide during the *in-vitro* release test or its average charge shift due to FITC conjugation. However, both problems will not affect the *in-vivo* release test or final application.

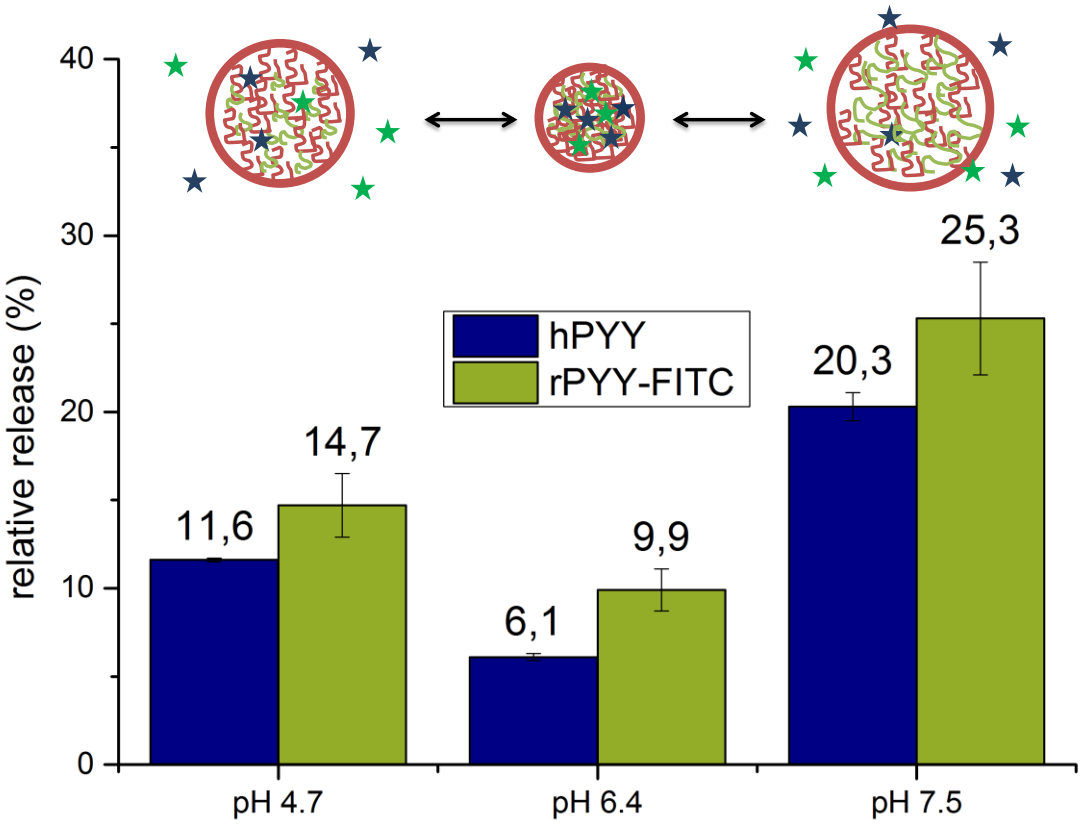

Figure 11. Comparison of released hPYY and rPYY-FITC. Both peptides were simultaneously encapsulated and released. Relative release: percentage of released PYY compared to total PYY. Inlet: stars represent hPYY (blue) and rPYY-FITC (green).

In this section, we studied the effect of surface crosslinking reaction on the polyelectrolyte complex, in terms of the relationship between the dosage of crosslinker and the final crosslinking density. The target drug peptide PYY was successfully encapsulated in these nanocarriers and was found to remain active after encapsulation. In the next section, we further adjusted the release profile of the encapsulated peptide drug by the degree of crosslinking, and the in-vitro pH-responsive release of PYY was studied in detail.

4.3. Control of the release kinetics by crosslinking

4.3.1. Degree of crosslinking and dosage of crosslinker

We further investigate the consumption of TDI at 10 min of reaction with the different amounts of TDI as a crosslinker. If we assume that all the TDI was consumed by GC, then we obtain a relation between the dosage of TDI and the corresponding crosslinking density at 10 min of reaction, as shown in **Figure 12**. The consumption of the crosslinker TDI at 10 min of reaction appears to scale linearly to the dosage of TDI added, which is expected because the amine groups were in excess compared to the isocyanate groups, therefore the reaction rate scales with the concentration of isocyanates. Such linear relation holds until 50% TDI and deviates at 100% TDI toward lower crosslinking density, which suggests that the concentration of isocyanates is no longer the main limiting factor for the reaction, but the reactive amines on the outer shell of polyplex NP. Hence, only a small amount of TDI is needed for the crosslinking reaction to reinforce the surface of polyplex NPs, especially

considering that the unreacted TDI could also cause unfavorable side reactions with the surfactants containing hydroxyl groups.

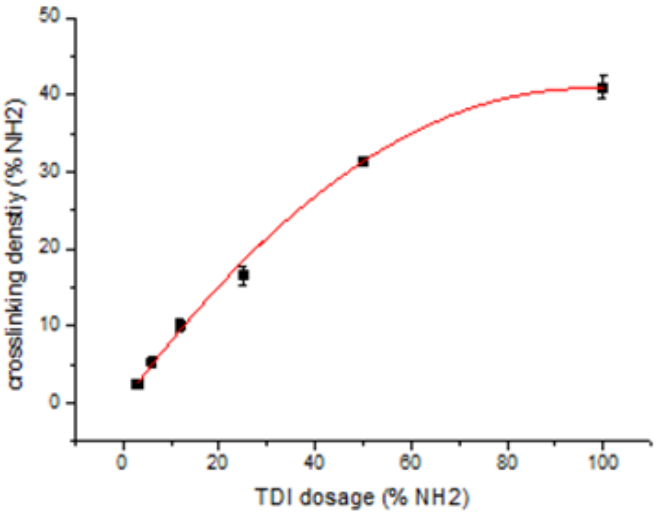

Figure 12. Estimation of crosslinking density at 10 min of crosslinking reaction with TDI. The curve is used to guide the eyes.

4.3.2. Influence of crosslinking density on the pH-responsiveness

To minimize the unfavored side reaction and to improve the recovery of NPs, we adopted the "cushion" method in the preparation of PEC-TDI NPs (The "cushion" method is described and discussed in detail in section 4.5). We studied the influence of crosslinking density on the pH-responsive release behaviors of these PEC-TDI NPs. The nanocarriers were crosslinked with a higher (25% TDI) or a lower (12% TDI) dosage of TDI. Both of the samples were reacted for 10 mins at room temperature. We confirmed that even at a lower dosage of crosslinker, the resulting NPs have a spherical shape (**Figure 13**), and the final dispersion of the GC-PGA-TDI NPs has minimum aggregates and does not require any surfactants for redispersion.

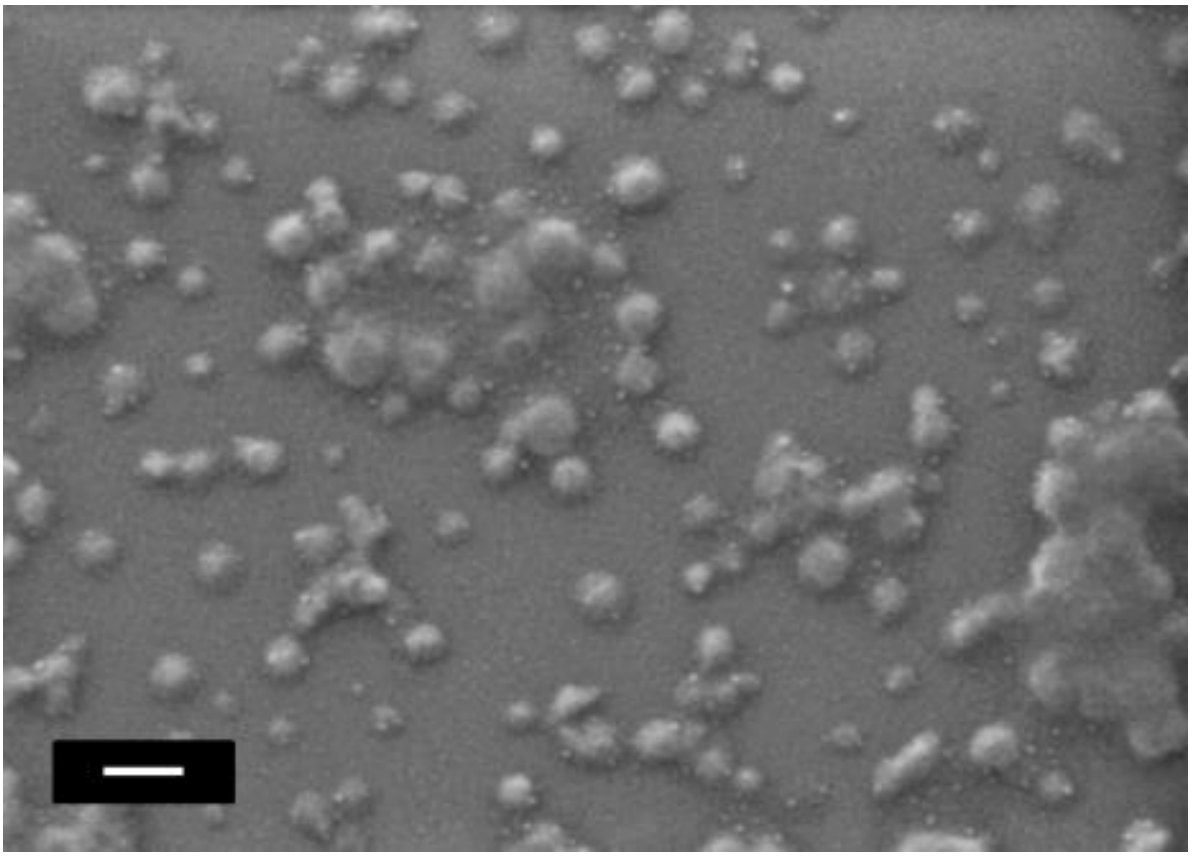

Figure 13. SEM micrograph of the crosslinked GC-PGA nanocarriers recovered with the "cushion" method (scale bar: 200 nm).

We studied the pH-responsive release behavior of the two samples of different crosslinking densities. For clarity, the release profiles are plotted in two ways. In **Figure 14**a-b, the pH responsiveness of the same sample is compared, while in **Figure 14**c-e, two samples of different crosslinking density are compared at different pH values. Generally, nanocarriers of higher crosslinking density tend to release the peptide at a higher rate, which is obvious in (c) and (d), when the pH value is lower. Besides, the release rate is higher at pH 4.5 compared to that at pH 6.0, which can be explained by the swelling behavior of polyplex NPs at lower pH values. However, at pH 7.4 in **Figure 14**e, the release of peptides is suppressed compared to that at pH 6.0 and pH 4.5. That is also observed in **Figure 14**a and **Figure 14**b, when one would normally expect an increased release of payload at higher and lower pH values from a polyplex nanocarrier. When we relate this phenomenon to the release profile in **Figure 9**, the

major difference between the two profiles lies in the “burst” release at pH 7.4. which leads us to speculate that surfactant could have influenced the release of the rPYY-FITC at pH 7.4, especially considering that the isoelectric point is of PYY is 7.6. The suppressed release of rPYY-FITC is probably due to the adsorption of the peptide on the surface of NPs or the container at pH 7.4, which is also observed during the FCS measurements (data not shown). On the other hand, when a surfactant is present in the release media, the majority of the surfaces are occupied by surfactants, and therefore the total amount of released peptide can be observed in the media. Therefore, we hypothesize that surface active molecules that are similar to surfactants can also facilitate the release of PYY at pH 7.4. In this sense, a cell growth media with various proteins is an ideal release media for our application.

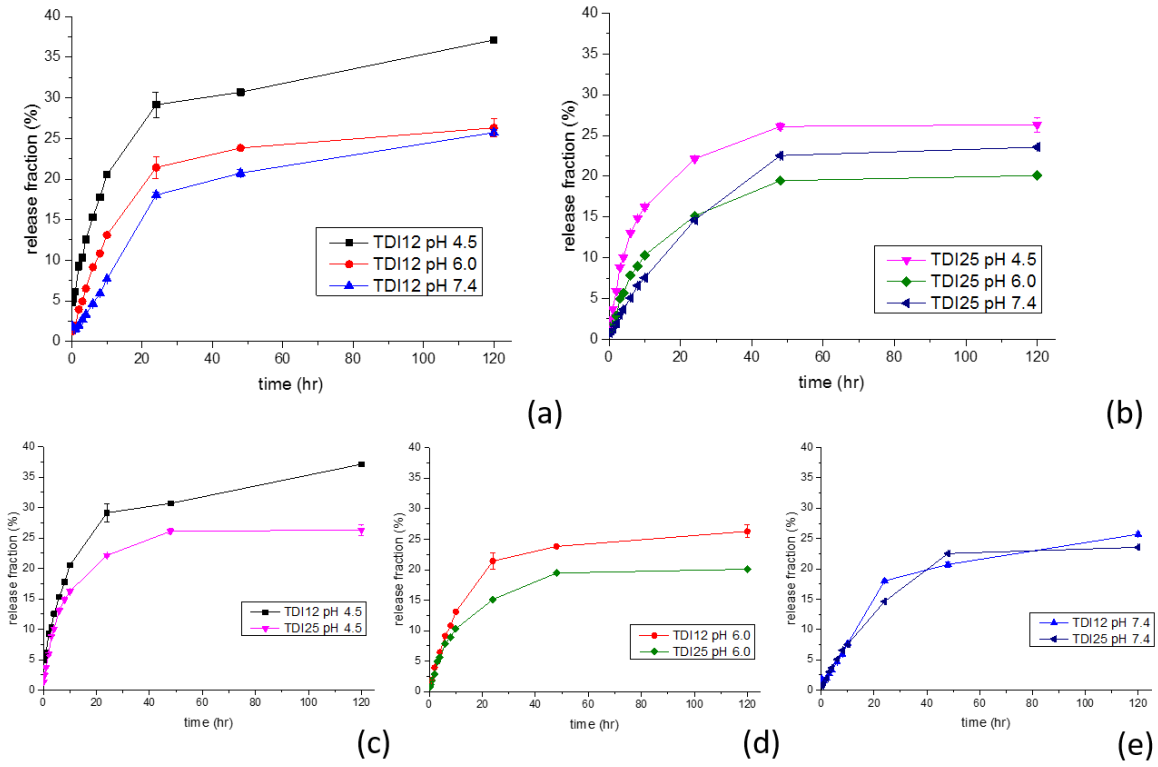

Figure 14. The release profile of rPYY-FITC from different crosslinked PEC-PGA nanocarriers. (a-b) comparison of the release profiles at pH values of 4.5, 6.0, and 7.4; (c-e) comparison of the release profiles with samples prepared with different dosage of crosslinkers: at 12%TDI, or 25%TDI.

We redispersed PEC-TDI nanocarriers into a standard cell growth medium Eagle's Minimum Essential Medium (EMEM) containing fetal calf serum (the pH of the medium is 7.4). As shown in **Figure 15**, a “burst” release at time zero that is similar to **Figure 9** is observed. Besides, an accelerated release rate in the first 24 h compared to that in **Figure 14**e is observed, which is typical for polyplex NPs. Thus, the unexpected suppression of the release of the rPYY-FITC at pH 7.4 can be attributed to the adsorption of the peptide on the surface of nanocarriers and the container.

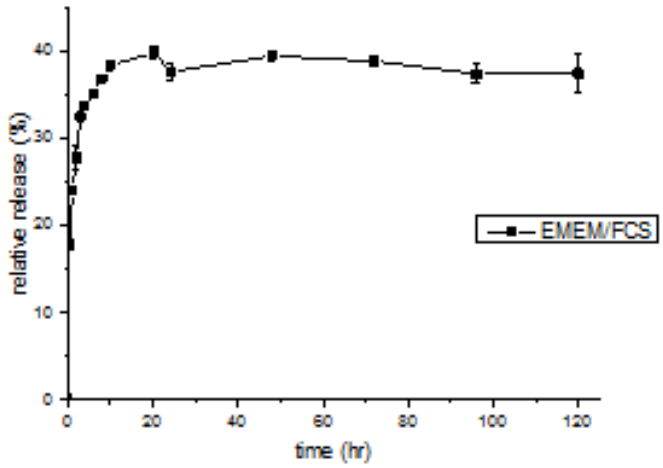

Figure 15. The release profile of rPYY-FITC from PEC-TDI12 in a cell growth media. Eagle's Minimum Essential Medium (EMEM) contains fetal calf serum, and *in vitro* release was conducted at 37 °C over 5 days (n = 3).

Hence, we can conclude that the release rate of PYY is not only determined by the properties of the drug carrier but also related to the pH value of the media. Besides, the surface-active moieties in the release media also play an important role in the release of peptide drugs.

So far, we have introduced a crosslinked polyplex that could be applied in the oral delivery of peptide drugs, because these GC coated carriers could protect the peptide from degradation or hydrolysis in the duodenum (pH = 6) and endothelial cells (pH = 4.5, cytosol, endosome), and then release the payload in the bloodstream (pH = 7.4). These nanocarriers should also be

protected in the stomach (pH = 2), and subsequently released individually in the duodenum (pH = 6). Therefore, we have designed a nanoparticle-in-nanofiber hierarchical structure, which is described in the next section.

4.4. Nanoparticles-in-nanofibers

To construct a peptide-drug delivery system that is suitable for oral administration route, we have further designed a nanoparticle-in-nanofiber hierarchical structure, so that the drug-containing nanocarriers and the target drug can be released step-wise upon a sequential change in pH values. The following section is based on our publication (He, C. W., Parowatkin, M., Mailander, V., Flechtner-Mors, M., Ziener, U., Landfester, K. and Crespy, D., Sequence-Controlled Delivery of Peptides from Hierarchically Structured Nanomaterials, Acs Applied Materials & Interfaces, 2017 [209]).

4.4.1. Fabrication of a multi-stage pH-responsive peptide delivery system

The multi-stage pH-responsive peptide delivery system is composed of two levels of hierarchy (**Figure 16**). The first level is represented by pH-responsive NPs. Crosslinked polyplex nanocarriers (NPs) were prepared according to the last chapter which is published in our paper [33]. The resulting nanocarriers had a z-average diameter of 229 ± 87 nm, which is in a reasonable range for the endocytosis of NPs by intestinal epidermal cells [210]. The zeta potential of the nanocarriers was +24.8 ± 3.8 mV. The positive surface charge enables colloidal stability in water and indicates that the surface is dominated by the presence of CS. Such property is suitable for oral drug delivery because the CS moiety allows better mucous adhesiveness. The morphology of crosslinked polyplex was further confirmed by SEM (**Figure 17**), showing that the crosslinked polyplex NPs are monolithic spherical particles. Most particles have a number-average size of 80 ± 34 nm as measured by SEM with the very low amount of aggregates (~ 380 nm, 0.7% by number), which is verified by dynamic light scattering (DLS) measurements (**Table 4**). The refractive index and the viscosity of the media use for the dynamic light scattering are corrected based on the concentration of EL55 (**Figure 18**).

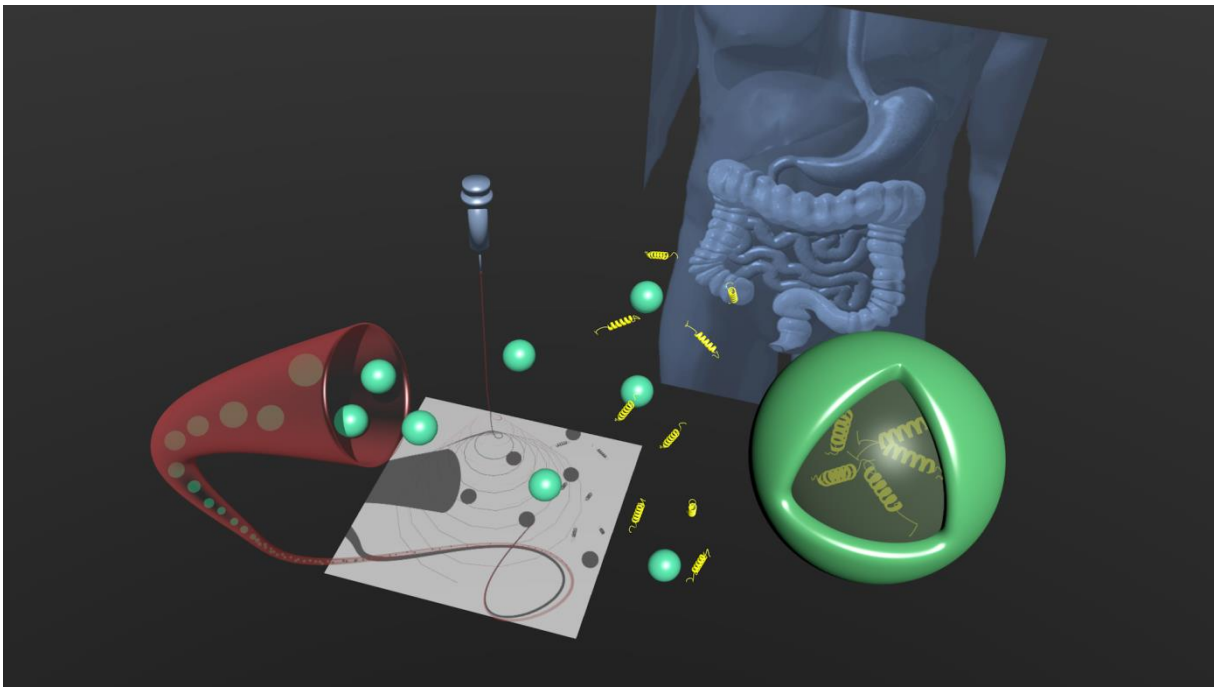

Figure 16. Structural hierarchy of multi-stage pH-responsive peptide delivery system.

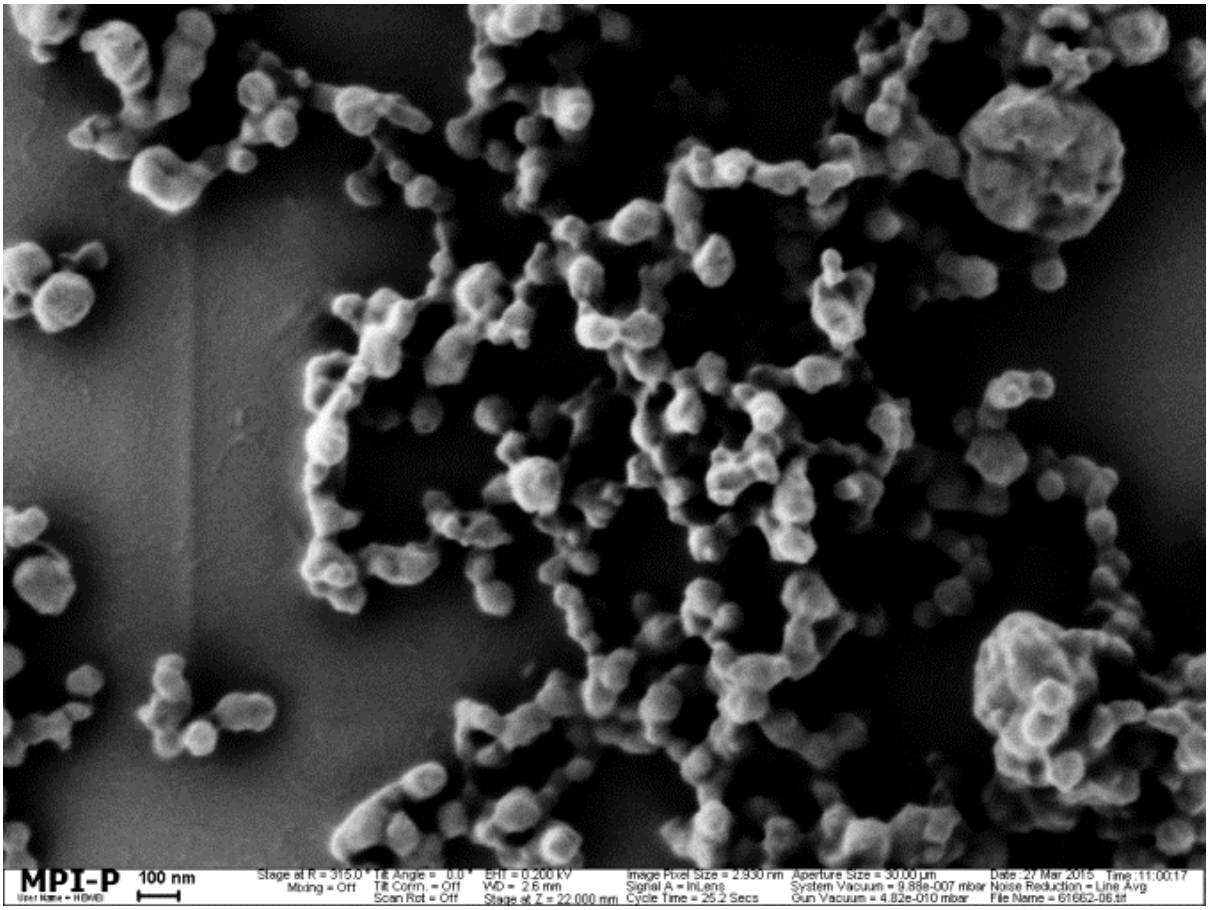

Figure 17. SEM micrograph of TDI crosslinked GC-PGA NPs TDI_25.

Table 4. Characteristics of the NPs before and after electrospinning

Sample	Diameter [nm]	Polydispersity	ζ-potential [mV]
NPs in water (pH = 6.0)	229 ± 87	0.144	+24.8 ± 3.8
NPs in buffer (pH = 7.4)	232 ± 74	0.104	+2.5 ± 4.1
NPs in water containing EL55 (pH = 6.0)*	242 ± 119	0.243	-37.2 ± 3.5
NPs released from NFs (pH = 7.4)*	290 ± 180	0.386	-38.0 ± 3.2

The hydrodynamic diameters of the NPs are expressed as z-average diameter ± standard deviation; ζ-potential is expressed as an average ζ-potential ± standard deviation.
*The refractive index and the viscosity of the media use for the dynamic light scattering is corrected with based on the concentration of EL55.

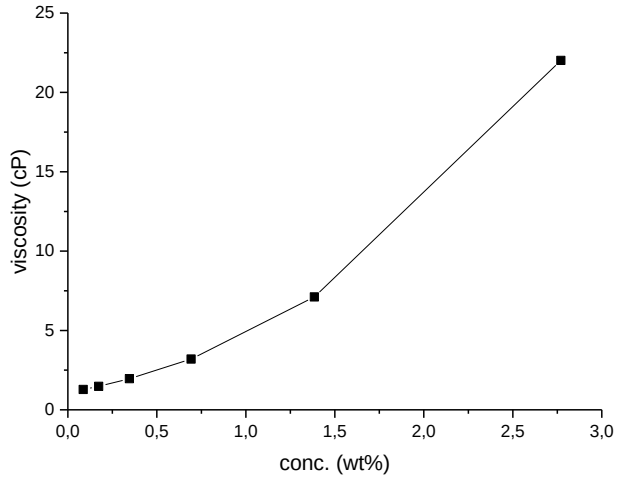

(a)

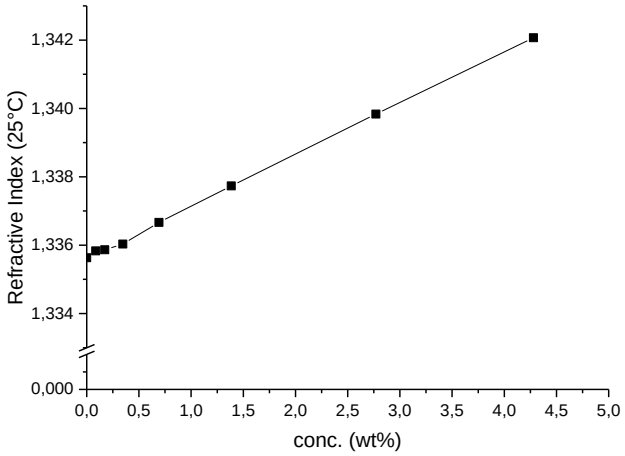

(b)

Figure 18. Evolution of the (a) viscosity and (b) refractive index of Eudragit L100-55 aqueous solution with its concentration expressed in wt%.

The second level of the hierarchy is given by the pH-responsive nanofibers that embed the NPs. The electrospun EL55 nanofibers have an average diameter of 382 ± 65 nm, which is much larger than the size of the NPs. The surface of the nanofibers is smooth, and no NPs can be detected at their surfaces (**Figure 19**a). Therefore, the NPs are loaded inside the fiber and thus protected by the fiber´s matrix. The fluorescently labeled NPs were electrospun with EL55 and therefore can be visualized under confocal light scanning microscopy (CLSM) (**Figure 19**b). The fluorescent NPs were separately distributed along the nanofiber without major aggregation, which is favorable for cellular uptake when the NPs are released near epidermal cells. The electrospinning procedure inherently provided simultaneously shearing force and fast drying of the polymer solution. Thus, the NPs were separated from each other during the elongation of the electrospinning jet and "frozen" when the fiber was dried.

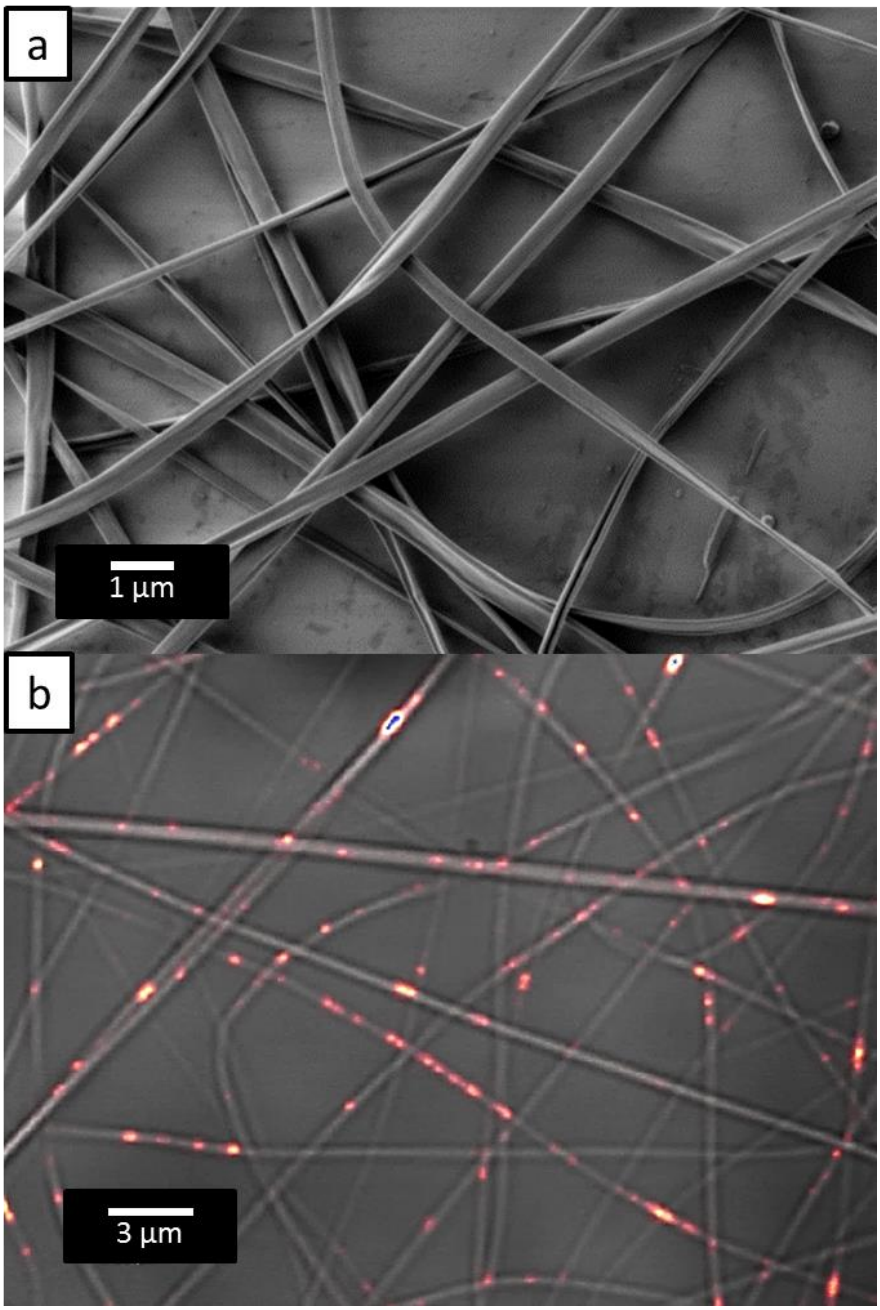

Figure 19. Morphology of EL55 NFs containing crosslinked polyplex NPs. (a) SEM, (b) CLSM: The fluorescence signal (NPs) is overlapped with transmission signals (NFs).

4.4.2. Release of NP from NF upon variation of pH value: The second level of the hierarchy

The next step was to verify that the NPs could be released from the nanofibers at selected pH values. A droplet of buffer solution was cast on nanofibers. The dissolution of fibers and the release of fluorescently labeled NPs was monitored in time by CLSM. The air-liquid

boundary of the droplet is shown in **Figure 20**. At low pH, the nanofibers remained intact. Immersed in the buffer (pH = 4.5) they showed no sign of swelling or dissolution and the NPs were constrained within the NFs throughout the experimental time (~ 30 min). At higher pH, the fibers dissolve instantly upon contact with the buffer solution (pH = 7.4). The droplet boundary proceeded toward dry NFs and led to the swelling of the NFs. The NPs were released without significant aggregation. Hence, the electrospun EL55 NFs serve as a smart matrix for the NPs. Indeed, they isolate the encapsulated NPs from the external environment at lower pH (pH < 5.5) because EL55 is hydrophobic and insoluble. At higher pH (pH > 5.5), EL55 NFs are dissolved and release the NPs.

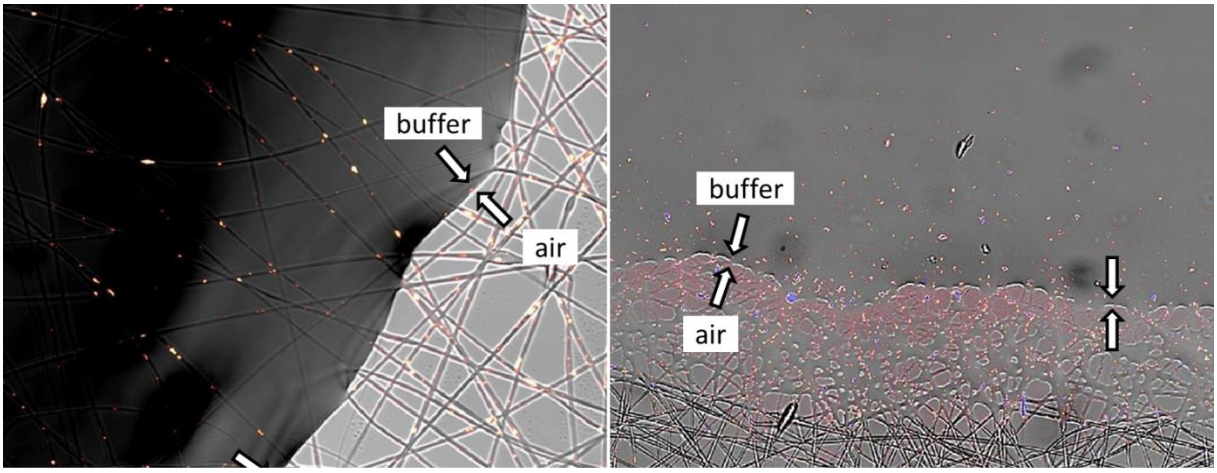

Figure 20. Dissolution of NPs from NFs studied by CLSM. At pH 7.4, the fiber was dissolved within 5 min and all the NPs were released, and > 80% NP was released within 110 s. At pH 6.0, the fibers dissolved gradually, and the NPs were released slowly. Complete dissolution requires > 1 h. At pH 4.5, the fiber was not dissolved, and no NP was released.

NFs containing fluorescently labeled NPs were immersed in various buffer solutions (pH = 4.5, 6.0, or 7.4) and the amount of released NPs was estimated by the fluorescence intensity of the released media (**Figure 21**). At pH 4.5, NFs were not wetted by the buffer and remained intact over the experimental time (~ 30 min). No fluorescent signal was detected in the media, which indicates that the NFs retained the NPs without leakage at lower pH value. At pH 6.0,

the NFs dissolved slowly. 80% of NPs was released over 25 min. At pH 7.4, the NFs were easily wetted and completely dissolved in 5 min. 82% of NPs were released in 2 min and 98% in 12 min.

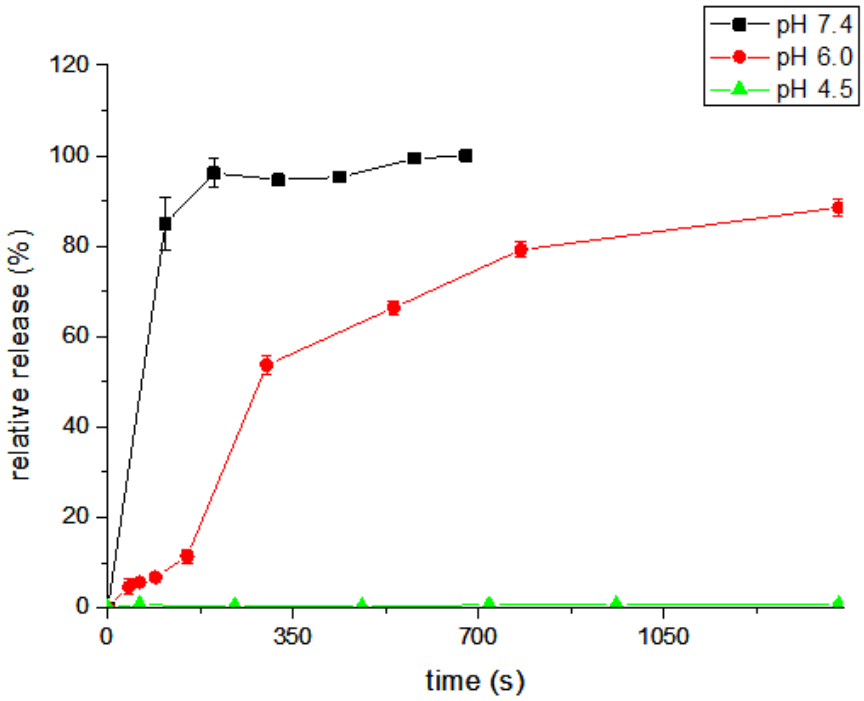

Figure 21. The release profile of fluorescently labeled NPs from NFs.

It is known that the size of the drug nanocarriers strongly affects particles' uptake in cells [210] and hence the transportation efficiency of the payload. Therefore, it is favorable that the NPs released from NFs remain in a non-aggregated state. We studied the aggregation of NPs by DLS before electrospinning and after the dissolution of the NFs (**Table 4**). The average size of the NPs released from EL55 NFs is 290 nm, which is higher than the size of the NP dispersion in water (229 nm) or in buffer solution (232 nm). The increase in polydispersity from 0.144 to 0.386 also suggests that the NPs partially aggregated. Despite a moderate aggregation of NPs after the dissolution of the NFs, the size of the released NPs is still within the suitable range for endocytosis of CS NPs.

To study the reason for the aggregation, an NP dispersion was mixed with an EL55 aqueous solution and compared with NPs without EL55. An increase in both size and polydispersity accompanied by an inversion of the ζ-potential was observed. These trends were also observed with NPs released from NFs. Therefore, we believe that the negatively charged EL55 contributed to the aggregation by complexing with the positively charged NPs and partially bridging multiple NPs.

4.4.3. Release of the peptide from the NP-in-NF system

We investigated the release profiles of a fluorescently labeled model peptide rPYY-FITC from NP-in-NF system in a medium simulating the gastrointestinal conditions at room temperature. In the first 2 h, the pH was 2.0, mimicking the pH in the stomach. Between 2 and 4 h after the beginning of the experiment, the pH was 6.0, which mimicked the condition in the lumen of the intestine. After 4 h, the pH was adjusted to 7.4 for reproducing the environment on the surface of intestinal epidermal cells or the bloodstream. Release profiles of rPYY-FITC from the NP-in-NF system were simultaneously recorded in the buffer solution with fixed pH values (4.5, 6.0, and 7.4) (**Figure 22**).

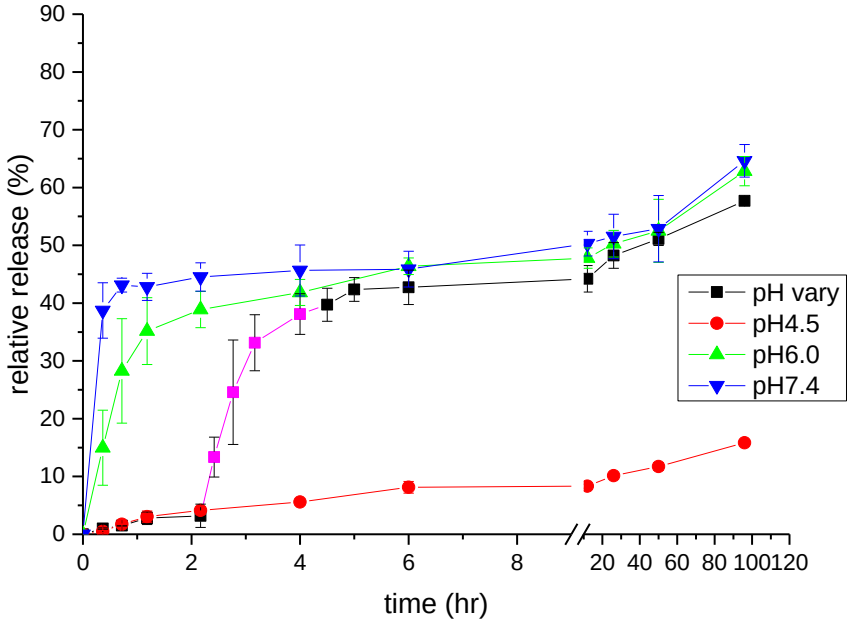

Figure 22. The release profile of the peptide from the NP-in-NF construct.

In the first two hours (pH = 2), a small amount of peptide (3%) leaked from the NFs despite the fact that NPs were not released from the NFs. The release profile in pH 4.5 buffer showed a similar slow leakage of peptide over 100 h. Such leakage indicated that the NF matrix is still permeable to an acidic environment although EL55 is practically insoluble at these conditions. At pH 6.0, the NFs dissolved gradually with a fast release of 35% of the peptide within 2 h. Such fast release indicates that a fraction of the peptide was released to the media due to the dissolution of fibers, *i.e.* part of the peptide was released from the NPs to the NFs before the dissolution of the NFs. Most of the peptide was however retained in the NFs because of the hydrophobic nature of NFs under acidic conditions. If we compare **Figure 21** to **Figure 22**, the release rate of the NPs from NFs is faster than the release rate of rPYY-FITC from the NP-in-NF system at pH 6.0, which suggests that part of the peptide also leaked out of the NPs during the dissolution of the NFs. The two fractions of the released peptide made up in total 35% release of the initially encapsulated peptide. After the pH was adjusted to 7.4, the release

of peptide continued over 100 h, and an extra amount of peptide was released from dispersed NPs (10% after 24 h, 13% at 48 h, and 20% at 96 h). The continuous sustained release of a peptide indicates that at least 20% PYY was still encapsulated in the NPs when they were released from the NFs. Such a trend can also be found in the release profile of peptides in a buffer solution at fixed pH values. Such property confers sustained release of the peptide on the NP-in-NF system after the dispersion of the NPs, thus taking full advantage of the hierarchically structured drug delivery system. Indeed, the peptide concentration is rapidly increased to the effective therapeutic concentration level and is maintained at the desired dosage for an extended period. This type of profile is favorable for some pharmaceutical applications such as drug delivery in the early stage of wound healing [27].

The release profile of the NP-in-NF systems is influenced by processing parameters. One major factor was the contact time between the peptide-loaded NPs and the EL55 solution before NF formation (**Figure 23**). The contact time between NPs and EL55 solution depends on the duration of the electrospinning process, which further scales with the amount of dispersion used for electrospinning. With the same crosslinking density, NFs prepared in smaller batch (contact time = ~ 40 min) compared with that in larger batch (contact time = 4 h) displays suppressed leakage in acidic medium, and the NPs can sustain the release during the experimental time after being released from the NFs. We speculate that such difference is caused by the partial deprotonation of EL55 during electrospinning: EL55 in ethanol reduces the pH upon mixing with the NP paste, which contains water, and the local acidic environment induces the leakage of payload during the electrospinning process. Therefore, a minimized contact time between NPs and EL55 solution achieved by the spinning of the smaller batch is desired to ensure minimized leakage of the peptide. Besides, the crosslinking density of the NPs also affects the retention ability of the NP-in-NF system. With the same spinning conditions, NFs loaded with NPs of 12% crosslinking degree shows a higher leakage

of the peptide, compared with those of 25% crosslinking. Therefore, a certain level of crosslinking is necessary to regulate the swelling of the NPs.

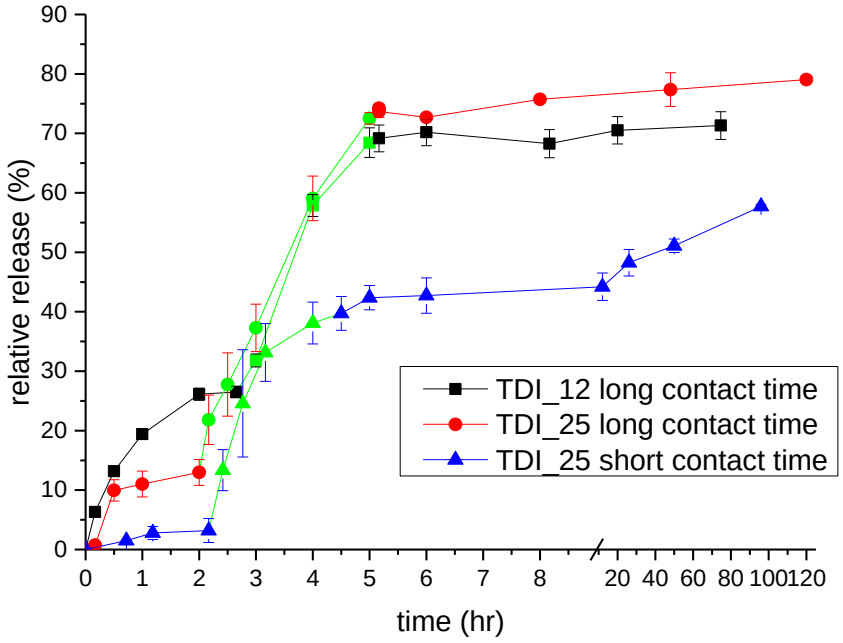

Figure 23. Effects of contact time and dosage of crosslinker on the release profile. TDI_12 long (squares) and TDI_25 long contact time (triangles) are NP-in-NF systems prepared in a larger batch, where the dispersions contain 10 mg NPs, with different dosage of crosslinker added during reaction: 12 and 25 indicate the molar percentage of isocyanate groups in TDI to amine groups in GC. TDI_25 short contact time (dots) corresponds to the NP-in-NF system prepared at a smaller batch, which contains 1.7 mg NPs and therefore implying a faster electrospinning process and shorter contact time between NPs and Eudragit L100-55® (EL55) solution in ethanol. Data collected at pH 6.0, which correspond to the release of NPs from NFs, are colored in green to guide the eyes.

So far, we have introduced a pH-responsive, hierarchical structured drug release system for fragile drugs. However, it is experimentally challenging to transfer the preformed nanoparticles into a matrix that is incompatible with the original media in which the

nanoparticles are synthesized. In the next section, we introduced a general method that addresses such a problem.

4.5. Re-dispersion of nanoparticles in water

The recovery of nanomaterials from inverse miniemulsion has been a challenge because a high recovery rate and a low degree of aggregation cannot be achieved simultaneously, especially when dealing with nanocarriers containing fragile payloads such as peptide drugs. To overcome such difficulty that hindered the construction of a nanoparticle-in-nanofiber hierarchical structure, we have developed a new approach, the "cushion" method, for the recovery of nanoparticles from the inverse emulsion. The following section is based on our publication (He, W., Graf, R., Vieth, S., Ziener, U., Landfester, K. and Crespy, D., The Cushion Method: A New Technique for the Recovery of Hydrophilic Nanocarriers, Langmuir, 2016 [211]).

4.5.1. The concept of molecular "cushion" in the recovery of nanoparticles

Nanocapsules based on crosslinked GC were prepared in an inverse miniemulsion as a model system, which is suitable for the encapsulation of hydrophilic moieties. A similar system has shown effective in the pH-responsive delivery of proteins (see section 4.1 to section 4.3, and [33]). To recover the GC nanocapsules (GCNCs) to aqueous media, our traditional approach involves a tedious process including removal of the hydrophobic surfactant, redispersion in an aqueous solution containing a hydrophilic surfactant, evaporation of the residual solvent, and further redispersion of nanocapsules via sonication. The resulting dispersion suffers from either a low recovery rate or aggregation, as the allowed dosage of surfactant is limited by its cytotoxicity [33]. Driven by these drawbacks, we sought for an alternative approach that is equally mild, surfactant free, simpler, and less time-consuming.

Our new approach to recovering GCNCs from the inverse emulsion is termed the "cushion" method, as a temporary protecting layer of water-soluble molecules, e.g. monosodium glutamate (GluNa), was introduced around the GCNCs to avoid their aggregation during the

preparation and purification of the GCNCs (**Figure 24**a). By ultrasonication and dilution of a mixture of two miniemulsions containing respectively a solution of "cushion" molecules and a dispersion of preformed NPs, the nanodroplets coalesce randomly and thereafter the preformed NPs are surrounded by "cushion" molecules. The resulting emulsion is subjected to purification by removing the hydrophobic surfactant.

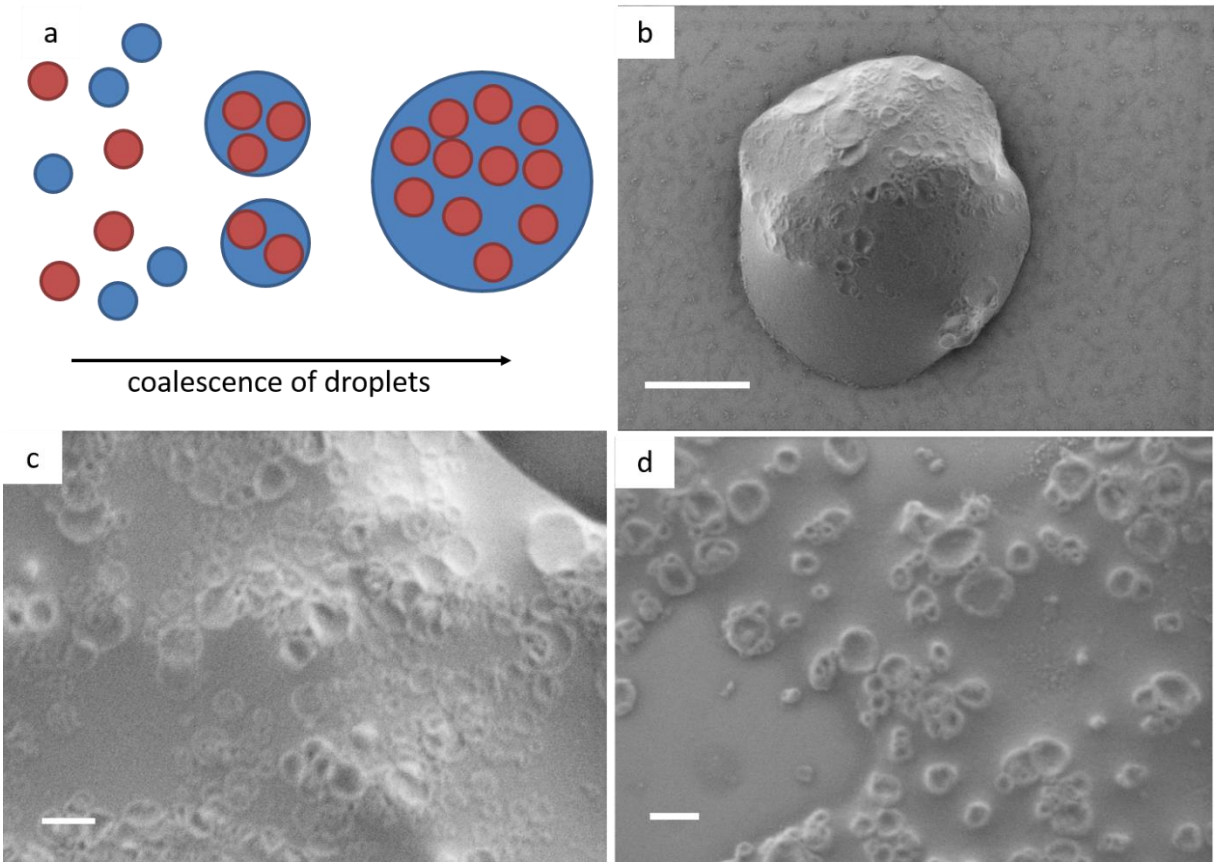

Figure 24. The concept of the "cushion" method. (a) Scheme for a water-in-oil emulsion. The background, the red circles, and the blue circles represent the cyclohexane phase, the NPs, and the aqueous droplets, respectively. (b−d) Scanning electron micrographs of dried samples from the emulsion during washing process: (b) sampled from the emulsion diluted in hexane; (c, d) sampled from the aqueous phase of the emulsion during the washing process. In (d), the water-soluble substance was partly removed via rinsing with water. The scale bars represent 1 μm in (b) and 200 nm in (c, d).

To monitor the dynamics of the "cushion" method, samples of the emulsion were collected at different steps of purification (**Figure 24**b-d). Immediately after dilution of the miniemulsion

with hexane, a sample of the emulsion was taken for SEM characterization. Multiple NPs were embedded in a matrix, presumably GluNa, in dried microdroplets (representative image is shown in **Figure 24**b). We attributed the formation of microdroplets to the coalescence of nanodroplets upon dilution of the emulsion. During the liquid−liquid extraction of surfactant, the microdroplets further coalesced and finally formed a single aqueous phase. A dried film of the aqueous phase was subjected to SEM (**Figure 24**c), in which GCNCs, although not observed as individual species owing to the surrounding matrix, can be identified. After carefully rinsing the same sample with water on the silicon wafer, individual nanocapsules can be then clearly observed (**Figure 24**d). This indicates that the embedding matrix is water-soluble and therefore suggests that the "cushion" molecules around the GCNCs can be easily dissolved in water during the redispersion process.

4.5.2. Colloidal characterizations of glycol chitosan nanocapsules prepared with the "cushion" method

The hydrodynamic diameters of the GCNC dispersion at different pH values are shown in **Figure 25**a. The z-average diameter determined by DLS lies around 240 nm, which implies a slight aggregation of GCNCs, as the diameter of a single GCNCs observed under SEM lies around 100 nm (**Figure 24**d). Besides, the size of GCNCs was slightly larger at lower pH than at higher pH, which can be explained by the swelling of GCNCs upon the protonation of amine groups from GC.

A sharp decrease of the ζ-potential of the GCNCs is observed above pH 6.2 (**Figure 25**b), which corresponds to the pK_a value of the amine groups in GC [175]. The similarity of GC and GCNCs implies that the surface of the GCNCs is predominantly GC, rather than the hydrolyzed isocyanates, which would have a much higher pK_a value. Besides, the ζ-potential –pH curve suggests that a desirable pH value of the "cushion" solution should be lower than pH 6.2, as a highly charged surface is favorable for the redispersion of GCNCs.

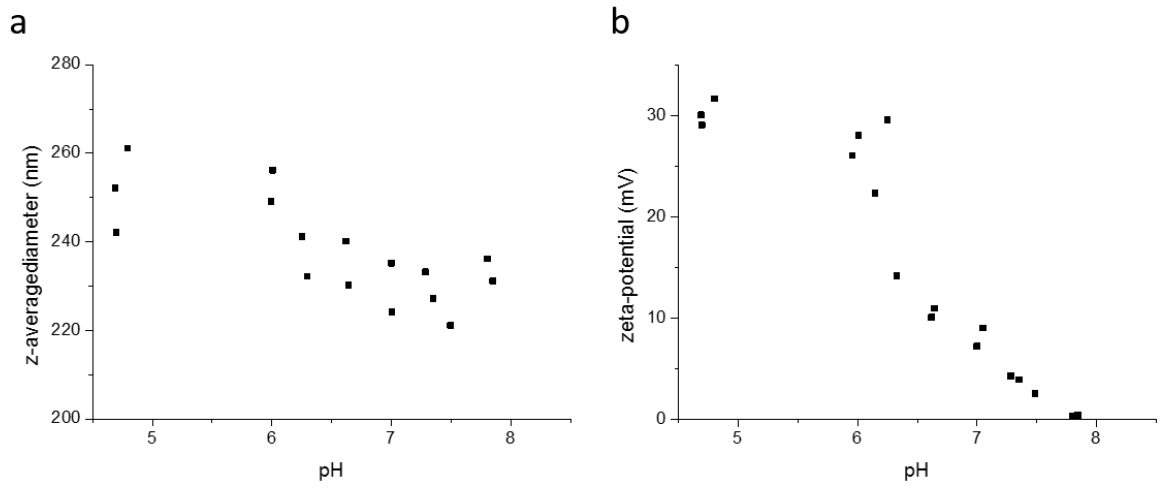

Figure 25. Characteristics of GC-TDI-NPs recovered by the "cushion" method. Data is accumulated from 3 independent batches. (a) the z-average hydrodynamic diameter of the GC-TDI capsules at different pH values; (b) ζ-potential of the GCNCs at different pH values.

The recovery rate of GCNCs by the "cushion" method is estimated by the GCNCs prepared with Rhodamine B isothiocyanate (RBITC) labeled GC (GC-RBITC), which has been fluorescently labeled. The fluorescence intensity of the final dispersion of the fluorescently labeled GCNCs is (98 ± 1)% compared to that of the reference GC-RBITC solution, which indicates that most of the starting materials were recovered after the washing process. Meanwhile, the fluorescence intensity of the supernatant of centrifuged dispersion is negligible (< 1%), and thus the fluorescence signal can be attributed to the GCNCs rather than the dissolved polymer. The high recovery rate during the phase transfer process contributes to the maximized overall encapsulation efficiency.

4.5.3. Monitoring of surfactant residue in the glycol chitosan nanocapsules

The fact that GCNCs can be dispersed in water without additional hydrophilic surfactant suggests that the surface of the GCNCs is GC and most of the hydrophobic surfactant polyglycerol polyricinoleate (PGPR) is removed. To monitor the residue of PGPR in GCNCs, the GluNa was further removed via dialysis and the freeze-dried GCNCs was subjected to

Fourier transform infrared (FTIR) analysis. In the search of a characteristic peak of PGPR, the carbonyl stretching band at 1735 cm^{-1}, in the spectra of GCNCs, an ambiguous shoulder peak was found (**Figure 26**). Hence, the majority of PGPR was removed, but the level of residual PGPR lies below the detection limit of FTIR.

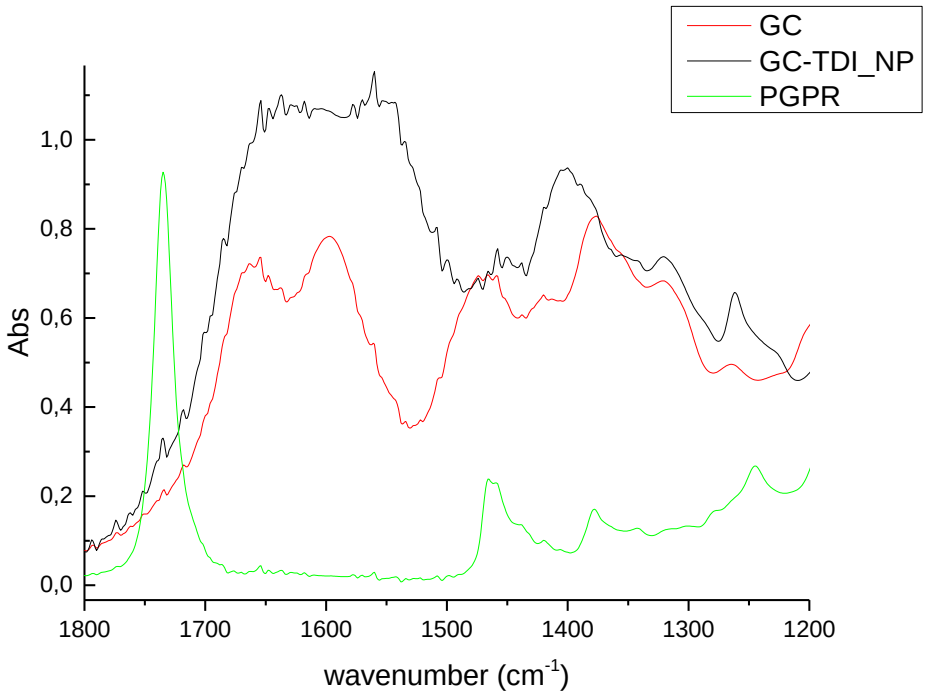

Figure 26. FTIR spectra of GC, PGPR, and GC-TDI_NP.

Further analysis of GCNCs with solid state C^{13}NMR also shows that the characteristic band between 125-132 ppm of the double bond in PGPR is overwhelmed by the band of the aromatic ring from TDI, while the aliphatic band between 20-40 ppm of PGPR is buried in the characteristic band of GluNa (**Figure 27**, right). Therefore, the residual PGPR level is significantly lower than the crosslinking unit and GluNa residue after dialysis. Despite the low level of residual PGPR present in GCNCs, its existence is still confirmed by solid-state ^{1}H NMR spectroscopy (**Figure 27** left). The significant peak broadening in ^{1}H NMR was expected as the GCNCs is solid. However surprisingly the peak broadening of PGPR is significantly lower, which indicates that PGPR has a higher mobility compared to that of the

GCNCs, that is, PGPR stays in a mobile (liquid) form. We speculate that PGPR is either in the pocket of interspace of GCNCs or on the surface of GCNCs, both indicate that surfactant is not incorporated into the shells of GCNCs. Due to the significant difference in mobility between PGPR and GCNCs, the quantification of PGPR in solid GCNCs is not available.

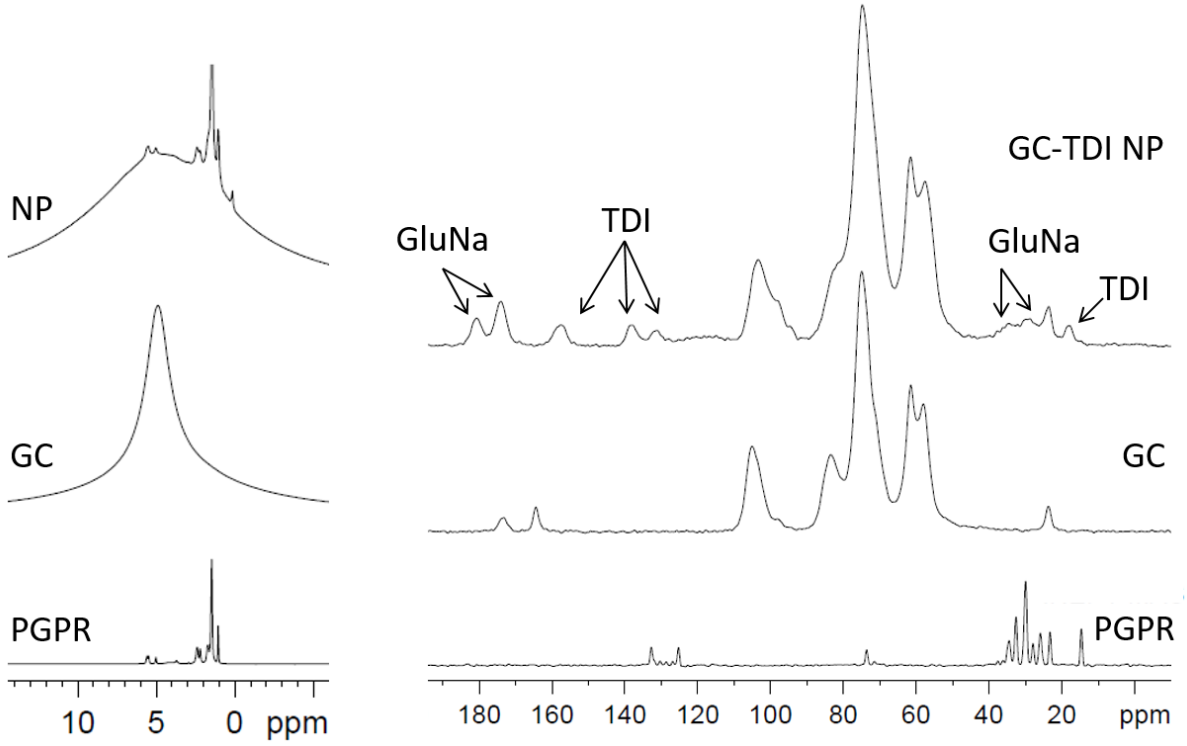

Figure 27. Solid-state NMR spectra of GC-TDI NPs, GC polymer, and surfactant PGPR. (left) solid-state-^{1}H NMR spectra; (right) solid-state-^{13}C NMR spectra. The spectra of NP and GC were taken with CP-MAS method, and the spectrum of PGPR was taken with INEPT-MAS method.

4.5.4. Application of the "cushion" method during redispersion of nanoparticles

One application of the "cushion" method is to prepare crosslinked polyelectrolyte complex-based GC nanocarriers for proteins for controlled peptide delivery (see also section 4.1 to section 4.3 and [33]) (**Figure 28**a). The peptides (rPYY-FITC) can be efficiently encapsulated and released from the NPs in a pH-responsive manner (**Figure 28**b). The advantage of the "cushion" method is that the current formulation does not require a surfactant for stabilization.

Therefore, the surface of NPs is dominated by the GC polymer rather than surfactants. Such property avoids the cytotoxicity issues [60] and the interference with protein from surfactants, especially in the studies of the particle-protein interactions [54]. Further biotests related to caco-2 cells including mucoadhesiveness, endocytosis, and cytotoxicity will be reported in a separated paper in detail, which shows the potential of GC based NPs prepared with "cushion" method as a good candidate for oral drug delivery.

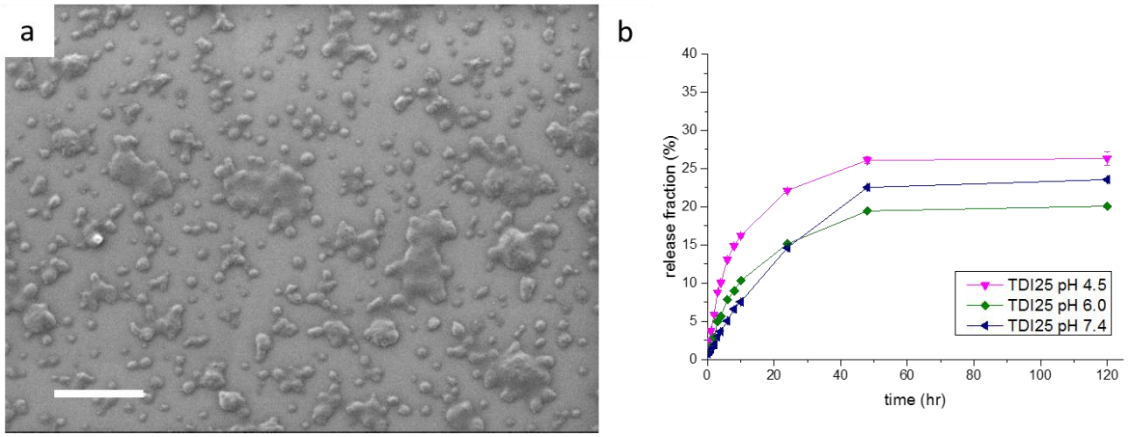

Figure 28. Polyplex based nanocarriers prepared with the "cushion" method. (a) SEM micrograph of NPs (scale bar = 1 µm), hydrodynamic diameter determined by DLS: 217 ± 64 nm (z-average ± standard deviation). (b) in-vitro release of a fluorescently labeled peptide, rPYY-FITC, from the NPs at different crosslinking density.

4.5.5. Generalized "cushion" method with other molecules

To generalize the concept of the "cushion" method, we substitute the GluNa with other water-soluble glucose derivatives because of their similarity to the repeating unit of CS. Glucosamine (Gluc-NH_2), glucuronic acid (Gluc-COOH), and trehalose were chosen to represent molecules bearing amine group, carboxylic acid group, or only hydroxyl groups respectively. When the pH value of this solution was adjusted to 6, good redispersion of GCNCs is achieved regardless of the nature of molecules (**Table 5**).

Table 5. Recovery of NPs with various molecules.

Molecule	**pK_a**	**contain NH_2**	**contain COOH**	**pH**	**diameter (nm)**

GluNa	2.1, 4.2, 9.5	Yes	Yes	6.01	229 ± 92
Gluc-NH_2	7.6	Yes	No	6.00	245 ± 90
Gluc-COOH	2.9	No	Yes	5.92	293 ± 132
Trehalose	-	No	No	5.81	254 ± 99

The diameter of GCNCs redispersed in water is represented as z-average hydrodynamic diameter ± standard deviation.

The underlining mechanism for the "cushion" method is currently not clear. We propose several possible roles of "cushion" molecules in the redispersion of GCNCs: (1) the physical separation between GCNCs that prevents direct contact, which is similar to the role of cryoprotectants as a matrix in freeze drying [66]; (2) the physical isolation between GCNCs and the TDI residue in organic phase, so that their possible reaction during the purification process is minimized; (3) hydrophilic molecule that increase Laplace pressure in the aqueous droplets, which inhibits the Ostwald ripening and the hydrophobization of GCNCs by hydrophobic surfactants [47]; (4) a salt or amino acid that decrease the adsorption of surfactants at the water-oil interface, thus facilitating the removal of surfactants during the purification [212]. (5) a buffer that keeps the amine group in GC in a non-reactive protonated form.

5. Experimental section

5.1. Crosslinked polyelectrolyte complex for peptide delivery

5.1.1. Materials

Rat PYY(1-36) and human PYY(1-36) (rPYY, hPYY > 95%, American Peptide), glycol chitosan (GC, 77% by titration, M_w ~ 210 kDa measured by GPC, Santa Cruz Biotechnology), poly(γ-glutamic acid) sodium salt (PGA, > 70%, M_w 100 kDa measured by GPC, Vedan), toluene diisocyanate (TDI, 95%, Sigma Aldrich), glutaraldehyde (GA, 50% aq. sol., Merck), dibutylamine (DBA, > 99% Merck), 1,4-dinitrobenzene (DNB, 98%, Sigma Aldrich), Pluronic F68 (10% sol., Sigma Aldrich), FITC antibody labelling kit (53027, Thermo Scientific), human-PYY ELISA kit (Millipore, #EZHPYYT66K), and Amicon centrifugal filters (UFC500396, Millipore) were used as received. Polyglycerol polyricinoleate (PGPR, 91%, E476, Danisco) was diluted in hexane and filtered (pore size: 0.45 μm, cellulose). PGPR was then concentrated by rotary evaporation and vacuum dried (40 mbar, 40 °C, overnight). Sterilized water (Aqua B. Braun) was used for all the experiments if not specifically mentioned.

5.1.2. Fluorescent labeling of the peptide

rPYY was fluorescently labeled with FITC antibody labeling kit, and the conjugated rPYY was named as rPYY-FITC. Briefly, rPYY was dissolved in sterilized water (2 mg/mL, 2 mL) and was mixed with FITC solution in anhydrous DMF (10 mg/mL, 77 μL). The mixture was stirred in darkness for 2 h at 4 °C and purified via chromatography and centrifugal filtration (Amicon Centrifugal Filters, 7500 G, 25 min, 10 °C, for 3 times). The purified rPYY-FITC conjugate was analyzed by HPLC. The recovery rate is 55% with an overall fluorophore/protein ratio of 1.21. The quantities of non-labeled and single-labeled PYY were 3% and 73%, respectively. No free FITC was detected with FCS.

5.1.3. Fluorescence correlation spectroscopy measurements of rPYY-FITC

Solutions of rPYY-FITC (< 50 µL, containing ca. 2 ng or ca. 200 ng peptide) were mixed with GC solution (1 mL, 1 mg/mL) or PGA solution (1 mL, 0.4 mg/mL). The autocorrelation functions of the fluorescence intensity the rPYY-FITC were recorded on a commercial FCS setup (ZEISS Axiovert 200M microscope, ConfoCor 2 FCS unit). The excitation was done by the 488 nm line of an argon laser and the collected fluorescence was filtered through an LP505 long pass emission filter. Eight-well polystyrene-chambered cover glass (Laboratory-Tek, Nalge Nunc International) was used as a sample cell. For each solution, a series of 10 measurements with a total duration of 5 min were performed. The confocal observation volume was calibrated using a reference dye with a known diffusion coefficient i.e. Alexa Fluor 488. The diffusion coefficient and hydrodynamic radius of FITC labels were obtained by fitting the experimental autocorrelation curves with a simple diffusion model [213].

5.1.4. Preparation of colloidal polyplexes in solution

Colloidal polyplexes were prepared according to a modified method that was previously reported [41]. Briefly, a stock solution of GC (10 mg/mL, pH 6.0) and PGA (10 mg/mL, pH 6.0) was prepared separately by dissolution at room temperature and pH adjustment. The PGA solution (1 mg/mL) was mixed with a rPYY-FITC solution (60 µL, 83.3 µg/mL), leading to a homogeneous PYY-PGA solution (0.3 mg/mL PGA). The PYY-PGA solution was injected into the GC solution (1 mg/mL) at mass ratio 5:1 (GC: PGA), and the GC-PGA NPs were formed instantly.

5.1.5. Preparation of colloidal polyplexes in miniemulsion and subsequent crosslinking

Crosslinked polyplex NPs were prepared in miniemulsion. An aliquot of PYY (~ 50 µg) was thawed, dissolved in 0.6 mL of water, and mixed with a PGA stock solution (0.4 mL, 6 mg PGA/mL). After pre-emulsification (0.5 h, 1000 rpm) in a PGPR solution (1wt% in

cyclohexane), the coarse emulsion was ultrasonicated for 1 min with ice-water cooling bath (Branson Sonifier W450, ½ inch probe). A GC stock solution (1 mL) was emulsified in the same way and was mixed with the PGA miniemulsion. The mixture was then ultrasonicated for 30 s. A predetermined amount of crosslinker (GA or TDI) was diluted with toluene and injected in the emulsion. After 20 min of reaction at room temperature, the reaction was stopped by dilution with toluene, and the oil phase was removed by centrifugation (2000 G, 15 °C, 5 min). The resulting crosslinked polyplex was washed 3 times against toluene and hexane by centrifugation-redispersion and was finally redispersed in an aqueous solution with slight sonication (1 min in an ultrasound bath, r.t.). The final dispersion contained crosslinked polyplex (ca. 1 mg/mL), Pluronic F68 (5 mg/mL), and phosphate buffer (0.01 M, pH 6.0). The residual hexane was removed by vacuum evaporation (40 mbar, r.t. *ca.* 30 min).

5.1.6. Quantification of consumed crosslinker in the reaction

The amount of TDI in the miniemulsion during the crosslinking reaction was quantified by ^{1}H-NMR spectroscopy. Briefly, aliquots of the miniemulsions were taken and injected in a toluene solution containing a known amount of DBA as a quenching agent for TDI and DNB as an external standard for NMR. After 10 min of reaction at room temperature, the solvents were removed by rotary evaporation (20 mbar, 40 °C) and vacuum drying (40 mbar, 40 °C, overnight). The dried product was extracted in deuterated toluene under sonication and the resulting suspension was centrifuged (15 °C, 20 min, 40000 G). The resulting supernatant was measured by ^{1}H-NMR spectroscopy (300 MHz, Bruker Avance). The signal of the amide H was normalized with the aromatic H peak of DNB to measure the concentration of quenched TDI.

5.1.7. Release of the peptide from the nanocarriers

Aliquots of frozen rPYY-FITC were thawed at room temperature and diluted with sterile water. A small fraction (typically 10 µL) of the peptide solution was further diluted and stored at 4 °C in the dark as a reference sample. The rPYY-FITC solution was then mixed with a PGA solution and finally encapsulated in GC-PGA-TDI NP. The NPs were then dispersed in aqueous solutions. Stock buffer solutions of different pH were injected to the aliquots. The pH value, average hydrodynamic diameter (DLS, Nicomp 380), and the zeta potential (Malvern Zetasizer) were recorded. The suspensions were stirred at room temperature and aliquots of the dispersions were sampled at a predetermined time and centrifuged (20,000 G, 15 °C, 20 min). The supernatant and the reference sample were collected, and 10-fold diluted with a phosphate buffer (0.1 M, pH 6.0) with dissolved Pluronic F68 (5 mg/mL). The fluorescence intensity (excitation: 490 nm, emission: 515 nm) was recorded and compared with the reference sample. The relative release was determined to be the ratio of the concentration of rPYY-FITC in the release medium to the concentration of originally encapsulated peptide. In some cases, the fluorescence intensity of the sampled NP dispersions was measured without centrifugation so that the overall fluorescence signal was recorded. This corresponded therefore to the total amount of rPYY-FITC in the dispersions.

5.1.8. Quantification of the peptide released from the nanocarriers

hPYY was mixed with rPYY-FITC with a 1:1 ratio. The mixture was then subjected to encapsulation and release procedures as for the fluorescence measurements. The released hPYY was quantified with a human PYY (total) kit. The test was performed according to the recommendation of the manufacturer. Since there are no interferences between hPYY and rPYY-FITC in the human PYY ELISA test and in the fluorescence measurements, hPYY and rPYY-FITC are encapsulated and released simultaneously.

5.2. Influence of crosslinking density on the release of peptides

5.2.1. Preparation of colloidal polyplexes in miniemulsion and subsequent crosslinking

Crosslinked polyplex NPs were prepared in miniemulsion. An aliquot of rPYY-FITC (~ 50 µg) was thawed, dissolved in 0.8 mL of water, and mixed with a PGA stock solution (0.2 mL, 6 mg PGA/mL). After pre-emulsification (0.5 h, 1000 rpm) in a PGPR solution (1wt% in cyclohexane), the coarse emulsion was ultrasonicated for 1 min with ice-water cooling bath (Branson sonifier W450, ½ inch probe). A GC stock solution (1 mL) was emulsified in the same way and was mixed with the PGA miniemulsion. The mixture was then ultrasonicated for 30 s. A predetermined amount of crosslinker (GA or TDI) was diluted with toluene and injected in the emulsion. After 20 min of reaction at room temperature, the reaction was stopped by dilution with toluene, and the oil phase was removed by centrifugation (2000 G, 15 °C, 5 min). The resulting crosslinked polyplex was washed 3 times against toluene and hexane by centrifugation-redispersion and was finally redispersed in an aqueous solution with slight sonication (1 min in an ultrasound bath, r.t.). The final dispersion contained crosslinked polyplex (ca. 1 mg/mL), Pluronic F68 (5 mg/mL), and phosphate buffer (0.01 M, pH 6.0). The residual hexane was removed by vacuum evaporation (40 mbar, r.t. *ca.* 30 min).

5.2.2. In-vitro release of peptides from colloidal polyplexes

Aliquots of frozen rPYY-FITC were thawed at room temperature and diluted with sterile water. A small fraction (typically 10 µL) of the peptide solution was further diluted and stored at 4 °C in the dark as a reference sample. The rPYY-FITC solution was then mixed with a PGA solution and finally encapsulated in GC-PGA-TDI NP. The NPs were then dispersed in aqueous solutions. Stock buffer solutions of different pH were injected to the aliquots. The pH value, average hydrodynamic diameter (DLS, Nicomp 380), and the zeta potential (Malvern Zetasizer) were recorded. The suspensions were stirred at room temperature and aliquots of

the dispersions were sampled at a predetermined time and centrifuged (20,000 G, 15 °C, 20 min). The supernatant and the reference sample were collected, and 10-fold diluted with a phosphate buffer (0.1 M, pH 6.0) with dissolved Pluronic F68 (5 mg/mL). The fluorescence intensity (excitation: 490 nm, emission: 515 nm) was recorded and compared with the reference sample. The relative release was determined to be the ratio of the concentration of rPYY-FITC in the release medium to the concentration of originally encapsulated peptide. In some cases, the fluorescence intensity of the sampled NP dispersions was measured without centrifugation so that the overall fluorescence signal was recorded. This corresponded therefore to the total amount of rPYY-FITC in the dispersions.

5.2.3. Quantification of the peptide released from the nanocarriers

hPYY was mixed with rPYY-FITC with a 1:1 ratio. The mixture was then subjected to encapsulation and release procedures as for the fluorescence measurements. The released hPYY was quantified with a human PYY (total) kit. The test was performed according to the recommendation of the manufacturer. Since there are no interferences between hPYY and rPYY-FITC in the human PYY ELISA test and in the fluorescence measurements, hPYY and rPYY-FITC are encapsulated and released simultaneously.

5.3. Sequence-controlled delivery of peptides from hierarchically structured nanomaterials

5.3.1. Materials

Rat PYY(1-36) (rPYY, > 95%, American Peptide), glycol chitosan (GC, 77% by titration, M_w = 210 kDa measured by gel permeation chromatography GPC, Santa Cruz Biotechnology), poly(γ-glutamic acid) sodium salt (PGA, > 70%, M_w = 100 kDa measured by GPC, Vedan), Eudragit® L100-55 (EL55, Evonik Industries), toluene diisocyanate (TDI, 95%, Sigma Aldrich), Rhodamine B isothiocyanate (RBITC, Sigma Aldrich), FITC antibody labelling kit (53027, Thermo Scientific), and Amicon centrifugal filters (UFC500396, Millipore) were used as received. Polyglycerol polyricinoleate (PGPR, 91%, E476, Danisco) was diluted in hexane and filtered (pore size: 0.45 µm, cellulose). PGPR was then concentrated by rotary evaporation and vacuum dried (40 mbar, 40 °C, overnight). Sterilized water (Aqua B. Braun) was used for all the experiments if not specifically mentioned. The buffer solution was prepared with monosodium phosphate, and acetic acid (Aldrich) at 0.1 M and was used for all the experiments if not specified.

5.3.2. Preparation of crosslinked polyplex nanocarriers

Polyplex-based nanocarriers were prepared in miniemulsion according to the procedure described in the previous paper [33]. Briefly, an aliquot of rPYY-FITC (ca. 50 µg) was thawed, dissolved in 0.6 mL of water, and mixed with a PGA stock solution (0.4 mL, 6 mg PGA/mL). After pre-emulsification (0.5 h, 1000 rpm magnetic stirring) in a PGPR solution (1wt% in 7.5 mL cyclohexane), the coarse emulsion was ultrasonicated for 1 min with ice-water cooling bath (Branson Sonifier W450, ½ inch probe). A GC stock solution (1 mL) was emulsified in the same way and was mixed with the PGA miniemulsion. An EL55 stock solution (3 mL, 2.5wt%, pH = 6.0) was emulsified in the same way. The mixture was then

ultrasonicated for 30 s. A predetermined amount of crosslinker, TDI, was diluted with toluene and injected in the emulsion. After 10 min of reaction at room temperature, the emulsion of EL55 (16 mL) was added and the mixture was ultrasonicated for 30 s. The final emulsion was diluted with 270 mL hexane and the oil phase was removed by centrifugation (2000 g, 15 °C, 5 min). The resulting crosslinked polyplex was washed 3 times against ethyl acetate by centrifugation-redispersion. The resulting paste of NP was ready for the next step. The NP can be redispersed in an aqueous solution with slight sonication (5 min in an ultrasound bath, r.t.). The final dispersion contained crosslinked polyplex (ca. 1 mg/mL), and phosphate buffer (0.01 M, pH 6.0). The residual ethyl acetate was removed by vacuum evaporation (40 mbar, r.t. ca. 10 min).

In the case of fluorescently labeled NP, GC was fluorescently labeled with RBITC and the resulting GC-RBITC was used instead of GC. The details for the preparation of GC-RBITC is available in the Supporting Information.

The final NPs were dispersed in water by applying ultrasound in a sonication bath (1 mg NP/mL water, 5 min). The resulting water dispersion was analyzed by DLS (ALV CGS, data fitted with cumulant method) and zeta potential (Zetasizer, Malvern). For SEM sampling, the NP dispersion was cast onto a silicon wafer and left to dry. The wafer surface was rinsed with a water droplet 3 times to remove the soluble fraction. Diameters of the NPs were measured manually (n = 435) based on the SEM image.

5.3.3. Electrospinning of pH-responsive nanofibers

EL55 nanofibers were produced by electrospinning. EL55 was dissolved in ethanol at 15wt% and then degassed in a vial in a sonication bath for 5 min. A known amount of a paste consisting of NPs dispersed in water (1wt%) was mixed with the solution of EL55 by magnetic stirring or pipetting. The contact time between NPs and the EL55 solution during

electrospinning depended on the amount of the dispersion. In a larger- or smaller-batch preparation, where 10 mg or 1.7 mg NPs were mixed with an EL55 solution at 1wt%, the electrospinning takes 4 h and 40 min, respectively. The NP dispersion in EL55/ethanol was used immediately for electrospinning (IME Technologies, 16 kV voltage, 1 mL/h feed rate, 10 cm working distance, 65% humidity, 25 °C, 0.15 mL of injected solution per sample). After spinning, the nanofiber mat was peeled off and weighed. For long-term storage, the fiber mat was sealed in a glass vial and stored in a desiccator. Samples for SEM and LCSM were collected. The fiber diameter was measured based on SEM micrograph (n = 20).

5.3.4. Monitoring the release of NP from pH-responsive NF

NP dissolution from NF was monitored by CLSM. NP containing NFs were collected onto a cover glass during electrospinning. A droplet of 0.1 M buffer solution (pH = 4.5 or pH = 7.4) was casted onto the NF. A CLSM micrograph was taken at the edge of the droplet to observe the dissolution process.

For quantification of the release of NPs from NFs, the nonwovens containing NP-RBITC were weighed (~ 20 mg) and immersed in 0.1 M buffer solutions (pH = 4.5 or pH = 6.0). At certain intervals, 200 µL of the sample was taken from the release medium and the fluorescence intensity of the dispersion was recorded. The relative release of particles (%) from the fibers was expressed as the ratio of the recorded intensity to the theoretical fluorescence intensity of the initial amount of GC-RBITC used for the synthesis of the NP.

The multi-stage release of the peptide from NP-in-NF system at different pH values

rPYY-FITC was present in NPs and NP-in-NF systems because it could be loaded during the synthesis of the particles. A fiber mat of known mass (~ 20 mg) was weighed and immersed in the release medium (10 mL, pH = 4.5). At certain intervals of time, 200 µL of the sample was taken from the release medium and centrifuged (15 °C, 20 min, 40000 g). The relative

release of the peptide (%) from the NP-in-NF system was expressed as the ratio of the recorded intensity to the theoretical fluorescence intensity of the initial amount of rPYY-FITC used for the synthesis of the NPs. For the multi-stage release profile of peptide under a sequence of pH values, the fiber mat was first immersed in a 0.01 M HCl solution (pH = 2.0). After 2 h, the release medium was changed to phosphate buffer (pH = 6.0). After 4 h, the pH of the buffer was adjusted to 7.4 with a 1.0 M NaOH solution.

5.4. Manipulation of nanodroplets for the recovery of nanoparticles

5.4.1. Materials

Glycol chitosan (GC, 77% by titration, M_w = 210 kDa measured by GPC, Santa Cruz Biotechnology), poly(γ-glutamic acid) sodium salt (PGA, > 70%, M_w = 100 kDa measured by GPC, Vedan), toluene diisocyanate (TDI, 95%, Sigma Aldrich), Glutamic acid monosodium salt (GluNa, > 99%, Sigma Aldrich), Trehalose (Trehl, > 98%, Sigma Aldrich), Glucosamine (Gluc-NH_2, > 99%, Sigma Aldrich), Glucuronic acid (Gluc-COOH, > 98%, Sigma Aldrich) Rhodamine B isothiocyanate (RBITC, Sigma Aldrich), FITC antibody labelling kit (53027, Thermo Scientific), and Amicon centrifugal filters (UFC500396, Millipore) were used as received. Polyglycerol polyricinoleate (PGPR, 91%, E476, Danisco) was diluted in hexane and filtered (pore size: 0.45 μm, cellulose). PGPR was then concentrated by rotary evaporation and vacuum dried (40 mbar, 40 °C, overnight). Rat PYY(1-36) (rPYY, > 95%, American Peptide) was labeled with FITC [33]. GC was labeled with RBITC. Sterilized water (Aqua B. Braun) was used for all the experiments if not specifically mentioned. The buffer solution was prepared with monosodium phosphate, and acetic acid (Aldrich) at 0.1 M and was used for all the experiments if not specified.

5.4.2. Glycol chitosan-based nanocapsules prepared with the “cushion” method

GC based nanocapsules (GCNCs) were prepared in miniemulsion modified based on the procedure described in our previous paper [7]. Briefly, a GC stock solution (10 mg/mL, 1 mL, pH = 6.0) was pre-emulsified in a PGPR solution (1wt% in 7.5 mL cyclohexane), the coarse emulsion was ultrasonicated for 1 min with ice-water cooling bath (Branson Sonifier W450, ½ inch probe, 2 min, 1 s pulse, 1 s pause). Right after emulsification, a predetermined amount of crosslinker (TDI) was diluted with toluene and injected in the emulsion. During the crosslinking reaction, a solution of GluNa (1.5 mL, 10wt%, pH = 6.0) was emulsified in

cyclohexane the same way. In a generalized process, GluNa was replaced by other molecules including Gluc-NH_2, Gluc-COOH, and trehalose. After 10 min of reaction at room temperature, the emulsion of GluNa (9 mL) was added, and the mixture was ultrasonicated for 30 s. The final emulsion was diluted with 180 mL hexane and the oil phase was removed by centrifugation (2000 g, 15 °C, 5 min). The organic phase was discarded, and the aqueous part was washed for three times via liquid-liquid extraction (water saturated ethyl acetate, ~ 10 mL) and centrifugation (< 1000 g, 3 min, 15 °C). After evaporation of the residue of ethyl acetate (200 mbar, ~ 5 min, r.t.), the resulting aqueous part was redispersed in water with slight sonication (5 min in an ultrasound bath, 1 W/cm^2, r.t.). The final dispersion contained GCNCs (1 mg/mL) and GluNa (15 mg/mL) and was subjected to further analysis including dynamic light scattering (DLS, Nicomp 380) and ζ-potential (Malvern Zetasizer). For IR and solid-state ^{13}C-NMR, ^{1}H-NMR analysis, the dispersion was further dialyzed against water for 4 days and the freeze dried. For SEM sampling, a droplet of hexane diluted emulsion (**Figure 24**b) and a droplet of the aqueous phase before redispersion (**Figure 24**c-d) was cast onto a silicon wafer and left to dry. For **Figure 24**d, the wafer surface was rinsed with a water droplet 3 times to remove the soluble fraction.

5.4.3. Quantification of the recovery rate of glycol chitosan nanocapsules

To quantify the amount of GCNCs in its aqueous dispersion, GC was fluorescently labeled with RBITC (available in supporting information), and the resulting GC-RBITC was used instead of GC in the synthesis of GCNCs. The fluorescence intensity (excitation: 556 nm, emission: 579 nm) of the GCNC dispersion, GC-RBITC reference, and the supernatant of centrifuged GCNC dispersion was monitored.

5.4.4. Polyplex-based nanocarriers prepared with the “cushion” method

polyplex-based nanocarriers were prepared in miniemulsion modified based on the above-mentioned method for GCNCs. Briefly, an aliquot of FITC labeled rPYY (rPYY-FITC) (ca. 50 μg) was thawed, dissolved in 0.6 mL of water, and mixed with a PGA stock solution (0.4 mL, 6 mg PGA/mL). After pre-emulsification in a PGPR solution (1wt% in 7.5 mL cyclohexane), the coarse emulsion was ultrasonicated for 1 min with ice-water cooling bath (Branson Sonifier W450, ½ inch probe). A GC stock solution (1 mL) was emulsified in the same way and was mixed with the PGA miniemulsion. A GluNa solution (3 mL, 10wt%, pH = 6.0) was emulsified in the same way. The mixture was then ultrasonicated for 30 s. A predetermined amount of crosslinker (TDI) was diluted with toluene and injected in the emulsion. After 10 min of reaction at room temperature, the emulsion of GluNa (16 mL) was added and the mixture was ultrasonicated for 30 s. The final emulsion was diluted with 360 mL hexane and the oil phase was removed by centrifugation (2000 g, 15 °C, 5 min). The further purification followed that for GCNCs. For SEM sampling, the final dispersion was cast onto a silicon wafer and left to dry. The wafer surface was rinsed with a water droplet 3 times to remove the soluble fraction.

5.4.5. In-vitro release of rPYY-FITC from polyplex-based nanocarriers

The release of rPYY-FITC from polyplex-based nanocarriers was monitored by the fluorescence intensity of the peptide [7]. Aliquots of frozen were thawed at room temperature and diluted with sterile water. A small fraction (typically 10 μL) of the rPYY-FITC solution was further diluted and stored at 4 °C in the dark as a reference sample. The suspensions were stirred at room temperature and aliquots of the dispersions were sampled at a predetermined time and centrifuged (20,000 G, 15 °C, 20 min). The supernatant and the reference sample were collected, and 10-fold diluted with a phosphate buffer (0.1 M, pH 6.0) with dissolved Pluronic F68 (5 mg/mL). The fluorescence intensity (excitation: 490 nm, emission: 515 nm)

was recorded and compared with the reference sample. The relative release was determined to be the ratio of the concentration of rPYY-FITC in the release medium to the concentration of originally encapsulated peptide. In some cases, the fluorescence intensity of the sampled NP dispersions was measured without centrifugation so that the overall fluorescence signal was recorded. This corresponded therefore to the total amount of rPYY-FITC in the dispersions.

6. Conclusions

In this work, we describe in section 4.1 to 4.3 a new strategy for the synthesis of pH-responsive nanocarriers based on polyelectrolyte complexes of GC and PGA for the controlled release of peptides. The main drawbacks of the widely used complexation method were successfully overcome by confining the complexation in nanodroplets and by subsequent interfacial crosslinking to stabilize the formed NPs. We studied the effect of surface crosslinking reaction on the polyelectrolyte complex, in terms of the relationship between the dosage of crosslinker and the final crosslinking density. Finally, the in-vitro pH-responsive release profile of the encapsulated peptide drug is studied. The target drug peptide PYY, known to hinder obesity was successfully encapsulated in the nanocarriers and was found to remain active after encapsulation. Such systems could also be applied for oral delivery of other peptides because these GC coated carriers could protect the peptide from degradation or hydrolysis in the duodenum (pH = 6) and endothelial cells (pH = 4.5, cytosol, endosome), and then release the payload in the bloodstream (pH = 7.4). The described method hence provides a new solution against overweight since it is the first approach against obesity that is based on NPs delivery. We anticipate that such an approach could be extended to other peptides and other polyelectrolytes allowing for a release of payloads at different pH values.

In section 4.4, we have described a hierarchically structured peptide delivery system, which can release multi-functional nanocarriers upon a first stimulus, while the peptide payload can be further released from the pH-responsive nanocarriers in a sustained manner. Such step-wise encapsulation strategy shows potential in complicated drug delivery tasks like oral delivery of peptide drugs. Further research like *in vivo* studies on the release profile and functionalization for the multi-stimulus response of NP-in-NF systems can be performed based on this system. Due to the high variability of the detailed composition of the system, we

believe that it can be adjusted to a variety of hydrophilic drugs and is, thus, of broad general interest.

In section 4.5, we have described a new method for the recovery of hydrophilic NPs in an efficient and mild manner, which enables the re-dispersion of chemically crosslinked CS particle in water without additional surfactant. As a proof of concept, the technique was developed for GC-based nanocarriers, because the polymer of the shell has good solubility in water. We believe that the “cushion” method is also suitable for polyamines based reactive encapsulations or other polymeric nanoparticles that have good compatibility in water. In this sense, further study on the usability of the “cushion” method on other materials is needed. Besides, a variety of non-toxic small molecules can be used instead of the monosodium glutamate for the “cushion” method. Thus, the selection criteria of the “cushion” molecule and their effect on the potential application would an interesting research topic.

7. References

1. Gupta, S., et al., *Oral Delivery of Therapeutic Proteins and Peptides: A Review on Recent Developments.* Drug Deliv, 2013. **20**(6). p. 237-46.

2. Win, K.Y. and S.S. Feng, *Effects of Particle Size and Surface Coating on Cellular Uptake of Polymeric Nanoparticles for Oral Delivery of Anticancer Drugs.* Biomaterials, 2005. **26**(15). p. 2713-22.

3. des Rieux, A., et al., *Nanoparticles as Potential Oral Delivery Systems of Proteins and Vaccines: A Mechanistic Approach.* J Control Release, 2006. **116**(1). p. 1-27.

4. Renukuntla, J., et al., *Approaches for Enhancing Oral Bioavailability of Peptides and Proteins.* Int. J. Pharm., 2013. **447**(1-2). p. 75-93.

5. Yun, Y., Y.W. Cho, and K. Park, *Nanoparticles for Oral Delivery: Targeted Nanoparticles with Peptidic Ligands for Oral Protein Delivery.* Adv Drug Deliv Rev, 2013. **65**(6). p. 822-32.

6. Mura, S., J. Nicolas, and P. Couvreur, *Stimuli-Responsive Nanocarriers for Drug Delivery.* Nat Mater, 2013. **12**(11). p. 991-1003.

7. Bhattarai, N., J. Gunn, and M. Zhang, *Chitosan-Based Hydrogels for Controlled, Localized Drug Delivery.* Adv Drug Deliv Rev, 2010. **62**(1). p. 83-99.

8. Serra, L., J. Domenech, and N.A. Peppas, *Engineering Design and Molecular Dynamics of Mucoadhesive Drug Delivery Systems as Targeting Agents.* Eur J Pharm Biopharm, 2009. **71**(3). p. 519-28.

9. Doane, T. and C. Burda, *Nanoparticle Mediated Non-Covalent Drug Delivery.* Adv Drug Deliv Rev, 2013. **65**(5). p. 607-21.

10. Liu, D., et al., *Microfluidic Assisted One-Step Fabrication of Porous Silicon@Acetalated Dextran Nanocomposites for Precisely Controlled Combination Chemotherapy.* Biomaterials, 2015. **39**. p. 249-59.

11. Shrestha, N., et al., *Multistage Ph-Responsive Mucoadhesive Nanocarriers Prepared by Aerosol Flow Reactor Technology: A Controlled Dual Protein-Drug Delivery System.* Biomaterials, 2015. **68**. p. 9-20.

12. Kovalainen, M., et al., *Mesoporous Silicon (Psi) for Sustained Peptide Delivery: Effect of Psi Microparticle Surface Chemistry on Peptide Yy3-36 Release.* Pharm. Res., 2012. **29**(3). p. 837-46.

13. Crespy, D., K. Friedemann, and A.M. Popa, *Colloid-Electrospinning: Fabrication of Multicompartment Nanofibers by the Electrospinning of Organic or/and Inorganic Dispersions and Emulsions.* Macromol. Rapid Commun., 2012. **33**(23). p. 1978-95.

14. Qi, R., et al., *Controlled Release and Antibacterial Activity of Antibiotic-Loaded Electrospun Halloysite/Poly(Lactic-Co-Glycolic Acid) Composite Nanofibers.* Colloids Surf B Biointerfaces, 2013. **110**. p. 148-55.

15. Bansal, P., et al., *Water-Stable All-Biodegradable Microparticles in Nanofibers by Electrospinning of Aqueous Dispersions for Biotechnical Plant Protection.* Biomacromolecules, 2012. **13**(2). p. 439-44.

16. Xue, J., et al., *Electrospun Microfiber Membranes Embedded with Drug-Loaded Clay Nanotubes for Sustained Antimicrobial Protection.* ACS Nano, 2015. **9**(2). p. 1600-12.

17. Yu, F., et al., *Enteric-Coated Capsules Filled with Mono-Disperse Micro-Particles Containing Plga-Lipid-Peg Nanoparticles for Oral Delivery of Insulin.* Int. J. Pharm., 2015. **484**(1-2). p. 181-91.

18. Kong, F., et al., *Inhibition of Multidrug Resistance of Cancer Cells by Co-Delivery of DNA Nanostructures and Drugs Using Porous Silicon Nanoparticles@Giant Liposomes.* Adv. Funct. Mater., 2015. **25**(22). p. 3330-3340.

19. Zhang, H., et al., *Fabrication of a Multifunctional Nano-in-Micro Drug Delivery Platform by Microfluidic Templated Encapsulation of Porous Silicon in Polymer Matrix.* Adv. Mater., 2014. **26**(26). p. 4497-503.

20. Khung, Y.L., et al., *Microencapsulation of Dye- and Drug-Loaded Particles for Imaging and Controlled Release of Multiple Drugs.* Adv Healthc Mater, 2012. **1**(2). p. 159-63.

21. DeVolder, R.J., et al., *Directed Blood Vessel Growth Using an Angiogenic Microfiber/Microparticle Composite Patch.* Adv. Mater., 2011. **23**(28). p. 3139-43.

22. Wei, G., et al., *Nano-Fibrous Scaffold for Controlled Delivery of Recombinant Human Pdgf-Bb.* J Control Release, 2006. **112**(1). p. 103-10.

23. Ionescu, L.C., et al., *An Anisotropic Nanofiber/Microsphere Composite with Controlled Release of Biomolecules for Fibrous Tissue Engineering.* Biomaterials, 2010. **31**(14). p. 4113-20.

24. Sonaje, K., et al., *Enteric-Coated Capsules Filled with Freeze-Dried Chitosan/Poly(Gamma-Glutamic Acid) Nanoparticles for Oral Insulin Delivery.* Biomaterials, 2010. **31**(12). p. 3384-94.

25. Kennedy, S., et al., *Sequential Release of Nanoparticle Payloads from Ultrasonically Burstable Capsules.* Biomaterials, 2016. **75**. p. 91-101.

26. Yilgor, P., et al., *An in Vivo Study on the Effect of Scaffold Geometry and Growth Factor Release on the Healing of Bone Defects.* J Tissue Eng Regen Med, 2013. **7**(9). p. 687-96.

27. Huang, X. and C.S. Brazel, *On the Importance and Mechanisms of Burst Release in Matrix-Controlled Drug Delivery Systems.* J Control Release, 2001. **73**(2-3). p. 121-36.

28. Zhang, C.L. and S.H. Yu, *Nanoparticles Meet Electrospinning: Recent Advances and Future Prospects.* Chem. Soc. Rev., 2014. **43**(13). p. 4423-48.

29. Hasan, A.S., et al., *Effect of the Microencapsulation of Nanoparticles on the Reduction of Burst Release.* Int. J. Pharm., 2007. **344**(1-2). p. 53-61.

30. Beck-Broichsitter, M., et al., *Novel 'Nano in Nano' Composites for Sustained Drug Delivery: Biodegradable Nanoparticles Encapsulated into Nanofiber Non-Wovens.* Macromol Biosci, 2010. **10**(12). p. 1527-35.

31. Li, L., et al., *Controlled Dual Delivery of Bmp-2 and Dexamethasone by Nanoparticle-Embedded Electrospun Nanofibers for the Efficient Repair of Critical-Sized Rat Calvarial Defect.* Biomaterials, 2015. **37**. p. 218-29.

32. Xu, X., et al., *The Release Behavior of Doxorubicin Hydrochloride from Medicated Fibers Prepared by Emulsion-Electrospinning.* Eur J Pharm Biopharm, 2008. **70**(1). p. 165-70.

33. He, W., et al., *Nanocarrier for Oral Peptide Delivery Produced by Polyelectrolyte Complexation in Nanoconfinement.* Biomacromolecules, 2015. **16**(8). p. 2282-7.

34. Wang, J.J., et al., *Recent Advances of Chitosan Nanoparticles as Drug Carriers.* Int J Nanomedicine, 2011. **6**. p. 765-74.

35. Bernkop-Schnurch, A. and S. Dunnhaupt, *Chitosan-Based Drug Delivery Systems.* Eur J Pharm Biopharm, 2012. **81**(3). p. 463-9.

36. Janes, K.A., P. Calvo, and M.J. Alonso, *Polysaccharide Colloidal Particles as Delivery Systems for Macromolecules.* Advanced Drug Delivery Reviews, 2001. **47**(1). p. 83-97.

37. Xia, W.S., et al., *Biological Activities of Chitosan and Chitooligosaccharides.* Food Hydrocolloids, 2011. **25**(2). p. 170-179.

38. Chaudhury, A. and S. Das, *Recent Advancement of Chitosan-Based Nanoparticles for Oral Controlled Delivery of Insulin and Other Therapeutic Agents.* AAPS PharmSciTech, 2011. **12**(1). p. 10-20.

39. Berger, J., et al., *Structure and Interactions in Covalently and Ionically Crosslinked Chitosan Hydrogels for Biomedical Applications.* Eur J Pharm Biopharm, 2004. **57**(1). p. 19-34.

40. Hamman, J.H., *Chitosan Based Polyelectrolyte Complexes as Potential Carrier Materials in Drug Delivery Systems.* Mar Drugs, 2010. **8**(4). p. 1305-22.

41. Liao, Z.X., et al., *Mechanistic Study of Transfection of Chitosan/DNA Complexes Coated by Anionic Poly(Gamma-Glutamic Acid).* Biomaterials, 2012. **33**(11). p. 3306-15.

42. Pergushov, D.V., A.H. Muller, and F.H. Schacher, *Micellar Interpolyelectrolyte Complexes.* Chem. Soc. Rev., 2012. **41**(21). p. 6888-901.

43. Lin, Y.H., et al., *Multi-Ion-Crosslinked Nanoparticles with Ph-Responsive Characteristics for Oral Delivery of Protein Drugs.* J Control Release, 2008. **132**(2). p. 141-9.

44. Berger, J., et al., *Structure and Interactions in Chitosan Hydrogels Formed by Complexation or Aggregation for Biomedical Applications.* Eur J Pharm Biopharm, 2004. **57**(1). p. 35-52.

45. Thunemann, A.F., et al., *Polyelectrolyte Complexes*, in *Polyelectrolytes with Defined Molecular Architecture Ii*, M. Schmidt, Editor. 2004, Springer-Verlag: Berlin Heidelberg. p. 113-171.

46. Klinger, D. and K. Landfester, *Stimuli-Responsive Microgels for the Loading and Release of Functional Compounds: Fundamental Concepts and Applications.* Polymer, 2012. **53**(23). p. 5209-5231.

47. Krumpfer, J.W., et al., *Make It Nano-Keep It Nano.* Nano Today, 2013. **8**(4). p. 417-438.

48. Maier, M., et al., *Highly Site Specific, Protease Cleavable, Hydrophobic Peptide-Polymer Nanoparticles.* Macromolecules, 2011. **44**(16). p. 6258-6267.

49. Dorresteijn, R., et al., *Polylactide-Block-Polypeptide-Block-Polylactide Copolymer Nanoparticles with Tunable Cleavage and Controlled Drug Release.* Adv. Funct. Mater., 2014. **24**(26). p. 4026-4033.

50. Andrieu, J., et al., *Live Monitoring of Cargo Release from Peptide-Based Hybrid Nanocapsules Induced by Enzyme Cleavage.* Macromol. Rapid Commun., 2012. **33**(3). p. 248-53.

51. Pellegrino, T., et al., *Hydrophobic Nanocrystals Coated with an Amphiphilic Polymer Shell: A General Route to Water Soluble Nanocrystals.* Nano Lett., 2004. **4**(4). p. 703-707.

52. Sperling, R.A., et al., *Size Determination of (Bio)Conjugated Water-Soluble Colloidal Nanoparticles: A Comparison of Different Techniques.* Journal of Physical Chemistry C, 2007. **111**(31). p. 11552-11559.

53. Bronstein, L.M., et al., *Hydrophilization of Magnetic Nanoparticles with Modified Alternating Copolymers. Part 1: The Influence of the Grafting.* J Phys Chem C Nanomater Interfaces, 2010. **114**(50). p. 21900-21907.

54. Huhn, D., et al., *Polymer-Coated Nanoparticles Interacting with Proteins and Cells: Focusing on the Sign of the Net Charge.* ACS Nano, 2013. **7**(4). p. 3253-63.

55. Lin, C.A., et al., *Design of an Amphiphilic Polymer for Nanoparticle Coating and Functionalization.* Small, 2008. **4**(3). p. 334-41.

56. Geidel, C., et al., *A General Synthetic Approach for Obtaining Cationic and Anionic Inorganic Nanoparticles Via Encapsulation in Amphiphilic Copolymers.* Small, 2011. **7**(20). p. 2929-34.

57. Dorresteijn, R., et al., *Biocompatible Polylactide-Block-Polypeptide-Block-Polylactide Nanocarrier.* Biomacromolecules, 2013. **14**(5). p. 1572-7.

58. Dorresteijn, R., et al., *Poly(L-Lactide) Nanoparticles Via Ring-Opening Polymerization in Non-Aqueous Emulsion.* Macromol. Chem. Phys., 2012. **213**(19). p. 1996-2002.

59. Dorresteijn, R., et al., *Polarity Reversal of Nanoparticle Surfaces by the Use of Light-Sensitive Polymeric Emulsifiers.* Journal of Polymer Science Part a-Polymer Chemistry, 2015. **53**(2). p. 200-205.

60. Ujhelyi, Z., et al., *Evaluation of Cytotoxicity of Surfactants Used in Self-Micro Emulsifying Drug Delivery Systems and Their Effects on Paracellular Transport in Caco-2 Cell Monolayer.* Eur J Pharm Sci, 2012. **47**(3). p. 564-73.

61. Machado, A.H., et al., *Preparation of Calcium Alginate Nanoparticles Using Water-in-Oil (W/O) Nanoemulsions.* Langmuir, 2012. **28**(9). p. 4131-41.

62. Machado, A.H., et al., *Encapsulation of DNA in Macroscopic and Nanosized Calcium Alginate Gel Particles.* Langmuir, 2013. **29**(51). p. 15926-35.

63. Ethirajan, A., et al., *Synthesis and Optimization of Gelatin Nanoparticles Using the Miniemulsion Process.* Biomacromolecules, 2008. **9**(9). p. 2383-9.

64. Groll, J., et al., *Biocompatible and Degradable Nanogels Via Oxidation Reactions of Synthetic Thiomers in Inverse Miniemulsion.* Journal of Polymer Science Part a-Polymer Chemistry, 2009. **47**(20). p. 5543-5549.

65. Lee, H., et al., *Target-Specific Intracellular Delivery of Sirna Using Degradable Hyaluronic Acid Nanogels.* J Control Release, 2007. **119**(2). p. 245-52.

66. Sundaramurthi, P. and R. Suryanarayanan, *Trehalose Crystallization During Freeze-Drying: Implications on Lyoprotection.* Journal of Physical Chemistry Letters, 2010. **1**(2). p. 510-514.

67. Liu, Z.H., et al., *Hydrophobic Modifications of Cationic Polymers for Gene Delivery.* Prog. Polym. Sci., 2010. **35**(9). p. 1144-1162.

68. Du, J.Z., et al., *Tailor-Made Dual Ph-Sensitive Polymer-Doxorubicin Nanoparticles for Efficient Anticancer Drug Delivery.* J. Am. Chem. Soc., 2011. **133**(44). p. 17560-3.

69. Radovic-Moreno, A.F., et al., *Surface Charge-Switching Polymeric Nanoparticles for Bacterial Cell Wall-Targeted Delivery of Antibiotics.* ACS Nano, 2012. **6**(5). p. 4279-87.

70. Gerweck, L.E., S. Vijayappa, and S. Kozin, *Tumor Ph Controls the in Vivo Efficacy of Weak Acid and Base Chemotherapeutics.* Mol Cancer Ther, 2006. **5**(5). p. 1275-9.

71. You, J.O. and D.T. Auguste, *Nanocarrier Cross-Linking Density and Ph Sensitivity Regulate Intracellular Gene Transfer.* Nano Lett., 2009. **9**(12). p. 4467-73.

72. Modi, S., et al., *A DNA Nanomachine That Maps Spatial and Temporal Ph Changes inside Living Cells.* Nat Nanotechnol, 2009. **4**(5). p. 325-30.

73. Jin, Y., et al., *Oxime Linkage: A Robust Tool for the Design of Ph-Sensitive Polymeric Drug Carriers.* Biomacromolecules, 2011. **12**(10). p. 3460-8.

74. Du, Y., et al., *Ph-Sensitive Degradable Chimaeric Polymersomes for the Intracellular Release of Doxorubicin Hydrochloride.* Biomaterials, 2012. **33**(29). p. 7291-9.

75. Griset, A.P., et al., *Expansile Nanoparticles: Synthesis, Characterization, and in Vivo Efficacy of an Acid-Responsive Polymeric Drug Delivery System.* J. Am. Chem. Soc., 2009. **131**(7). p. 2469-71.

76. Ahmed, M. and R. Narain, *Intracellular Delivery of DNA and Enzyme in Active Form Using Degradable Carbohydrate-Based Nanogels.* Mol Pharm, 2012. **9**(11). p. 3160-70.

77. Deng, Z., et al., *Hollow Chitosan-Silica Nanospheres as Ph-Sensitive Targeted Delivery Carriers in Breast Cancer Therapy.* Biomaterials, 2011. **32**(21). p. 4976-86.

78. Min, K.H., et al., *Tumoral Acidic Ph-Responsive Mpeg-Poly(Beta-Amino Ester) Polymeric Micelles for Cancer Targeting Therapy.* J Control Release, 2010. **144**(2). p. 259-66.

79. Gao, G.H., et al., *The Use of Ph-Sensitive Positively Charged Polymeric Micelles for Protein Delivery.* Biomaterials, 2012. **33**(35). p. 9157-64.

80. Lee, C.H., et al., *Synthesis and Characterization of Positive-Charge Functionalized Mesoporous Silica Nanoparticles for Oral Drug Delivery of an Anti-Inflammatory Drug.* Adv. Funct. Mater., 2008. **18**(20). p. 3283-3292.

81. Lee, E.S., et al., *Super Ph-Sensitive Multifunctional Polymeric Micelle for Tumor Ph(E) Specific Tat Exposure and Multidrug Resistance.* J Control Release, 2008. **129**(3). p. 228-36.

82. Koren, E., et al., *Multifunctional Pegylated 2c5-Immunoliposomes Containing Ph-Sensitive Bonds and Tat Peptide for Enhanced Tumor Cell Internalization and Cytotoxicity.* J Control Release, 2012. **160**(2). p. 264-73.

83. Quan, C.Y., et al., *Core-Shell Nanosized Assemblies Mediated by the Alpha-Beta Cyclodextrin Dimer with a Tumor-Triggered Targeting Property.* ACS Nano, 2010. **4**(7). p. 4211-9.

84. Chang Kang, H. and Y.H. Bae, *Co-Delivery of Small Interfering Rna and Plasmid DNA Using a Polymeric Vector Incorporating Endosomolytic Oligomeric Sulfonamide.* Biomaterials, 2011. **32**(21). p. 4914-24.

85. Su, X., et al., *In Vitro and in Vivo Mrna Delivery Using Lipid-Enveloped Ph-Responsive Polymer Nanoparticles.* Mol Pharm, 2011. **8**(3). p. 774-87.

86. Zhang, C.Y., et al., *Self-Assembled Ph-Responsive Mpeg-B-(Pla-Co-Pae) Block Copolymer Micelles for Anticancer Drug Delivery.* Biomaterials, 2012. **33**(26). p. 6273-83.

87. Lee, E.S., et al., *A Virus-Mimetic Nanogel Vehicle.* Angew. Chem. Int. Ed. Engl., 2008. **47**(13). p. 2418-21.

88. Kim, D., et al., *Doxorubicin-Loaded Polymeric Micelle Overcomes Multidrug Resistance of Cancer by Double-Targeting Folate Receptor and Early Endosomal Ph.* Small, 2008. **4**(11). p. 2043-50.

89. Dehousse, V., et al., *Development of Ph-Responsive Nanocarriers Using Trimethylchitosans and Methacrylic Acid Copolymer for Sirna Delivery.* Biomaterials, 2010. **31**(7). p. 1839-49.

90. Zhang, J., et al., *The Targeted Behavior of Thermally Responsive Nanohydrogel Evaluated by Nir System in Mouse Model.* J Control Release, 2008. **131**(1). p. 34-40.

91. Tagami, T., et al., *Mri Monitoring of Intratumoral Drug Delivery and Prediction of the Therapeutic Effect with a Multifunctional Thermosensitive Liposome.* Biomaterials, 2011. **32**(27). p. 6570-8.

92. Cheng, Y., et al., *Thermally Controlled Release of Anticancer Drug from Self-Assembled Gamma-Substituted Amphiphilic Poly(Epsilon-Caprolactone) Micellar Nanoparticles.* Biomacromolecules, 2012. **13**(7). p. 2163-73.

93. Al-Ahmady, Z.S., et al., *Lipid-Peptide Vesicle Nanoscale Hybrids for Triggered Drug Release by Mild Hyperthermia in Vitro and in Vivo.* ACS Nano, 2012. **6**(10). p. 9335-46.

94. Chen, K.J., et al., *A Thermoresponsive Bubble-Generating Liposomal System for Triggering Localized Extracellular Drug Delivery.* ACS Nano, 2013. **7**(1). p. 438-46.

95. Macewan, S.R. and A. Chilkoti, *Digital Switching of Local Arginine Density in a Genetically Encoded Self-Assembled Polypeptide Nanoparticle Controls Cellular Uptake.* Nano Lett., 2012. **12**(6). p. 3322-8.

96. Sun, Y., et al., *Disassemblable Micelles Based on Reduction-Degradable Amphiphilic Graft Copolymers for Intracellular Delivery of Doxorubicin.* Biomaterials, 2010. **31**(27). p. 7124-31.

97. Koo, A.N., et al., *Disulfide-Cross-Linked Peg-Poly(Amino Acid)S Copolymer Micelles for Glutathione-Mediated Intracellular Drug Delivery.* Chem Commun (Camb), 2008(48). p. 6570-2.

98. Li, Y., et al., *Well-Defined, Reversible Disulfide Cross-Linked Micelles for on-Demand Paclitaxel Delivery.* Biomaterials, 2011. **32**(27). p. 6633-45.

99. Ryu, J.H., et al., *Self-Cross-Linked Polymer Nanogels: A Versatile Nanoscopic Drug Delivery Platform.* J. Am. Chem. Soc., 2010. **132**(48). p. 17227-35.

100. Li, J., et al., *Redox-Sensitive Micelles Self-Assembled from Amphiphilic Hyaluronic Acid-Deoxycholic Acid Conjugates for Targeted Intracellular Delivery of Paclitaxel.* Biomaterials, 2012. **33**(7). p. 2310-20.

101. Kim, H., et al., *Glutathione-Induced Intracellular Release of Guests from Mesoporous Silica Nanocontainers with Cyclodextrin Gatekeepers.* Adv. Mater., 2010. **22**(38). p. 4280-3.

102. Ong, W., et al., *Redox-Triggered Contents Release from Liposomes.* J. Am. Chem. Soc., 2008. **130**(44). p. 14739-44.

103. Kurtoglu, Y.E., et al., *Poly(Amidoamine) Dendrimer-Drug Conjugates with Disulfide Linkages for Intracellular Drug Delivery.* Biomaterials, 2009. **30**(11). p. 2112-21.

104. Suma, T., et al., *Smart Multilayered Assembly for Biocompatible Sirna Delivery Featuring Dissolvable Silica, Endosome-Disrupting Polycation, and Detachable Peg.* ACS Nano, 2012. **6**(8). p. 6693-705.

105. Wilson, D.S., et al., *Orally Delivered Thioketal Nanoparticles Loaded with Tnf-Alpha-Sirna Target Inflammation and Inhibit Gene Expression in the Intestines.* Nat Mater, 2010. **9**(11). p. 923-8.

106. Zhang, L., et al., *General Route to Multifunctional Uniform Yolk/Mesoporous Silica Shell Nanocapsules: A Platform for Simultaneous Cancer-Targeted Imaging and Magnetically Guided Drug Delivery.* Chemistry, 2012. **18**(39). p. 12512-21.

107. Hua, M.Y., et al., *The Effectiveness of a Magnetic Nanoparticle-Based Delivery System for Bcnu in the Treatment of Gliomas.* Biomaterials, 2011. **32**(2). p. 516-27.

108. Katagiri, K., et al., *Magnetoresponsive on-Demand Release of Hybrid Liposomes Formed from Fe3 O4 Nanoparticles and Thermosensitive Block Copolymers.* Small, 2011. **7**(12). p. 1683-9.

109. Plassat, V., et al., *Anti-Estrogen-Loaded Superparamagnetic Liposomes for Intracellular Magnetic Targeting and Treatment of Breast Cancer Tumors.* Adv. Funct. Mater., 2011. **21**(1). p. 83-92.

110. Huang, H.Y., et al., *Self-Assembling Pva-F127 Thermosensitive Nanocarriers with Highly Sensitive Magnetically-Triggered Drug Release for Epilepsy Therapy in Vivo.* J. Mater. Chem., 2012. **22**(17). p. 8566-8573.

111. Qin, J., et al., *Injectable Superparamagnetic Ferrogels for Controlled Release of Hydrophobic Drugs.* Adv. Mater., 2009. **21**(13). p. 1354-1357.

112. Cai, K.Y., et al., *Magnetically Triggered Reversible Controlled Drug Delivery from Microfabricated Polymeric Multireservoir Devices.* Adv. Mater., 2009. **21**(40). p. 4045-+.

113. Zhang, F., et al., *Mesoporous Multifunctional Upconversion Luminescent and Magnetic "Nanorattle" Materials for Targeted Chemotherapy.* Nano Lett., 2012. **12**(1). p. 61-7.

114. Tang, Y.S., et al., *Bacterial Magnetic Particles as a Novel and Efficient Gene Vaccine Delivery System.* Gene Ther, 2012. **19**(12). p. 1187-95.

115. Arias, J.L., et al., *Squalene Based Nanocomposites: A New Platform for the Design of Multifunctional Pharmaceutical Theragnostics.* ACS Nano, 2011. **5**(2). p. 1513-21.

116. Park, J.W., et al., *Clustered Magnetite Nanocrystals Cross-Linked with Pei for Efficient Sirna Delivery.* Biomacromolecules, 2011. **12**(2). p. 457-65.

117. Prijic, S., et al., *Surface Modified Magnetic Nanoparticles for Immuno-Gene Therapy of Murine Mammary Adenocarcinoma.* Biomaterials, 2012. **33**(17). p. 4379-91.

118. Jenkins, S.I., et al., *Magnetic Nanoparticle-Mediated Gene Transfer to Oligodendrocyte Precursor Cell Transplant Populations Is Enhanced by Magnetofection Strategies.* ACS Nano, 2011. **5**(8). p. 6527-38.

119. Al-Deen, F.N., et al., *Superparamagnetic Nanoparticles for Effective Delivery of Malaria DNA Vaccine.* Langmuir, 2011. **27**(7). p. 3703-12.

120. Chorny, M., et al., *Endothelial Delivery of Antioxidant Enzymes Loaded into Non-Polymeric Magnetic Nanoparticles.* J Control Release, 2010. **146**(1). p. 144-51.

121. Pradhan, P., et al., *Targeted Temperature Sensitive Magnetic Liposomes for Thermo-Chemotherapy.* J Control Release, 2010. **142**(1). p. 108-21.

122. Hoare, T., et al., *Magnetically Triggered Nanocomposite Membranes: A Versatile Platform for Triggered Drug Release.* Nano Lett., 2011. **11**(3). p. 1395-400.

123. Satarkar, N.S. and J. Zach Hilt, *Hydrogel Nanocomposites as Remote-Controlled Biomaterials.* Acta Biomater, 2008. **4**(1). p. 11-6.

124. Thomas, C.R., et al., *Noninvasive Remote-Controlled Release of Drug Molecules in Vitro Using Magnetic Actuation of Mechanized Nanoparticles.* J. Am. Chem. Soc., 2010. **132**(31). p. 10623-5.

125. Stanley, S.A., et al., *Radio-Wave Heating of Iron Oxide Nanoparticles Can Regulate Plasma Glucose in Mice.* Science, 2012. **336**(6081). p. 604-8.

126. Derfus, A.M., et al., *Remotely Triggered Release from Magnetic Nanoparticles.* Adv. Mater., 2007. **19**(22). p. 3932-+.

127. Ruiz-Hernandez, E., A. Baeza, and M. Vallet-Regi, *Smart Drug Delivery through DNA/Magnetic Nanoparticle Gates.* ACS Nano, 2011. **5**(2). p. 1259-66.

128. Vrignaud, S., J.P. Benoit, and P. Saulnier, *Strategies for the Nanoencapsulation of Hydrophilic Molecules in Polymer-Based Nanoparticles.* Biomaterials, 2011. **32**(33). p. 8593-604.

129. Wang, W., *Protein Aggregation and Its Inhibition in Biopharmaceutics.* Int. J. Pharm., 2005. **289**(1-2). p. 1-30.

130. Lu, Y., W. Sun, and Z. Gu, *Stimuli-Responsive Nanomaterials for Therapeutic Protein Delivery.* J Control Release, 2014. **194**. p. 1-19.

131. Prego, C., et al., *Chitosan-Peg Nanocapsules as New Carriers for Oral Peptide Delivery. Effect of Chitosan Pegylation Degree.* J Control Release, 2006. **111**(3). p. 299-308.

132. Qu, W., et al., *A Silica-Based Ph-Sensitive Nanomatrix System Improves the Oral Absorption and Efficacy of Incretin Hormone Glucagon-Like Peptide-1.* Int J Nanomedicine, 2012. **7**. p. 4983-94.

133. Pan, Y., et al., *Bioadhesive Polysaccharide in Protein Delivery System: Chitosan Nanoparticles Improve the Intestinal Absorption of Insulin in Vivo.* Int. J. Pharm., 2002. **249**(1-2). p. 139-47.

134. Sadeghi, A.M., et al., *Permeation Enhancer Effect of Chitosan and Chitosan Derivatives: Comparison of Formulations as Soluble Polymers and Nanoparticulate Systems on Insulin Absorption in Caco-2 Cells.* Eur J Pharm Biopharm, 2008. **70**(1). p. 270-8.

135. Gu, Z., et al., *Protein Nanocapsule Weaved with Enzymatically Degradable Polymeric Network.* Nano Lett., 2009. **9**(12). p. 4533-8.

136. Vauthier, C. and K. Bouchemal, *Methods for the Preparation and Manufacture of Polymeric Nanoparticles.* Pharm. Res., 2009. **26**(5). p. 1025-58.

137. Kim, S.H., et al., *Vegf Sirna Delivery System Using Arginine-Grafted Bioreducible Poly(Disulfide Amine).* Mol Pharm, 2009. **6**(3). p. 718-26.

138. Vader, P., et al., *Disulfide-Based Poly(Amido Amine)S for Sirna Delivery: Effects of Structure on Sirna Complexation, Cellular Uptake, Gene Silencing and Toxicity.* Pharm. Res., 2011. **28**(5). p. 1013-22.

139. Mok, H., et al., *Multimeric Small Interfering Ribonucleic Acid for Highly Efficient Sequence-Specific Gene Silencing.* Nat Mater, 2010. **9**(3). p. 272-8.

140. Takemoto, H., et al., *Polyion Complex Stability and Gene Silencing Efficiency with a Sirna-Grafted Polymer Delivery System.* Biomaterials, 2010. **31**(31). p. 8097-105.

141. Lin, Y.H., et al., *Preparation and Characterization of Nanoparticles Shelled with Chitosan for Oral Insulin Delivery.* Biomacromolecules, 2007. **8**(1). p. 146-52.

142. Chen, M.C., et al., *The Characteristics, Biodistribution and Bioavailability of a Chitosan-Based Nanoparticulate System for the Oral Delivery of Heparin.* Biomaterials, 2009. **30**(34). p. 6629-37.

143. Peng, S.F., et al., *Effects of Incorporation of Poly(Gamma-Glutamic Acid) in Chitosan/DNA Complex Nanoparticles on Cellular Uptake and Transfection Efficiency.* Biomaterials, 2009. **30**(9). p. 1797-808.

144. Lee, P.W., et al., *The Use of Biodegradable Polymeric Nanoparticles in Combination with a Low-Pressure Gene Gun for Transdermal DNA Delivery.* Biomaterials, 2008. **29**(6). p. 742-51.

145. Reis, C.P., et al., *Nanoencapsulation Ii. Biomedical Applications and Current Status of Peptide and Protein Nanoparticulate Delivery Systems.* Nanomedicine, 2006. **2**(2). p. 53-65.

146. Chen, M.C., et al., *Recent Advances in Chitosan-Based Nanoparticles for Oral Delivery of Macromolecules.* Adv Drug Deliv Rev, 2013. **65**(6). p. 865-79.

147. Wang, X.Q. and Q. Zhang, *Ph-Sensitive Polymeric Nanoparticles to Improve Oral Bioavailability of Peptide/Protein Drugs and Poorly Water-Soluble Drugs.* Eur J Pharm Biopharm, 2012. **82**(2). p. 219-29.

148. Sung, H.W., et al., *Ph-Responsive Nanoparticles Shelled with Chitosan for Oral Delivery of Insulin: From Mechanism to Therapeutic Applications.* Acc. Chem. Res., 2012. **45**(4). p. 619-29.

149. Rinaudo, M., *Chitin and Chitosan: Properties and Applications.* Prog. Polym. Sci., 2006. **31**(7). p. 603-632.

150. Prashanth, K.V.H. and R.N. Tharanathan, *Chitin/Chitosan: Modifications and Their Unlimited Application Potential - an Overview.* Trends in Food Science & Technology, 2007. **18**(3). p. 117-131.

151. Mathur, N.K. and C.K. Narang, *Chitin and Chitosan, Versatile Polysaccharides from Marine Animals.* J. Chem. Educ., 1990. **67**(11). p. 938-942.

152. Aiba, S., *Studies on Chitosan: 3. Evidence for the Presence of Random and Block Copolymer Structures in Partially N-Acetylated Chitosans.* Int. J. Biol. Macromol., 1991. **13**(1). p. 40-4.

153. Kubota, N. and Y. Eguchi, *Facile Preparation of Water-Soluble N-Acetylated Chitosan and Molecular Weight Dependence of Its Water-Solubility.* Polym. J., 1997. **29**(2). p. 123-127.

154. Tabujew, I. and K. Peneva, *Chapter 1. Functionalization of Cationic Polymers for Drug Delivery Applications*, in *Cationic Polymers in Regenerative Medicine*. 2014, The Royal Society of Chemistry. p. 1-29.

155. Morimoto, M., H. Saimoto, and Y. Shigemasa, *Control of Functions of Chitin and Chitosan by Chemical Modification.* Trends in Glycoscience and Glycotechnology, 2002. **14**(78). p. 205-222.

156. Fukamizo, T., *Chitinolytic Enzymes: Catalysis, Substrate Binding, and Their Application.* Current Protein & Peptide Science, 2000. **1**(1). p. 105-124.

157. Xia, W., P. Liu, and J. Liu, *Advance in Chitosan Hydrolysis by Non-Specific Cellulases.* Bioresour. Technol., 2008. **99**(15). p. 6751-62.

158. Allan, G.G. and M. Peyron, *Molecular Weight Manipulation of Chitosan. I: Kinetics of Depolymerization by Nitrous Acid.* Carbohydr. Res., 1995. **277**(2). p. 257-72.

159. Suzuki, K., et al., *Antitumor Effect of Hexa-N-Acetylchitohexaose and Chitohexaose.* Carbohydr. Res., 1986. **151**. p. 403-8.

160. Varum, K.M., et al., *Determination of Enzymatic Hydrolysis Specificity of Partially N-Acetylated Chitosans.* Biochim. Biophys. Acta, 1996. **1291**(1). p. 5-15.

161. Fukamizo, T., et al., *Reaction Mechanism of Chitosanase from Streptomyces Sp. N174.* Biochem. J, 1995. **311**(part 2). p. 377-83.

162. Roberts, G.A.F. and F.A. Wood, *A Study of the Influence of Structure on the Effectiveness of Chitosan as an Anti-Felting Treatment for Wool.* J. Biotechnol., 2001. **89**(2-3). p. 297-304.

163. Rinaudo, M., P. Ledung, and M. Milas, *A New and Simple Method of Synthesis of Carboxymethylchitosans*. Advances in Chitin and Chitosan, ed. C.J. Brine, P.A. Sandford, and J.P. Zikakis. 1992, Barking Essex: Elsevier Appl Sci Publ Ltd. 516-525.

164. Xu, P., et al., *Zwitterionic Chitosan Derivatives for Ph-Sensitive Stealth Coating.* Biomacromolecules, 2010. **11**(9). p. 2352-8.

165. Nishimura, S.I., et al., *Regioselective Syntheses of Sulfated Polysaccharides: Specific Anti-Hiv-1 Activity of Novel Chitin Sulfates.* Carbohydr. Res., 1998. **306**(3). p. 427-33.

166. Terbojevich, M., et al., *Solution Studies of Chitosan 6-O-Sulfate.* Makromolekulare Chemie-Macromolecular Chemistry and Physics, 1989. **190**(11). p. 2847-2855.

167. Holme, K.R. and A.S. Perlin, *Chitosan N-Sulfate. A Water-Soluble Polyelectrolyte.* Carbohydr. Res., 1997. **302**(1-2). p. 7-12.

168. Khanal, D.R., et al., *Protective Effects of Phosphated Chitin (P-Chitin) in a Mice Model of Acute Respiratory Distress Syndrome (Ards).* Carbohydr. Polym., 2001. **44**(2). p. 99-106.

169. Heras, A., et al., *N-Methylene Phosphonic Chitosan: A Novel Soluble Derivative.* Carbohydr. Polym., 2001. **44**(1). p. 1-8.

170. Varma, A.J., S.V. Deshpande, and J.F. Kennedy, *Metal Complexation by Chitosan and Its Derivatives: A Review.* Carbohydr. Polym., 2004. **55**(1). p. 77-93.

171. Domard, A., M. Rinaudo, and C. Terrassin, *New Method for the Quaternization of Chitosan.* Int. J. Biol. Macromol., 1986. **8**(2). p. 105-107.

172. Domard, A., M. Rinaudo, and C. Terrassin, *Adsorption of Chitosan and a Quaternized Derivative on Kaolin.* J. Appl. Polym. Sci., 1989. **38**(10). p. 1799-1806.

173. Suzuki, K., et al., *New Selectively N-Substituted Quaternary Ammonium Chitosan Derivatives.* Polym. J., 2000. **32**(4). p. 334-338.

174. Knight, D.K., S.N. Shapka, and B.G. Amsden, *Structure, Depolymerization, and Cytocompatibility Evaluation of Glycol Chitosan.* J Biomed Mater Res A, 2007. **83**(3). p. 787-98.

175. Bajaj, G., W.G. Van Alstine, and Y. Yeo, *Zwitterionic Chitosan Derivative, a New Biocompatible Pharmaceutical Excipient, Prevents Endotoxin-Mediated Cytokine Release.* PLoS One, 2012. **7**(1). p. e30899.

176. Desbrieres, J. and V.G. Babak, *Interfacial Properties of Amphiphilic Natural Polymer Systems Based on Derivatives of Chitin.* Polym. Int., 2006. **55**(10). p. 1177-1183.

177. Fujii, S., H. Kumagai, and M. Noda, *Preparation of Poly(Acyl)Chitosans.* Carbohydr. Res., 1980. **83**(2). p. 389-393.

178. Hirano, S., K. Hayashi, and K. Hirochi, *Some N-Acyl Derivatives of O-Carboxymethylchitosan.* Carbohydr. Res., 1992. **225**(1). p. 175-178.

179. Ramos, V.M., et al., *Modified Chitosan Carrying Phosphonic and Alkyl Groups.* Carbohydr. Polym., 2003. **51**(4). p. 425-429.

180. Sun, T., et al., *Graft Copolymerization of Methacrylic Acid onto Carboxymethyl Chitosan.* Eur. Polym. J., 2003. **39**(1). p. 189-192.

181. Desbrieres, J., C. Martinez, and M. Rinaudo, *Hydrophobic Derivatives of Chitosan: Characterization and Rheological Behaviour.* Int. J. Biol. Macromol., 1996. **19**(1). p. 21-8.

182. Holme, K.R. and L.D. Hall, *Chitosan Derivatives Bearing C-10-Alkyl Glycoside Branches - a Temperature-Induced Gelling Polysaccharide.* Macromolecules, 1991. **24**(13). p. 3828-3833.

183. Auzely, R. and M. Rinaudo, *Controlled Chemical Modifications of Chitosan. Characterization and Investigation of Original Properties.* Macromolecular Bioscience, 2003. **3**(10). p. 562-565.

184. Desbrieres, J., M. Rinaudo, and L. Chtcheglova, *Reversible Thermothickening of Aqueous Solutions of Polycations from Natural Origin.* Macromolecular Symposia, 1997. **113**. p. 135-149.

185. Rinaudo, M., et al., *Specific Interactions in Modified Chitosan Systems.* Biomacromolecules, 2005. **6**(5). p. 2396-407.

186. Babak, V.G., et al., *The Effect of Alkyl Chain Length of a Polysoap on the Surface Activity of Its Complexes with Cationic Surfactants.* Mendeleev Commun., 1997(4). p. 149-151.

187. Illum, L., *Chitosan and Its Use as a Pharmaceutical Excipient.* Pharm. Res., 1998. **15**(9). p. 1326-1331.

188. Kong, M., et al., *Antimicrobial Properties of Chitosan and Mode of Action: A State of the Art Review.* Int J Food Microbiol, 2010. **144**(1). p. 51-63.

189. Kim, I.Y., et al., *Chitosan and Its Derivatives for Tissue Engineering Applications.* Biotechnol. Adv., 2008. **26**(1). p. 1-21.

190. Riva, R., et al., *Chitosan and Chitosan Derivatives in Drug Delivery and Tissue Engineering*, in *Chitosan for Biomaterials Ii*, R. Jayakumar, M. Prabaharan, and A.R.A. Muzzarelli, Editors. 2011, Springer Berlin Heidelberg: Berlin, Heidelberg. p. 19-44.

191. Harris, J.M., et al., *Synthesis and Characterization of Poly(Ethylene Glycol) Derivatives.* Journal of Polymer Science Part a-Polymer Chemistry, 1984. **22**(2). p. 341-352.

192. Aiba, S., N. Minoura, and Y. Fujiwara, *Graft-Copolymerization of Amino-Acids onto Partially Deacetylated Chitin.* Int. J. Biol. Macromol., 1985. **7**(2). p. 120-121.

193. Wang, X., et al., *Chitosan-Nac Nanoparticles as a Vehicle for Nasal Absorption Enhancement of Insulin.* J Biomed Mater Res B Appl Biomater, 2009. **88**(1). p. 150-61.

194. Shahnaz, G., et al., *Thiolated Chitosan Nanoparticles for the Nasal Administration of Leuprolide: Bioavailability and Pharmacokinetic Characterization.* Int. J. Pharm., 2012. **428**(1-2). p. 164-70.

195. Chung, T.W., et al., *Preparation of Alginate/Galactosylated Chitosan Scaffold for Hepatocyte Attachment.* Biomaterials, 2002. **23**(14). p. 2827-34.

196. Park, I.K., et al., *Galactosylated Chitosan as a Synthetic Extracellular Matrix for Hepatocytes Attachment.* Biomaterials, 2003. **24**(13). p. 2331-2337.

197. Yalpani, M. and L.D. Hall, *Some Chemical and Analytical Aspects of Polysaccharide Modifications .3. Formation of Branched-Chain, Soluble Chitosan Derivatives.* Macromolecules, 1984. **17**(3). p. 272-281.

198. Auzely-Velty, R. and M. Rinaudo, *Chitosan Derivatives Bearing Pendant Cyclodextrin Cavities: Synthesis and Inclusion Performance.* Macromolecules, 2001. **34**(11). p. 3574-3580.

199. Casettari, L. and L. Illum, *Chitosan in Nasal Delivery Systems for Therapeutic Drugs.* J Control Release, 2014. **190**. p. 189-200.

200. Fernandez-Urrusuno, R., et al., *Enhancement of Nasal Absorption of Insulin Using Chitosan Nanoparticles.* Pharm. Res., 1999. **16**(10). p. 1576-1581.

201. Schmidtke, K., et al., *Complex Inorganic/Organic Core-Shell Particles by an Inverse Emulsion Technique*, in *Modern Trends in Polymer Science-Epf 09*, F. Stelzer and E. Wiesbrock, Editors. 2010, Wiley-V C H Verlag Gmbh: Weinheim. p. 28-37.

202. Hood, M.A., et al., *Controlling Hydrophobicity of Silica Nanocapsules Prepared from Organosilanes.* Colloids and Surfaces a-Physicochemical and Engineering Aspects, 2017. **532**. p. 172-177.

203. Sjoback, R., J. Nygren, and M. Kubista, *Absorption and Fluorescence Properties of Fluorescein.* Spectrochimica Acta Part a-Molecular and Biomolecular Spectroscopy, 1995. **51**(6). p. L7-L21.

204. Dautzenberg, H., *Polyelectrolyte Complex Formation in Highly Aggregating Systems. 1. Effect of Salt: Polyelectrolyte Complex Formation in the Presence of Nacl.* Macromolecules, 1997. **30**(25). p. 7810-7815.

205. Staff, R.H., et al., *Particle Formation in the Emulsion-Solvent Evaporation Process.* Small, 2013. **9**(20). p. 3514-22.

206. Migneault, I., et al., *Glutaraldehyde: Behavior in Aqueous Solution, Reaction with Proteins, and Application Ro Enzyme Crosslinking.* Biotechniques, 2004. **37**(5). p. 790-6, 798-802.

207. Crespy, D., et al., *Polymeric Nanoreactors for Hydrophilic Reagents Synthesized by Interfacial Polycondensation on Miniemulsion Droplets.* Macromolecules, 2007. **40**(9). p. 3122-3135.

208. Hungerford, G., et al., *Effect of the Labelling Ratio on the Photophysics of Fluorescein Isothiocyanate (Fitc) Conjugated to Bovine Serum Albumin.* Photochem Photobiol Sci, 2007. **6**(2). p. 152-8.

209. He, C.W., et al., *Sequence-Controlled Delivery of Peptides from Hierarchically Structured Nanomaterials.* ACS Appl. Mater. Interfaces, 2017. **9**(4). p. 3885-3894.

210. Sahay, G., D.Y. Alakhova, and A.V. Kabanov, *Endocytosis of Nanomedicines.* J Control Release, 2010. **145**(3). p. 182-95.

211. He, W., et al., *The Cushion Method: A New Technique for the Recovery of Hydrophilic Nanocarriers.* Langmuir, 2016. **32**(51). p. 13669-13674.

212. Harutyunyan, L.R., *Effect of Amino Acids on Micellization, Surface Activity and Micellar Properties of Nonionic Surfactant Hexadecyl Alcohol Ethoxylate (25eo) in Aqueous Solutions.* Journal of Surfactants and Detergents, 2015. **18**(1). p. 73-81.

213. Koynov, K. and H.J. Butt, *Fluorescence Correlation Spectroscopy in Colloid and Interface Science.* Current Opinion in Colloid & Interface Science, 2012. **17**(6). p. 377-387.

8. Acknowledgments

I would like to express my sincere gratitude to my advisor Prof. Katharina Landfester for her continuous support during my Ph.D. study, great patience, and immense knowledge. As a big fan of her since I was a master student, I felt proud and lucky to have had the opportunity to work on the topic of miniemulsion in Landfester´s Group. I could not imagine a better place for research.

I would like to thank Assoc. Prof. Daniel Crespy, who has supervised my study as project leader in AK-Landferster. I am very grateful that he also supported me to finish my Ph.D. thesis in his group in VISTEC. I felt happy to be surrounded by a delightful group of fellow students, and I really enjoyed the time I spent in VISTEC. Daniel's guidance helped me throughout all the time of my research and writing of this thesis. I have benefited a lot from his advice, mentorship, and encouragement. I feel extremely lucky to have met such a great supervisor, mentor, and friend.

I would also like to thank Prof. Ulrich Ziener, who supervised my project and provided me with numerous insightful suggestions. He has taken care of me throughout my study. Moreover, Ulrich encouraged me to pursue my Ph.D. in AK-Landfester ever since I was an internship student in Ulm. Without him, nothing would have happened.

My thanks also go to my fellow colleagues and friends in AK-Landfester, and in MPIP, for stimulating discussions, fantastic technical support, and for all the fun we have had in all these years. They have made my life much more colorful and enjoyable. AK-Landfester was not only a workplace for me but also like a family, not to mention that this is the place where I have met Yiran, my lovely wife.

Last but not the least, I would give my special thanks to my family, for supporting me spiritually throughout my study and my life in general.

9. Abbreviations

CLSM	confocal light scanning microscopy
CS	chitosan
DA%	degree of acetylation
DD%	degree of deacetylation
DLS	dynamic light scattering
EL55	Eudragit L100-55 ®
ELISA	enzyme-linked immunosorbent assay
EMEM	Eagle's Minimum Essential Medium
FCS	fluorescence correlation spectroscopy
FTIR	Fourier transform infrared
GA	glutaraldehyde
GC	glycol chitosan
GCNC	glycol chitosan nanocapsule
GC-RBITC	RBITC labeled GC
GlcN	D-glucosamine
GlcNAc	N-acetyl-D-glucosamine
Gluc-COOH	glucuronic acid
Gluc-NH2	glucosamine
GluNa	monosodium glutamate

PEC	polyelectrolyte complexation
PEG	polyethylene glycol
PGA	poly-γ-glutamic acid
PGPR	polyglycerol polyricinoleate
pK_a	acid dissociation constant
PYY, hPYY , rPYY	polypeptide YY, human PYY, rat PYY
RBITC	Rhodamine B isothiocyanate
rPYY-FITC	FITC labelled rPYY
SDS	sodium dodecyl sulfate
SEM	scanning electron microscopy
TAT	transactivator of transcription
TDI	toluene diisocyanate
TEM	transmission electron microscopy
UV	ultraviolet

10. List of figures

11. List of tables

12. SUMMARY

We discuss here several strategies to answer key challenges related to the delivery of fragile hydrophilic molecules in the body from nanoparticles. The questions associated with these questions are: How to encapsulate a hydrophilic fragile drug while preserving its function and integrity? How to ensure that the nanoparticles encapsulating the fragile payload are not aggregated when dispersed in aqueous media? And finally, is it possible to fabricate a material that would allow for the delivery of a fragile drug in the blood when the drug is taken orally?

In this work, we first discuss the state of the art related to the relevant topics. We summarized the currently available strategies to preserve fragile molecules. Moreover, we give also an insight into the techniques used to recover nanoparticles produced in inverse emulsions.

We report a new strategy for the synthesis of pH-responsive nanocarriers for the controlled release of peptides. The main drawbacks of the common polyelectrolyte complexation method were overcome by confining the complexation reaction in nanodroplets of inverse miniemulsion and by subsequent interfacial crosslinking. The resulting nanocarriers released encapsulated peptide drug in response to changes in pH values.

Afterward, the pH-responsive nanocarriers were further loaded into nanofibers constructed with a pH-responsive polymer, allowing for a stepwise release of payloads at sequential events of pH change. The hierarchically structured nanoparticle-in-nanofiber systems showed potential in complicated drug delivery tasks such as oral delivery of peptide drugs.

Finally, the “cushion” method, a new method for the recovery of hydrophilic NPs was introduced. The fast, mild, and efficient “cushion” method enabled the re-dispersion of a CS-based nanocarrier in water without additional surfactant. We believe that the “cushion” method is also suitable for other water compatible nanocarriers.

13. ZUSAMMENFASSUNG

Wir diskutieren hier einige Strategien, um die wichtigsten Herausforderungen im Zusammenhang mit der Abgabe von fragilen hydrophilen Molekülen im Körper aus Nanopartikeln zu beantworten. Die Fragen, die mit diesen Fragen verbunden sind, lauten: Wie kann ein hydrophiles, fragiles Medikament eingekapselt werden, während seine Funktion und Integrität erhalten bleiben? Wie kann sichergestellt werden, dass die Nanopartikel, die die fragile Nutzlast einkapseln, nicht aggregiert sind, wenn sie in wässrigen Medien dispergiert sind? Und schließlich, ist es möglich, ein Material herzustellen, das die Abgabe eines fragilen Medikaments im Blut ermöglicht, wenn das Medikament oral eingenommen wird?

In dieser Arbeit diskutieren wir zunächst den Stand der Technik zu den relevanten Themen. Wir haben die derzeit verfügbaren Strategien zum Erhalt fragiler Moleküle zusammengefasst. Darüber hinaus geben wir einen Einblick in die Techniken zur Gewinnung von Nanopartikeln in inversen Emulsionen.

Wir berichten über eine neue Strategie für die Synthese von pH-abhängigen Nanocarriern für die kontrollierte Freisetzung von Peptiden. Die Hauptnachteile des herkömmlichen Polyelektrolyt-Komplexierungsverfahrens wurden überwunden, indem die Komplexierungsreaktion in Nanotröpfchen der inversen Miniemulsion und durch anschließende Grenzflächenvernetzung eingeschränkt wurde. Die resultierenden Nanoträger setzten verkapselte Peptidarzneimittel in Reaktion auf Änderungen der pH-Werte frei.

Danach wurden die pH-ansprechenden Nanoträger weiter in Nanofasern geladen, die mit einem auf pH ansprechenden Polymer konstruiert waren, was eine schrittweise Freisetzung von Nutzlasten bei aufeinanderfolgenden Ereignissen der pH-Änderung ermöglichte. Die hierarchisch strukturierten Nanopartikel-in-Nanofasersysteme zeigten ein Potenzial bei

komplizierten Wirkstoffabgabeaufgaben wie der oralen Verabreichung von Peptidarzneimitteln.

Schließlich wurde mit der "Cushion" -Methode (cushion = Kissen) eine neue Methode zur Gewinnung hydrophiler NPs eingeführt. Die schnelle, milde und effiziente "Cushion" -Methode ermöglichte die erneute Dispersion eines CS-basierten Nanoträgers in Wasser ohne zusätzliches Tensid. Wir glauben, dass die "Cushion" -Methode auch für andere wasserkompatible Nanoträger geeignet ist.

14. Erklärung

Hiermit versichere ich gemäß § 10 Abs. 3d der Promotionsordnung vom 24.07.2007, dass ich die als Dissertation vorgelegte Arbeit selbst angefertigt und alle benutzten Hilfsmittel (Literatur, Apparaturen, Material) in der Arbeit angegeben habe.

Mainz,den _____

Wei He